2016

An Optical Character Recognition Engine for Graphical Processing Units

Jeremy Reed
University of Kentucky, jp_reed@yahoo.com
Author ORCID Identifier:
http://orcid.org/0000-0001-7491-9683
Digital Object Identifier: https://doi.org/10.13023/ETD.2016.506

An Optical Character Recognition Engine for Graphical Processing Units

DISSERTATION

A dissertation submitted in partial fulfillment of the requirements for the degree of Doctor of Philosophy in the College of Engineering at the University of Kentucky

By
Jeremy Reed
Lexington, Kentucky

Director: Dr. Raphael Finkel
Professor of Computer Science
Lexington, Kentucky 2016

ABSTRACT OF DISSERTATION

An Optical Character Recognition Engine for Graphical Processing Units

This dissertation investigates how to build an optical character recognition engine (OCR) for a graphical processing unit (GPU). I introduce basic concepts for both building an OCR engine and for programming on the GPU. I then describe the SegRec algorithm in detail and discuss my findings.

KEYWORDS: OCR, CUDA, GPU

Author's signature: Jeremy Reed

Date: November 22, 2016

An Optical Character Recognition Engine for Graphical Processing Units

By
Jeremy Reed

Director of Dissertation:	Raphael Finkel
Director of Graduate Studies:	Miroslaw Truszczyński
Date:	November 22, 2016

ACKNOWLEDGMENTS

My wife, Anrea, first and foremost, is the reason this dissertation exists in a finished form. Her support and encouragement over the years to "finish my OCR" served as a driving force to help keep me on track. My advisor, Dr. Raphael Finkel, follows at a close second. He served — and continues to serve — as a sounding board upon which ideas are bounced and as a source of wisdom and advice. I am grateful to him for all he has helped me do and look forward to ever more.

I would also like to thank the members of my committee for their time, effort, and feedback.

Special thanks goes to NVIDIA for providing the Tesla K40 upon which I tested SegRec.

TABLE OF CONTENTS

LIST OF FIGURES

LIST OF TABLES

Chapter 1: Introduction

1.1 Motivation

This dissertation describes research and development for an optical character recognition (OCR) engine that runs on a graphical processing unit (GPU). The purpose of this endeavor is to significantly increase the speed of the image-processing and glyph-recognition steps while maintaining accuracy and precision measures that favorably compare to existing commercial engines.

OCR was first introduced in the early 1900s as a technology designed to enable sight-impaired people to read. The "Type-reading Optophone", introduced in 1914, converts light reflected off of type-written text into sounds — each glyph emitting a unique tone. With training, a person could learn to discern the tones and "read" the text [11]. A later invention, patented in 1931 and dubbed the "Statistical Machine", was designed to help speed the search for text in microfilm archives [16]. A light source positioned below the microfilm and "search plates", solid, opaque plates with the search text carved out, positioned above the microfilm provides a variable light-source to a light detector positioned above the search plate. As the microfilm moves, the light level above the search plate varies such that when the text matches exactly with the search plate, very little light passes through the film to the detector. The detector then records the occurrence as a possible text match [16].

This dissertation describes an OCR engine that processes glyphs that have already been captured in image form, but much of the same process occurs as in the devices described previously. Modern optical character recognition can be segmented into four main phases: pre-processing, isolation, identification and post-processing. The **pre-processing** phase prepares the image for the next phase and includes such tasks as noise reduction and rotation correction. The **isolation** phase deals with dividing an image into sub-images, delineating where lines, words and, ultimately, characters begin and end. The **identification** phase accepts the output from the isolation phase and attempts to recognize the sub-images passed to it as characters. The **post-processing** phase attempts to reassemble the characters into words and sentences. The main focus of this dissertation is on the isolation and identification phases.

1.2 Contribution

In this dissertation, I present a series of algorithms for quickly isolating and identifying characters from a large number of images containing typewritten text. As a whole, this work comprises a framework for a GPU-enabled OCR engine.

During my research, I invented a number of algorithms:

- **PathFind** is a path-finding algorithm that operates on bi-tonal images and requires no recursion or complex data structures. PathFind is discussed on page 18.

- **EdgeWalk** is an edge-walking algorithm that traverses the edges of a glyph in a bi-tonal image using pixel-based heuristics to decide the next step. EdgeWalk is discussed on page 53.
- **SegRec Version 1** is a naïve implementation of the isolation phase that introduces a parallel algorithm similar to the **x-y cut segmentation** algorithm. The x-y cut segmentation algorithm from which Version 1 is partially derived is discussed on page 20. SegRec Version 1 is discussed in section 4.1 on page 48.
- **SegRec Version 2** is a reimplementation of SegRec Version 1 and discards the similarities to x-y cut altogether. Version 2 uses the EdgeWalk algorithm to compute glyph boundaries. SegRec Version 2 is discussed in section 4.2 on page 51.
- **SegRec Version 3** is a reimplementation of SegRec Version 2 and forms the bulk of my contribution. Version 3 introduces a novel algorithm to discover and process glyphs in a parallel manner. Version 3 is discussed in section 4.3 on page 53.

1.3 Structure of the dissertation

This dissertation outlines the methods and algorithms I chose for handling the first three phases within the GPU OCR engine and the reasons for those choices.

Chapter 2, Preliminaries

In section 2.1, I introduce the fundamental terminology upon which the concepts of OCR are built.

In sections 2.2 through 2.9, I describe, in greater detail, the four phases of OCR, the typical problems and solutions associated with each phase and the base concepts and ideas that I reference throughout the dissertation. These sections also include a literature review that outlines the current state of the field and provides background information relevant to the particular phase of OCR under discussion.

This chapter assumes no prior experience with OCR or related fields.

Chapter 3, OCR on GPUs

This chapter provides an introduction to GPU hardware and a basic introduction to GPU programming.

This chapter assumes no prior experience with GPUs.

Chapter 4, The SegRec Algorithm

This chapter describes each of the three versions of the SegRec algorithm in detail.

Chapter 5, Results and Findings

This chapter compares SegRec against other open-source and commercial OCR engines.

Chapter 6, Conclusion and Future Work

This chapter summarizes the results presented in this dissertation and details future research that could improve SegRec.

Chapter 2: Preliminaries

Figures and images

Unless otherwise noted in the caption, I created every figure and image with my own implementation of the algorithm the figure or image illustrates.

2.1 Terminology

We introduce some of the basic terminology here; we introduce more definitions later as they become relevant.

Base
: The core portion of a character; for instance, in the character â, the base is ‘a’.

Mark
: A character accent not physically connected to the base, for instance, in the character â, the mark is ‘ˆ’.

Glyph
: The pictorial representation of a character.

2.2 OCR Phases

Pre-processing

The purpose of the pre-processing phase is to prepare a given image for the isolation phase — primarily, to make it easier for the isolation phase to determine where character glyphs begin and end. Section 2.3 describes this phase and its associated problems in detail.

Isolation

The isolation phase analyzes the cleaned image data from the pre-processing phase in an effort to locate and isolate pockets of text. These pockets are then further broken down into lines and, finally, into single glyphs. Section 2.5 describes this phase and its associated problems in detail.

Identification

The identification phase examines the isolated glyphs and attempts to classify each of them as a particular character. Section 2.7 describes this phase and its associated problems in detail.

Post-processing

Post-processing attempts to construct text from the output provided by the identification phase. The output might include spacing and formatting. Section 2.9 provides an overview of this phase and gives a brief introduction to its associated problems.

2.3 Pre-processing phase: Problems

The pre-processing phase must deal with pixel noise, varying degrees of contrast, bleed-through text, multiple colors, and document rotation. Below is a breakdown of these issues and a brief description about why they pose a problem.

Pixel noise

Pixel noise usually refers to the random marks, streaks or other image artifacts found throughout low-quality images, but it can also refer to unwanted background images, borders or other document flourishes that impede the isolation or identification phases. Removing the noise is key for accurately isolating and identifying glyphs, because untreated noise can disrupt the use of white space to find paragraphs and lines or cause incorrect identification.

Degrees of contrast

In faxed documents, poorly scanned documents, and historical documents, the quality of the image may vary from one page to another. Often, documents contain varying levels of contrast within the text itself. This situation affects the ability of the OCR algorithm to choose an appropriate threshold for converting to a binary image and could affect the overall effectiveness of noise-removal techniques.

Bleed-through text

Bleed-through text, where ink from one side of a piece of paper is visible on the other side, is often found in historical documents or on images scanned from documents printed on thin paper. Because differentiating between bleed-through text and text that is merely low-contrast or faded is difficult, bleed-through text, like varying degrees of contrast, interferes with most noise-removal techniques.

Multiple colors

Some images contain characters of varying colors on backgrounds of varying colors. The OCR application must be able to differentiate background from character. There is some overlap between this problem and the isolation phase “Complex Page Layout” problem, because colors are typically blocked and grouped in a complex manner.

Rotation detection, estimation and correction

The whole image can be rotated, lines can be skewed or individual letters can be skewed. The OCR algorithm must recognize the transformation and correct it prior to identification. Alternatively, the identification phase must be aware of the transformation and adjust its training data or other internal recognition mechanisms accordingly.

2.4 Pre-processing phase: Techniques and solutions

Thresholding

All thresholding[1] techniques fall under the class of "data-reduction" algorithms. That is, the techniques seek to compress or reduce the information contained within a given image in order to reduce computational complexity. The purpose then, is to remove or reduce the unwanted information or "noise" and leave the "important" information intact, such as removing the background of a bank check so the OCR application can read the signature panel.

For OCR applications, data reduction is usually confined to reducing a grayscale or color image to a black and white (binary or bi-tonal) image. This reduction is accomplished by calculating a level of intensity against which individual pixel values are compared. The values that fall below the threshold are included in the binary image as black pixels; the others are white [48]. The threshold value can be calculated on a global or local level, and the techniques implementing each method are referred to as **global** or **adaptive**[2] thresholding, respectively. Global methods calculate the threshold using the entire image, whereas local or adaptive thresholds readjust the threshold based on the area of the image around which processing is taking place [4]. Adaptive techniques typically calculate a "running value" for the threshold and make the black or white decision based on comparisons against this value [56].

These thresholding techniques are also appropriate for removing bleed-through text, because such text generally appears on the page at a much lighter contrast than normal text. However, for severely degraded text or in cases where a document exhibits both varying degrees of contrast and bleed-through text, thresholding is usually avoided [5].

1. Histogram-based thresholding techniques build a histogram of grayscale values and then analyze the histogram topology. The analysis finds groups of peaks that are then combined by averaging the grayscale values within the group, thereby reducing the total number of grayscale values. Figure 2.1 shows an example of this method. Figure 2.1a contains 6 grayscale values. The histogram groups the peaks. Averaging the groupings results in the image Figure 2.1c, which gives a reduction in grayscale values of 50% [46].

2. The clustering technique (or **Otsu's method**) attempts to find the threshold that separates the grayscale values into classes that maximize the between-class variance [37]. In simpler terms, the technique attempts to find the histogram grouping that maximizes the

[1]Also referred to as **binarization**.

[2]Also referred to as **local** thresholding.

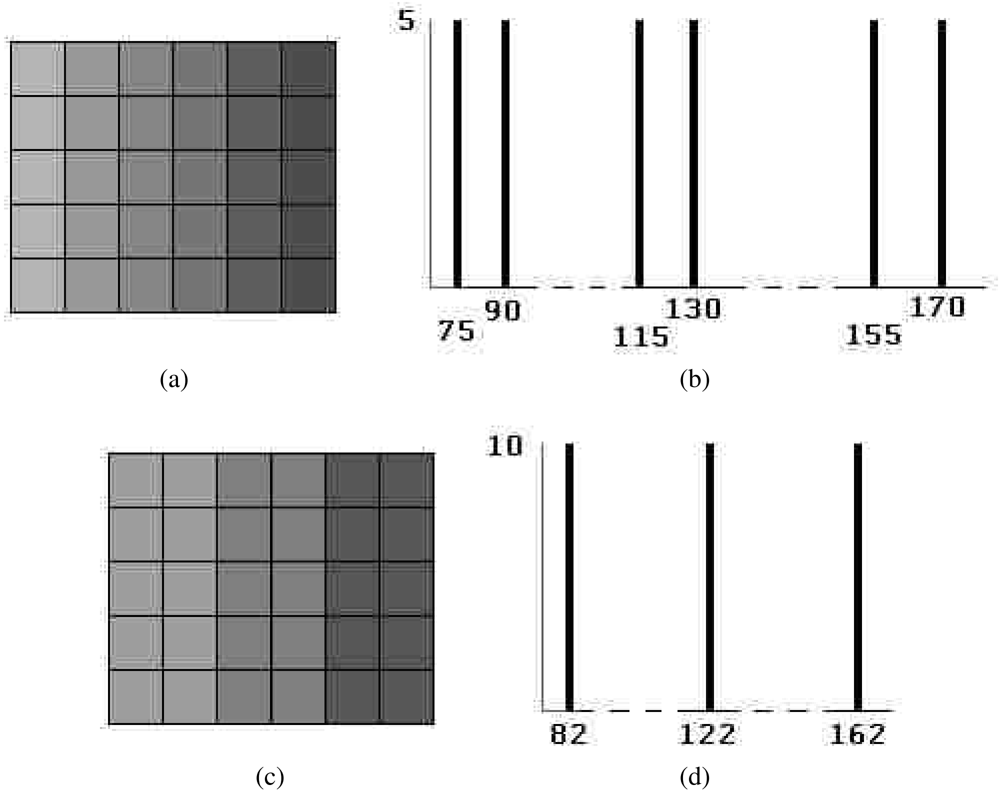

Figure 2.1: The original image with 6 grayscale values (a) and its histogram (b). The reduced image with 3 grayscale values (c) and its histogram (d).

difference in intensity between two groups of grayscale values. In the final grouping, the lighter values are drawn as white pixels and the darker values as black pixels. The threshold is the value that splits the class groupings.

Singh et al. parallelized Otsu's method for an average speedup of 1.6× over serial methods [51].

3. Entropy methods select a threshold based upon entropic calculations performed on the histogram [3, 8, 21]. In the simplest form, the chosen threshold splits the pixel count equally, as entropy is maximized when a pixel is equally as likely to be black as it is to be white. See Figures 2.3 and 2.4.

4. An **object-attribute method** examines a particular attribute of an object (in this case, a glyph) and utilizes some specific feature of that object to perform a function. An example of such an algorithm utilizes edge detection to perform thresholding. First, the algorithm applies a heuristic to choose the initial threshold values based upon the peak values within the grayscale histogram of the image. Next, an edge detection routine runs on both the original image and the thresholded image. If the edges match, the thresholds are kept and the process is complete. If not, the image is broken down into smaller chunks and the whole process repeats. Thus, this technique utilizes global thresholding at the beginning and selectively applies adaptive thresholding as the need arises [19].

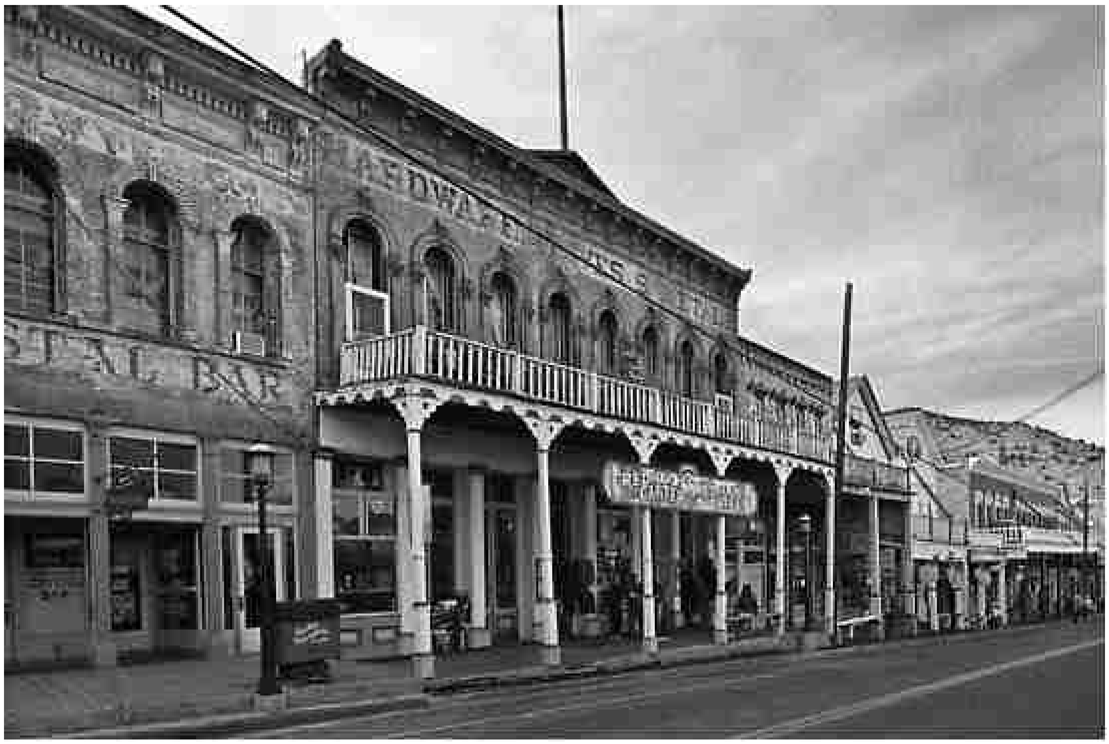

Figure 2.2: Original grayscale image (resized to fit). Image by QT Luong
`http://www.terragalleria.com/america/nevada/virginia-city/`

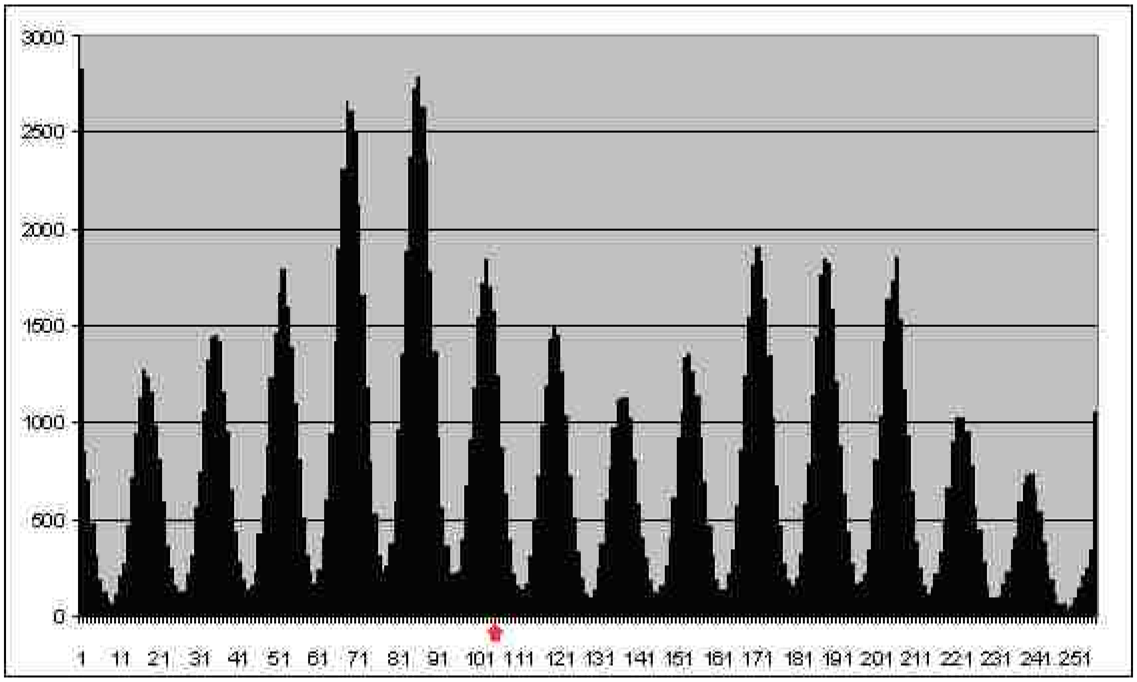

Figure 2.3: The grayscale histogram of Figure 2.2. The arrow denotes the point at which half the pixels are on the left and half are on the right.

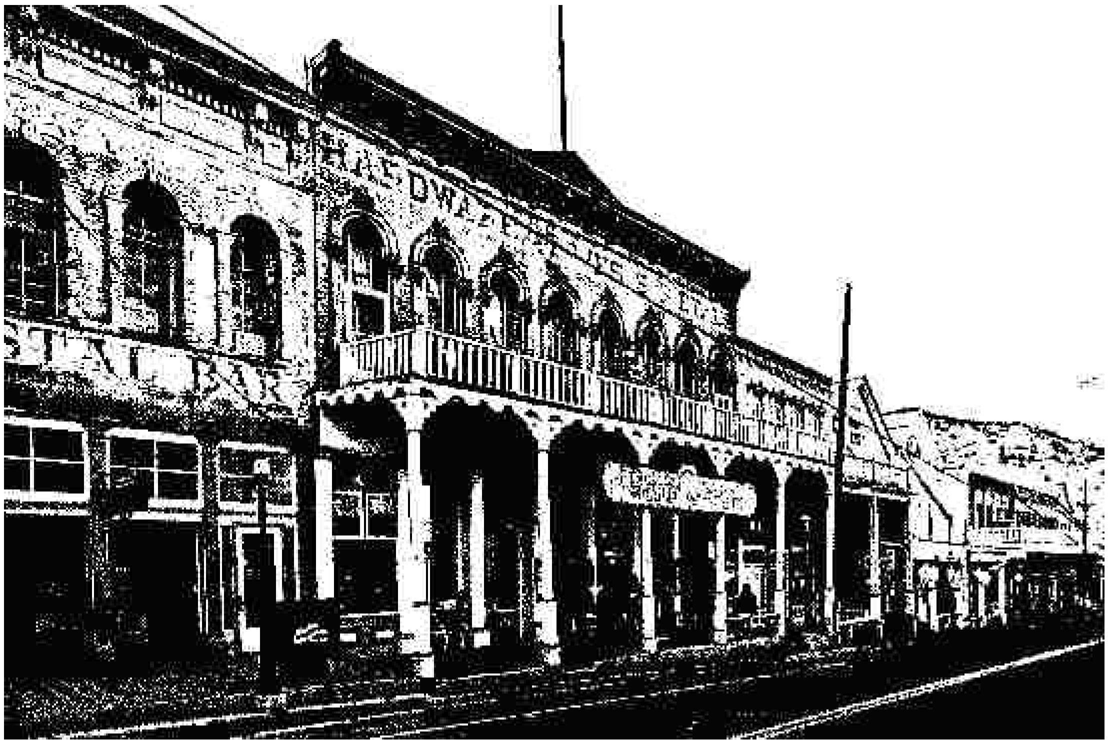
Figure 2.4: Original image after the threshold from Figure 2.3 is applied.

5. A dynamic algorithm, called the **integrated function algorithm**, is able to separate text from backgrounds with as little as 20% difference in contrast. The algorithm first identifies edges of sharp contrast (similar to the previous method) and then assumes that character strokes range in width from 0.2mm to 1mm in order to determine if an identified region is a character or an area of high-contrast background. The algorithm marks regions identified as characters black and all other regions as white [55].

6. The basic adaptive thresholding technique is called the **Niblack binarization algorithm**. The algorithm works by calculating the threshold value within a sliding window using the mean and the standard deviation and includes or excludes the pixels in the area according to the calculated value. The window shape is up to the implementation and can vary based upon the requirements of the images being processed [31]. **Sauvola's algorithm** modifies Niblack to store and use the dynamic range of standard deviation, which adapts the threshold to ignore noisy backgrounds [45].

   Singh et al. parallelized Niblack's binarization algorithm for a speedup of 20× to 22× over serial methods [50]. Singh et al. and Chen et al. also parallelized Souvala's algorithm for a speedup of 20× to 22× and 38×, respectively, over serial methods [9, 52].

7. A variation on Niblack's algorithm is **pixel density thresholding**. This method determines the average pixel density within a sliding window and includes or excludes the pixels in that area accordingly. The window shape is up to the implementation and can vary based upon the requirements of the images being processed. This technique is useful for removing streaks and marks due to poor image quality and can also oper-

ate in conjunction with another thresholding algorithm. The pixel density thresholding technique is not mentioned in any paper I have found.

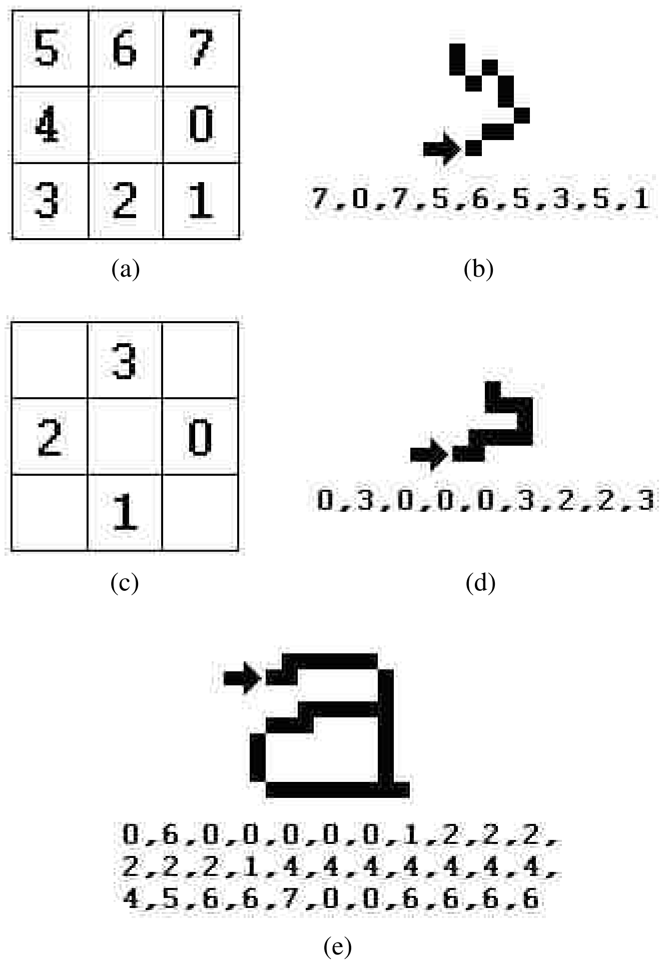

Figure 2.5: (a) and (c) show the two chain code scoring methods; (b) and (d) show a sample chain using their respective scoring methods; (e) shows an ‘a’ and its corresponding chain code. The arrow denotes the starting position for each chain code.

8. Another algorithm for a noise-reduction thresholding technique is called **chain code thresholding**. A chain code is a data structure that consists of a start point and a string of digits representing a list of directions. The digit string contains numerals in the range 0-7 (or 0-3) that represent all possible directions on a 2D image. A chain code is formed by choosing a starting point, moving one pixel in an allowed direction and appending that direction to the digit list. Thus, the chain code is a representation of a path in 2D space. Chain code thresholding constructs chain codes representing the border of each pixel group and analyzes the resultant digit string. During the isolation phase, if a chain code has a length below a certain threshold, it can be discarded. This method is not mentioned in the literature, though chain codes are described in detail by Freeman [14].

DIBCO, the Document Image Binarization Contest, was started in 2009 in order to evaluate and test the best thresholding techniques [1]. The contest ran from 2009 through 2014. The winning entries for each year are all hybrid algorithms that break down the thresholding process and use the best-of-breed algorithm for each part. For example, the winning submission in 2009 was by Lu et al., a team from the Institute for Infocomm Research in Singapore. Lu's submission incorporates Otsu's method, Niblack's algorithm, stroke edge detection and a post-process clean-up step [15]. Unfortunately, the published results from 2010 to 2014 are too brief to glean any meaningful detail about the algorithms. However, I include references for each of the yearly result papers for completeness: 2009 [15], 2010 [40], 2011 [41], 2012 [42], 2013 [43], and 2014 [32].

Otsu's method provides an excellent general-purpose algorithm for thresholding that many authors still reference as a baseline for comparing their methods. However, advancements made in adaptive thresholding, such as the object-attribute edge detection and the integrated function algorithms described above, and increased document complexity limit the appeal of global thresholding as a whole. This shift to adaptive algorithms is because the cost of each type of algorithm is similar, but the adaptive methods handle contrast gradients and variations within documents better. Ultimately, choosing a thresholding algorithm is context- and domain-specific. For example, Otsu's method is a simple, parameterless algorithm that will give good results on documents with high contrast between text and background, whereas the adaptive methods, such as the integrated function algorithm, are more complex, require tuning and are required only for more complex documents.

Rotation detection, estimation and correction

There are four basic types of rotation-detection algorithms: projection profile, nearest neighbor clustering, component labeling, and the Hough transform [12].

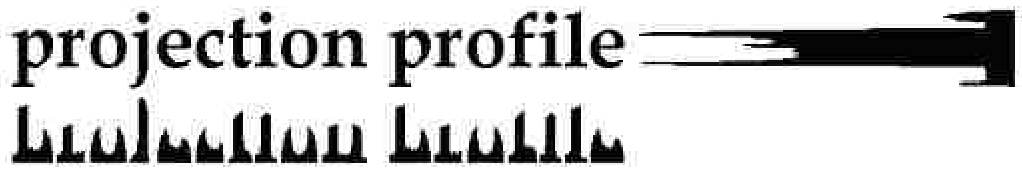

Figure 2.6: Horizontal and vertical projection profiles. Figure recreated from Abdelwahab et al. [56].

1. The **projection profile** technique projects the document at different angles, then, for each angle, constructs a graph based on the sum of black pixels in each line. Peaks are due to scanlines with high pixel density and troughs are due to white space and scanlines with low pixel density. The document angle that gives the maximum difference between the peaks and troughs is the rotation angle [12]. This technique can be applied horizontally or vertically. The horizontal application of the projection profile technique works better for the languages written in rows (i.e. right to left or left to right), such as English, whereas the vertical application works better for languages written in columns, such as Chinese. See Figure 2.6.

2. The **nearest-neighbor clustering** method constructs "pixel groups" from directly connected pixels. Every pixel group contains at least one glyph (this technique assumes there are no groups with only noise). The method calculates the vertical center of each pixel group and uses it to calculate the angle between the closest pixel groups and a horizontal reference line. Next, the algorithms constructs a histogram from these results, and the angle found to be most common, indicated by the highest peak in the histogram, is the rotation angle [12]. See Figure 2.7.

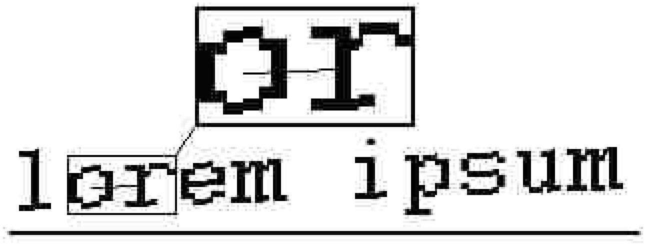

Figure 2.7: Nearest-neighbor clustering uses the angle between pixel groups to compute rotation. In this example, the glyphs themselves form the pixel groups.

3. **Component labeling**, a technique adapted from graph theory, attempts to calculate the average height of the characters in a line in order to identify the mean line and baseline. Once identified, these lines can be used to calculate the rotation. The **mean line** is roughly defined as the equivalent to the top of a lowercase character, excluding those characters with ascenders or descenders (e.g. d, t, g, y, etc.). The **baseline** is the line upon which the characters are printed. The algorithm groups and labels sets of pixels as belonging to either the mean line, baseline or neither by maintaining a running average for the height of a character and excluding outliers, such as tall characters, marks, and letters with ascenders or descenders. Once the process is complete and the average height is known, the mean line and baseline estimate the rotation angle [12].

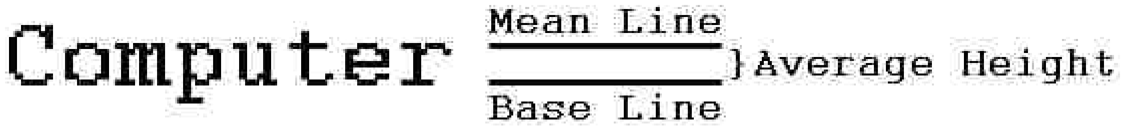

Figure 2.8: Depiction of the mean line and base line. Figure recreated from Das et al. [12].

4. The **Hough transform** also attempts to discover the mean lines and baselines in an image of text as a way to calculate rotation. The algorithm maintains a two-dimensional array indexed by line slope and origin that functions as an accumulator. A naïve implementation of the transform projects lines at varying angles through each black pixel and counts the number of intersections with other black pixels. If the number of intersections is above a threshold, the algorithm increments the corresponding slots for the line angle and origin within the accumulator array. This algorithm operates under the assumption that the mean lines and baselines for a given page of text have the highest pixel density. The angle represented by the bucket with the highest value is taken as the angle of either

the mean line or the base line (or both) and is the rotation angle [29]. This algorithm can be applied on a global or local scale. The main drawback for implementing the Hough transform is its computational complexity [12]. See Figure 2.9.

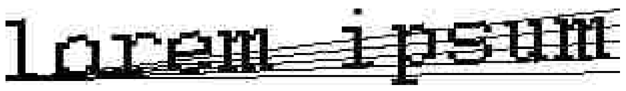

Figure 2.9: The Hough transform projects lines through pixels and counts the intersections to find the mean line and the baseline.

5. The **Das and Chanda morphology method** calculates rotation by performing the morphological close operation (described below) with a 12×1-pixel horizontal line structuring element to reduce each line of text into a black band. The algorithm smooths each band with a morphological open operation (described below) and marks the bottoms with a line. The algorithm measures these lines and averages their rotations. The average of the angles is the rotation angle.

   A morphological **close** operation works by sliding a **structuring element** across a binary image. Everywhere the structuring element overlaps only white pixels remains white; the white pixels where the element does not fit are made black. See Figure 2.10.

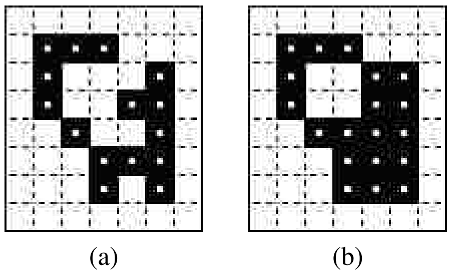

Figure 2.10: An example 2×2-pixel morphological close operation. (a) the original shape, (b) the shape after the structuring element is applied.

   After the algorithm applies the 12×1-pixel horizontal line structuring element via the morphological close, each black band contains rough edges corresponding to the presence of ascenders and descenders. The algorithm smooths these bumps by applying the morphological open operation with a 5×5-pixel structuring element. The **open** operation works like the close operation, except instead of sliding around on the white pixels, the algorithm places the open structuring element on the black pixels in an image. Everywhere the opening structuring element fits, the pixels remain black; the black pixels where the element does not fit are made white. See Figure 2.11.

   Once the black bands are smoothed, the algorithm scans the document top to bottom and marks black to white transitions. Essentially, this step captures the baseline of each text line. If the line length exceeds some threshold, the angles of the lines are measured and averaged and the resultant angle is the rotation angle [12]. See Figure 2.12 on page 14.

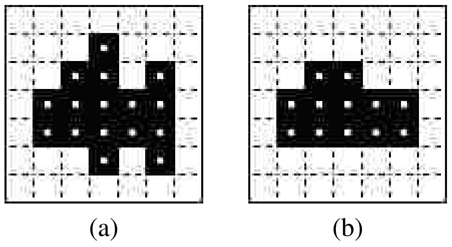

Figure 2.11: An example 2×2-pixel morphological open operation. (a) the original shape, (b) the shape after the structuring element is applied.

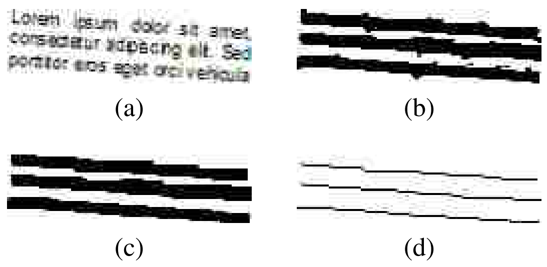
Lorem ipsum dolor sit amet, consectetur adipiscing elit. Sed porttitor eros eget orci vehicula
(a)
(b)
(c)
(d)

Figure 2.12: The Das and Chanda morphology method. (a) the original text, (b) the text after the close operation using a 12 pixel horizontal structuring element. (c) the text after the open operation with a 5 pixel x 5 pixel structuring element. (d) the transitions from black to white pixels, representing the baseline of the text.

6. The **bounding-box reduction** method subdivides the image into sections by global and adaptive thresholding, then attempts to reduce the bounding boxes around each subsection through a brute-force rotation mechanism. The algorithm rotates each subsection of the document by a step angle, then re-calculates the bounding box for that subsection. The algorithm accepts the angle that minimizes the overall area of the bounding box as the rotation angle for that subsection. This method allows for multiple rotation angles to be present on a document. This method also works on documents that include graphics, as each graphic is treated as just another subsection [4]. See Figure 2.13.

All these algorithms are adequate at finding the rotation angle on a rotated document. Typical results from each of the corresponding references report deviations from the actual rotation value of less than several tenths of a degree. However, the clear winner is the bounding-box reduction method. This algorithm can be used with mixed graphics and text documents and can handle multiple rotation angles on the same page, since it processes each section separately. For text-only documents, the Das and Chanda morphology method is viable, though the implementation depends heavily on the efficiency of the open and close morphology operations.

In general, the rotation angle in scanned text tends to be less than a few degrees and, in such cases, a shear transformation (or shear mapping) is an efficient corrective measure; rotation is much more expensive.

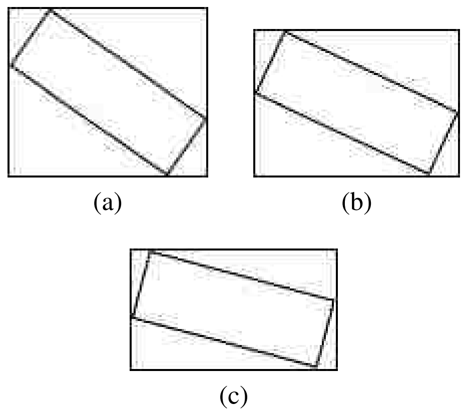

Figure 2.13: The bounding-box reduction method. (a) through (c) show progressively smaller bounding boxes as the object being rotated progresses towards being horizontal.

A **shear transformation** is a type of linear transformation in which pixels are moved in a particular direction. The distance the pixels are moved is proportional to the signed distance (i.e. the scaling can be positive or negative) from an arbitrary line that denotes the intended shear angle. See Figure B.5.

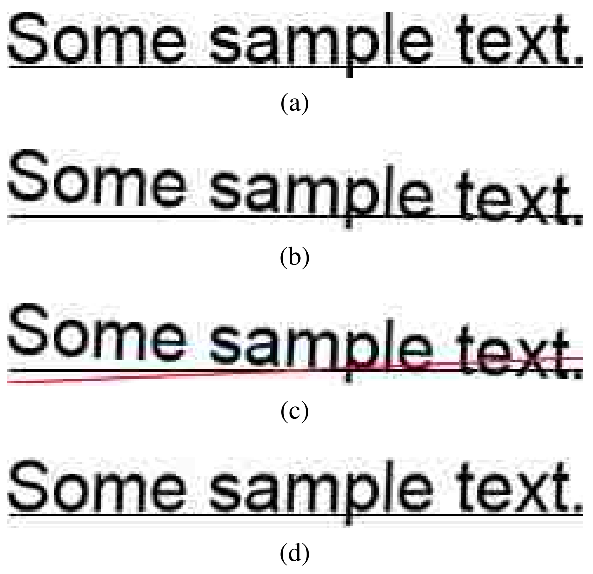

Figure 2.14: Sample text rotated then corrected with a shear transformation. (a) the original text, (b) the text rotated by 2.5°, (c) the rotated text overlayed by a line denoting the target −2.5° vertical shear angle, and (d) the corrected text.

2.5 Isolation phase: Problems

The problems encountered during this phase have to do with handling kerning and character ligatures, associating marks with the correct base, and handling complex page layouts.

Kerning

Some fonts and handwriting styles contain characters that project into the vertical space of surrounding characters, which makes isolating individual characters more complex as compared to fonts with clearly separated characters. For example, the characters “WJ’ are not separated by vertical white space.

Character ligatures

Ligatures are strokes that connect one letter to another. Small fonts, cursive English handwriting and Arabic all exhibit characters that are connected via a continuous stroke. Connected characters are hard to separate.

Marks

In many languages, letters have various accents and accompanying strokes (marks) that are unconnected to the rest of the letter, such as the dot in the English lower case ‘i’. Because the meaning of a glyph can change based on these marks, the OCR application must correctly group them with the base. Marks can appear above or below a base.

Complex page layout

If a page is multi-columnar or contains sidebars of text or textual graphics such as solid lines separating sections, the OCR application needs to be able to group the appropriate lines of text together and discard the graphics as noise.

2.6 Isolation phase: Techniques and solutions

Kerning

1. Chain codes representing boundaries are an effective way to capture entire characters even if they are kerned. The chain code moves around the border, operating on either the black pixels of the character itself or the white pixels directly adjacent to the character, until the entire character has been enveloped. This algorithm fails if characters are not separated by white space.

2. An alternative method is to find the best-fit bounding box. A **best-fit bounding box** is a rectangle that surrounds the character and is bounded by the most likely horizontal location where one character ends and another begins. An algorithm finds these locations by calculating the horizontal and vertical pixel density of the area and choosing the valley locations [28]. These bounding boxes may intersect and include portions of other characters, so this method requires additional processing to remove any extra pixels caused by this inclusion. Noise reduction algorithms, such as chain-code thresholding, can remove the extra pixels. An enhancement to the algorithm is to calculate the average size of each letter and impose minimum and maximum widths (or heights) for the bounding box. See Figure 2.16.

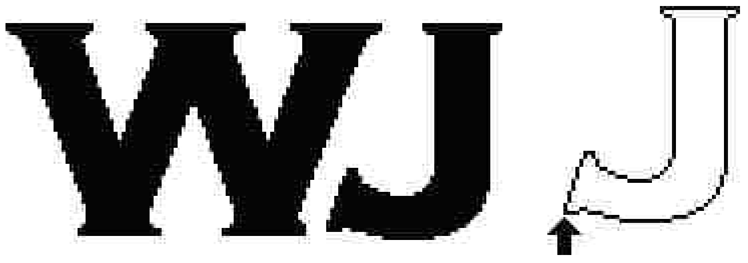

(a) (b)

```
6,6,7,6,6,7,6,6,7,6,6,7,6,7,6,0,0,2,1,2,1,0,1,0,1,0,0,1,0,0,0,0,0,7,0,7,7,
7,6,7,6,6,6,6,6,6,6,6,6,6,6,6,6,6,6,6,6,6,6,6,6,6,6,6,6,6,6,6,6,6,6,6,6,6,
5,4,5,6,0,0,0,0,0,0,0,0,0,0,0,0,0,0,0,0,0,0,2,3,4,3,2,2,2,2,2,2,2,2,2,2,
2,2,2,2,2,2,2,2,2,2,2,2,2,2,2,2,2,2,2,2,2,2,2,2,2,2,2,3,2,2,3,2,3,3,3,3,
4,3,4,3,4,4,4,3,4,4,4,4,4,4,4,4,4,4,4,4,5,4,4,4,5,4,4,4,5,4,3,4,4,4
```

(c)

Figure 2.15: Chain codes can isolate kerned characters like those in (a). The chain code in (c) represents the outside edge of the 'J' character in (b).

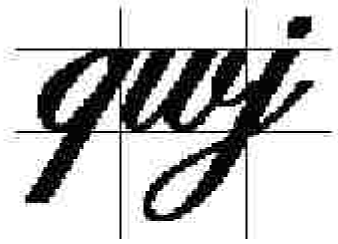

Figure 2.16: Borders for a best-fit bounding box.

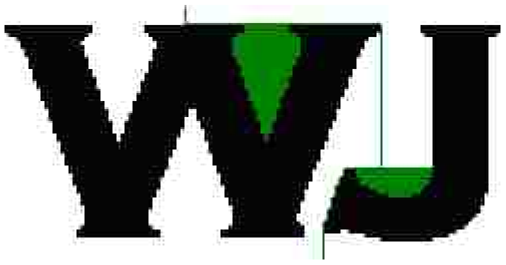

Figure 2.17: The execution of the path-finding algorithm to find the white space between characters.

3. Another method is to find a path between kerned characters. This method creates a bounding polygon that isolates the characters from each other. The downside to this algorithm is its computational complexity.

   I developed a pathing algorithm, PathFind, that operates on a bi-tonal image as shown in Figure 2.18 on page 19. This path-finding algorithm requires no recursion or complex data structures, results in an array of fixed size, requires no target ‘end point’ (it only tries to find a path to some x at $image\_height - 1$), and requires very little memory. These features make it especially good for GPU processing.

Of the methods described, the PathFind algorithm seems to be the most likely candidate for a general-purpose solution. The best-fit bounding box suffers from the problem of determining where the “best-fit” actually occurs. For example, in the case of Figure 2.16 on page 17, a reasonable alternative for a best-fit box may only capture half the “w”. The algorithm using chain codes must check and process every pixel on the border of a glyph and must convert a finished chain code into a bounding polygon, which generally requires more processing than the PathFind algorithm (the cost of the chain code algorithm is proportional to the border length of a glyph; the cost of PathFind is proportional to the height of a glyph).

Marks

1. The only technique in the literature for dealing with marks is to use the overall height-to-width ratio to determine if a mark belongs with a particular character [29]. If pairing the mark with a specific character increases the height-to-width ratio of the character beyond a threshold, the mark is excluded; otherwise it is included with the character. Since most marks are placed above or below their bases, this method is particularly effective. The OCR engine could also try to recognize the character both with and without the mark, accepting whichever version is recognized. If both versions are recognized, confidence values can be relied upon to determine a winner. The OCR engine could also recognize marks and bases separately and combine them in post-processing.

2. Using the bounding boxes of isolated glyphs, one can easily compute the distance between smaller boxes (most likely marks) to the nearest larger box (most likely a base) to determine to which base the mark belongs. This technique allows the creation of entire characters from the constituent strokes in the image. This method is not mentioned in the literature.

This problem needs more research, because there is no good generic algorithm for associating marks with their base. The lack of any generic algorithm is probably because the types of marks seen in an alphabet vary widely with the alphabet under consideration, so any generic algorithm would need to account for this variability. An algorithm could be derived from the bounding-box idea described above, though heuristic workarounds would be necessary for some alphabets. If the algorithm is processing a language where there are no marks under the baseline, English for example, it would never need to consider character bases above the mark. However, for a language such as Hebrew, bases both above and below the mark are candidates.

```
int x_arr[IMAGE_HEIGHT];
// y increases downward, the origin is at the top-left
int cur_y = 1;
//starting x-value is the middle of the glyph
x_arr[0] = IMAGE_WIDTH / 2;
while (cur_y < IMAGE_HEIGHT)  {
  if (GetPixel(x_arr[cur_y], cur_y + 1) == White)
  {  // down
    x_arr[cur_y + 1] = x_arr[cur_y];
    cur_y = cur_y + 1;
    MarkPixel(x_arr[cur_y], cur_y);
  }
  else if (GetPixel(x_arr[cur_y] + 1, cur_y + 1) == White)
  {  // down right
    x_arr[cur_y + 1] = x_arr[cur_y] + 1;
    cur_y = cur_y + 1;
    MarkPixel(x_arr[cur_y], cur_y);
  }
  else if (GetPixel(x_arr[cur_y] - 1, cur_y + 1) == White)
  {  // down left
    x_arr[cur_y + 1] = x_arr[cur_y] - 1;
    cur_y = cur_y + 1;
    MarkPixel(x_arr[cur_y], cur_y);
  }
  else if (GetPixel(x_arr[cur_y] + 1, cur_y) == White)
  {  // right
    x_arr[cur_y] = x_arr[cur_y] + 1;
    MarkPixel(x_arr[cur_y], cur_y);
  }
  else if (GetPixel(x_arr[cur_y] - 1, cur_y) == White)
  {  // left
    x_arr[cur_y] = x_arr[cur_y] - 1;
    MarkPixel(x_arr[cur_y], cur_y);
  }
  else if (cur_y == 0)
  {  // no path, stop
    return;
  }
  // we have checked the right path
  // so we reset so to check the left path
  else if (GetPixel(x_arr[cur_y - 1] - 1, cur_y - 1) == White)
  {
    x_arr[cur_y] = x_arr[cur_y - 1];
  }
  else
  {  // backtrack
    cur_y = cur_y - 1;
  }
}
```

Figure 2.18: PathFind pseudo code.

Character ligatures

1. The best-fit bounding box is the only method in the surveyed literature for determining where to separate characters connected via ligatures [28]. See Figure 2.16 on page 17 for an example.

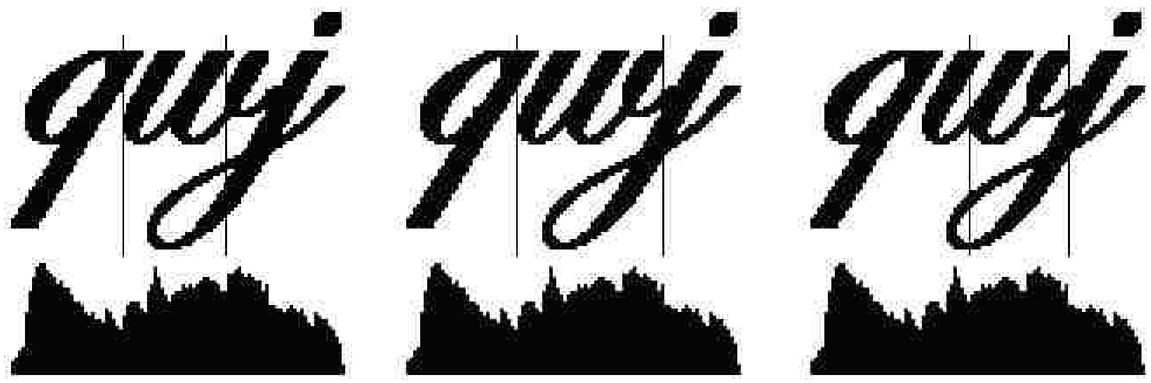

Figure 2.19: Possible vertical boundary borders of a best-fit bounding box.

2. An alternative method is to calculate the vertical pixel density of the text line and then create a set of best-fit bounding boxes. Each member of the set corresponds to a bounding box with borders that fall in the valleys for the vertical density graph, as in Figure 2.19. Each set of borders is processed as a best-fit bounding box (with noise reduction, partial character removal, etc.) and the boxes that are found to contain valid characters are kept. This method is not mentioned in the literature.

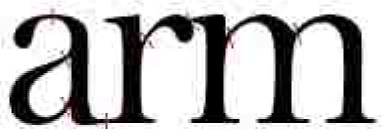

Figure 2.20: Several potential chop points that the Tesseract OCR engine might use to overcome ligatures. Figure recreated from Smith [53].

3. A method suggested by the Tesseract OCR engine is to determine "chop points" or thin points on a glyph. The glyphs are then separated at the chop points and recognition is attempted on the pieces [53].

Complex page layout

1. The **x-y cut segmentation** algorithm uses recursion to construct a tree-based representation of the document, with the root as the whole document and each leaf comprising a single section of similar content (text, graphics, etc.) from the image. First, the algorithm computes the horizontal and vertical projection profile (see Figure 2.6 on page 11) of the document and splits it into two or more segments based on the valleys in the density graphs. In Figure 2.21, the vertical density graph shows two potential split points corresponding to the white space between the columns, and the horizontal density graph

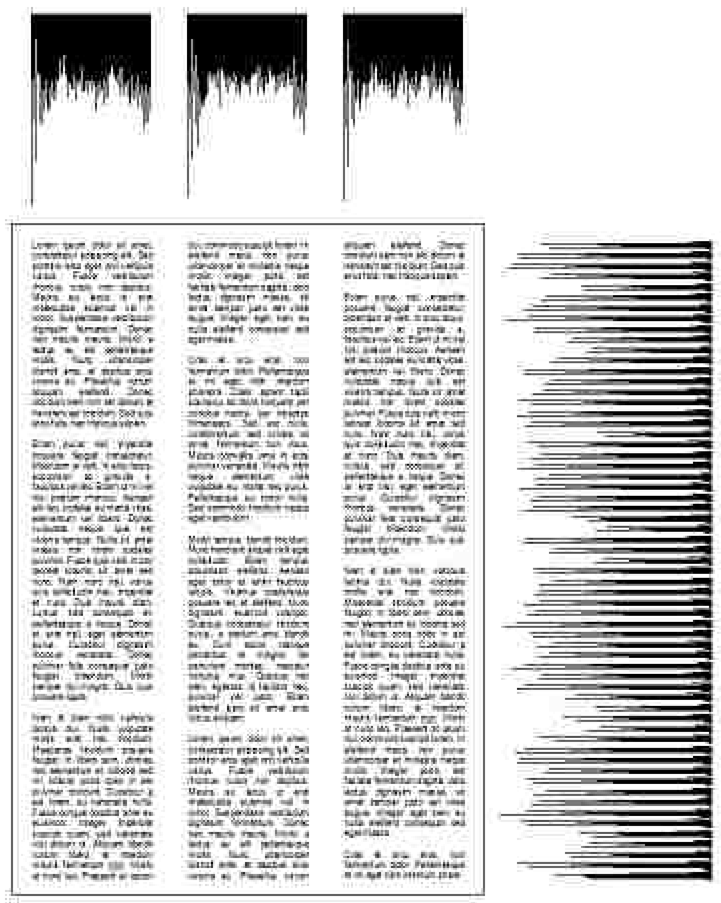

Figure 2.21: A complex page layout with horizontal and vertical projection graphs. Valleys in the graphs show potential split points.

shows many potential split points, one between each line. Once split, these segments are connected as children to the root node. Then, for each newly created child, the process recurses. When no more splits can be made, the algorithm is finished [13, 47].

Singh et al. [49] implemented a version of the x-y cut algorithm for segmenting Devanagari text lines and words. The paper did not provide a clear explanation of their implementation, but, according to their results, the authors saw a 20× to 30× speedup over serial methods.

2. The **smearing** algorithm operates horizontally or vertically on binary images by "smearing" the black pixels across white space if the number of consecutive white pixels falls below some threshold. This algorithm has the effect of connecting neighboring black areas that are separated by less than a threshold value. Connected-component analysis connects the smeared pixel groups to form segments, and the set of segments comprises the page layout. Typically, horizontal smearing works best for alphabets written horizontally, such as English [47]. See Figure 2.22.

3. **White-space analysis** finds a set of maximal rectangles whose union is the complete background. The rectangles are sorted according to their height-to-width ratios, with

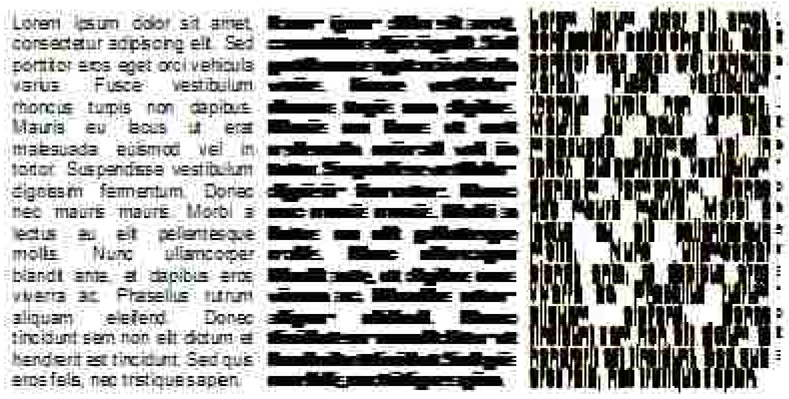

Figure 2.22: (a) the original paragraph, (b) and (c) horizontal and vertical smearing, respectively, using a 6 pixel threshold.

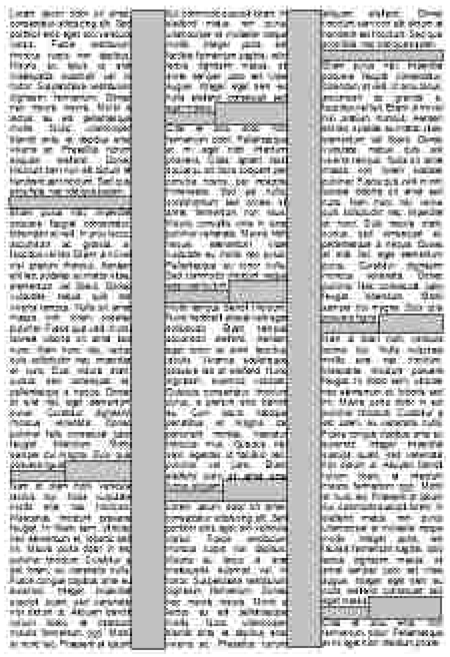

Figure 2.23: White-space analysis finds set of rectangles that comprise white space within the document. The gray rectangles indicate white space.

an additional weight assigned to tall and wide blocks, since these blocks typically represent breaks between text blocks. Figure 2.23 depicts “tall” blocks between columns and “wide” blocks between paragraphs. The blocks left uncovered are the text-block segments [47].

4. The **Docstrum algorithm** is based on nearest-neighborhood clustering of connected components. The algorithm partitions the connected components into two groups, one with characters of the dominant font size, and one with the remaining characters. For each component, the algorithm identifies *k* nearest neighbors and calculates the distance and angle to each neighbor. The neighbors with the shortest distance and smallest angles are considered to be on the same line. The whole text line is determined by combining the series of these within-line pairings. The final text block segmentation is formed by merging text lines based on location, similar rotation angles and line lengths [47].

5. The **area Voronoi diagram** method is based on the concept of Voronoi diagrams. In the simplest case, a Voronoi diagram on an x-y plane consists of a set of regions, each containing a center point and a set of points such that the distance from each point to the center point is less than the distance from that point to any other center point. The simplest measure is Euclidean distance, but other measures can be used. See Figure 2.24. The algorithm creates Voronoi regions around each character glyph. The algorithm removes boundaries between regions that are below a minimum distance from each other. It also removes boundaries between regions whose area is similar in order to cover cases where images contain graphics and figures. The underlying idea is that, for any individual character, the area of the Voronoi region is roughly the same, whereas the area for a graphic or figure is much larger [23].

There is no clear choice for the best page-segmentation algorithm; each has merits under certain document conditions. To summarize the results of the performance evaluation by Shafait et al. [47]: the x-y cut algorithm is best for clean documents with little to no rotation; the Docstrum and Voronoi algorithms are appropriate for homogeneous documents that contain similar font sizes and styles; white-space analysis works well on documents containing many font sizes and styles; and the Voronoi method excels at segmenting page layouts with text oriented in different fashions [47].

Multiple colors

I was unable to locate any papers describing methods to handle multiple-colored documents, though one can hypothesize ways to remove solid-color backgrounds and deal with different-colored foregrounds. One naïve method is to separate a full color image into 3 sub-images, each sub-image containing only the R, G or B color components. Convert these sub-images to grayscale, then process each of them as a normal grayscale image and combine the results.

Figure 2.25 contains an example of splitting the R, G and B components from a full-color image. The colors in the original image, Figure 2.25a, comprise the full list of colors created by using all combinations of the values 0, 64, 128, 192 and 255 for each component.

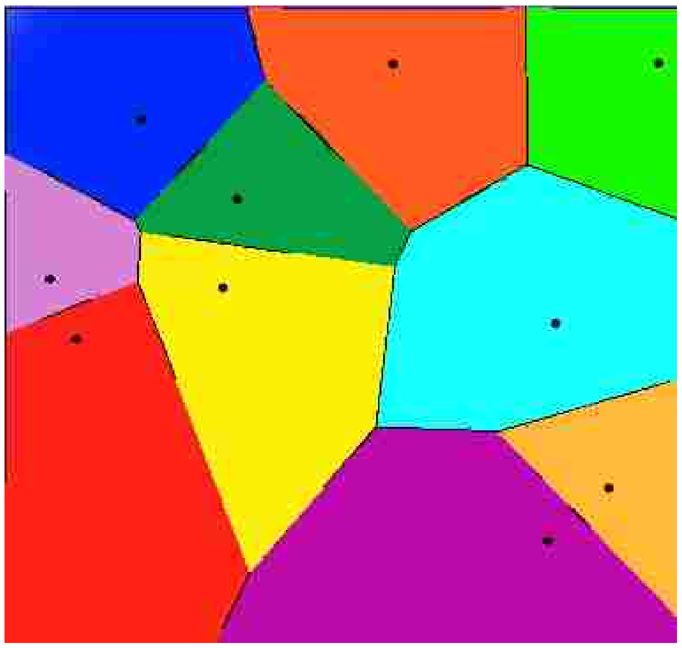
(a)

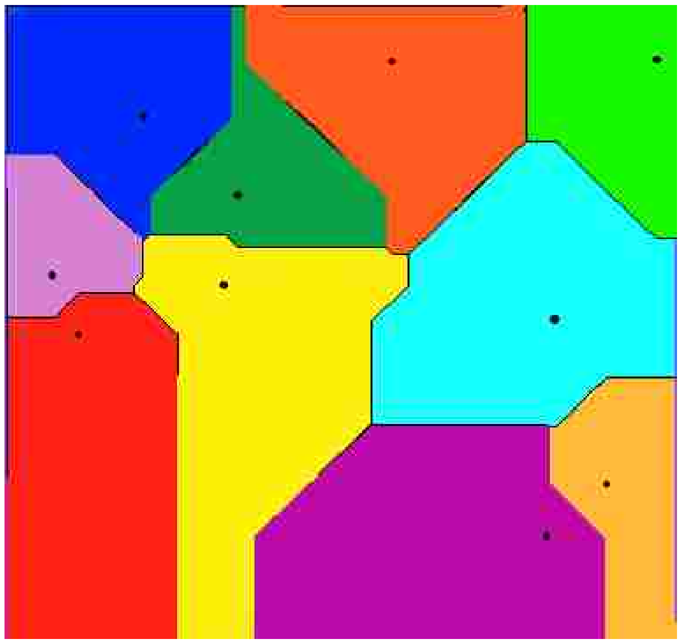
(b)

Figure 2.24: Voronoi diagrams, (a) pixel membership based on Euclidean distance, (b) pixel membership based on Manhattan (i.e. driving) distance
Images from `http://en.wikipedia.org/wiki/Voronoi_diagram`

The text color is the **negative color** of the background. The components of the negative color are calculated as 255 − *original_component*.

For each component image, the algorithm performs adaptive thresholding to convert the grayscale image to monochrome. To determine which pixels are the "text pixels", it might analyze the histogram and look for the most common value (black or white) — presumably the background pixels comprise the majority of the image. For images such as those in 2.25, a new analysis method might be useful — **adaptive histogram analysis**[3]. This method constructs a histogram for a section of an image in order to perform analysis on that section. The analysis enables an application to adapt to multi-colored backgrounds and successfully separate the text.

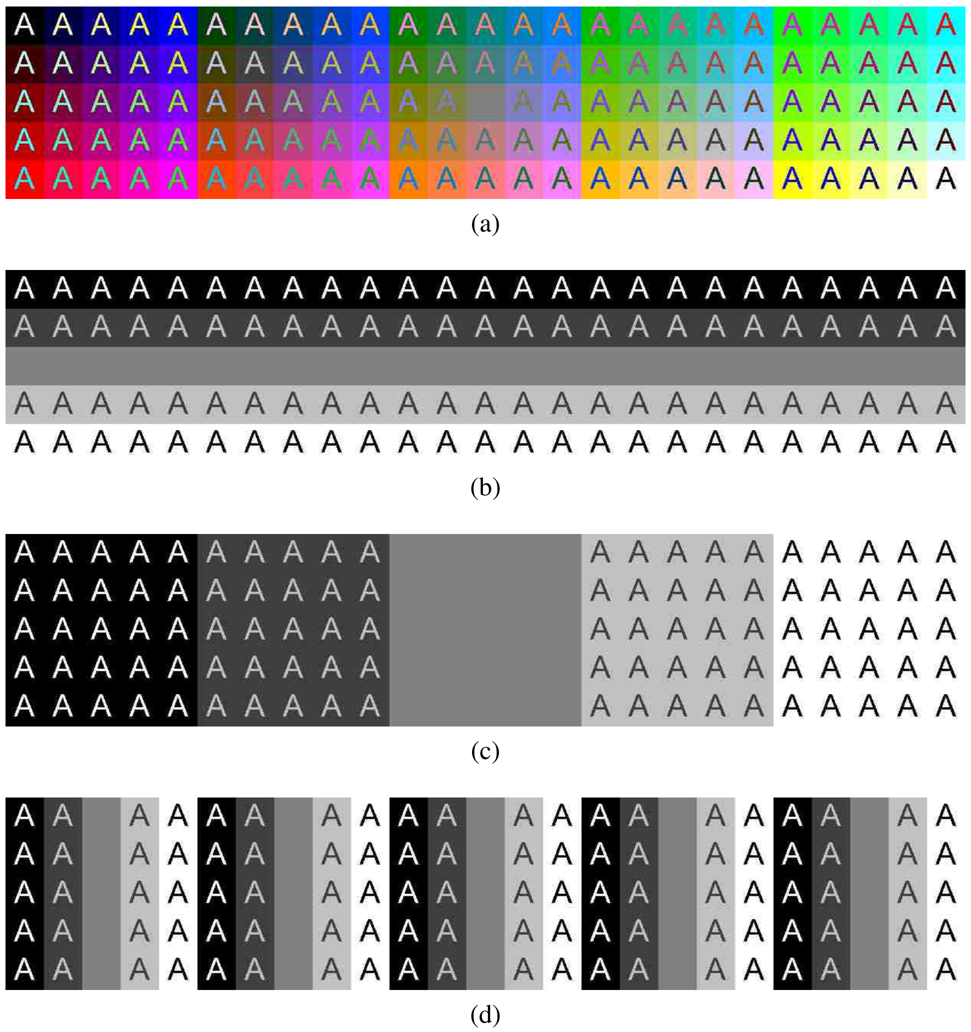

Figure 2.25: Multiple color image with negative color text and isolated color components, (a) the original image, (b) the R component, (c) the G component, (d) the B component.

[3]This method is similar to **adaptive histogram equalization**, which is a technique used to improve contrast in images and credited to Ketcham et al., Hummel and Pizer [20, 22, 38, 39]

2.7 Identification phase: Problems

The identification phase must account for deficiencies in the isolation phase. The problems this phase must overcome are partial letters, multiple font types and handwriting styles, character normalization, data extraction and the confusing character set.

Partial letters

Images scanned from books, handwritten documents or historical documents may contain partially erased, occluded or faded letters. These letters must be recognized in their partial state.

Multiple font types and handwriting styles

A **font** refers to the typeface of a particular set of characters. In machine-printed text and handwritten text, all the various styles and ways to write each character must be recognized as that specific character.

Character normalization

Often, recognition techniques require normalizing glyph image sizes to a standard image size in order to match training data. The normalization technique can alter the recognition rate of the normalized glyph because of differences in the way the technique handles thick fonts versus thin fonts or tall versus short fonts. Different sizes of fonts also tend to have different relative stroke thicknesses, but a normalized character glyph maintains its thickness ratio across scales [24].

Data extraction

The identification phase relies on extracting characteristic data from character glyphs that can then classify the glyph as a specific character. There are two main options for character data extraction: feature extraction and image transformation. **Feature extraction** techniques extract data directly from the glyph of a character. **Image transformation** techniques transform the glyph into another representation, such as a waveform, and then extract data from the transformed glyph.

The choice of features to extract or transformations to apply is crucial to OCR accuracy. If character data are poorly extracted, too similar or insufficient, the OCR application may misidentify the characters.

Confusing character set

The **confusing character set** contains those characters within a given alphabet and font that are commonly misrecognized by OCR techniques. For English, the confusing character set might contain: the uppercase ‘I’ and lowercase ‘l’ (lowercase ‘L’), the number ‘1’ and lowercase ‘l’, the uppercase ‘O’ and the number ‘0’ and the lowercase ‘e’ and lowercase ‘c’.

2.8 Identification Phase: Techniques and solutions

Partial Characters and Multiple Font/Handwriting Types

Skeletonization or “thinning” is a technique that captures the overall shape of a character by reducing each character stroke to one pixel wide. This process recreates the essence of the “human” capability to reduce a shape to its constituent parts and capture the overall shape. This method is able to handle multiple fonts and handwriting types since, theoretically, the algorithm removes the extra “noise” generated by different fonts and styles.

1. The generic process to skeletonize a character involves removing pixels from each side of a stroke until only one pixel remains. This process “thins” the character while retaining the overall shape [26]. The technique can be applied both horizontally and vertically. See Figure 2.26.

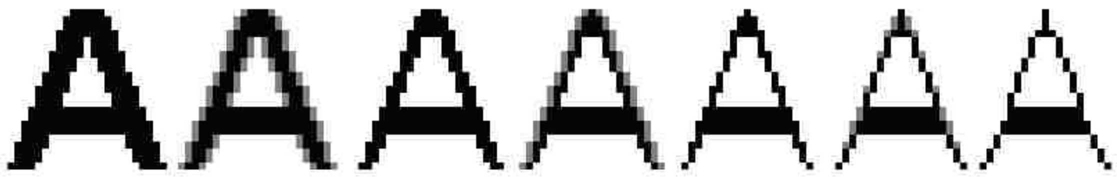
Figure 2.26: The letter ‘A’ undergoing horizontal skeletonization. The gray pixels indicate pixels selected for deletion.

2. Another method for skeletonization projects successively lower horizontal scanlines across a character and then groups the lines as splitting, merging or continuous (see Figure 2.27). A splitting line is a scanline that is split by white space, such as a line projected horizontally through the middle of an English ‘W’. A merging scanline is a line directly adjoining (above or below) a group of split lines, indicating the character is no longer split. All other lines are continuous. Adjoining lines of the same type are merged into blocks. The vertical and horizontal center, called the **centroid**, of each block serves as the representative of each block and acts an an endpoint for a **connection path** (see Figure 2.28). Centroids that lie on the same vertical or horizontal as another centroid are connected using a straight line; all others are connected using either a line with a single 90 degree turn or a line with a single 120 degree turn. The lines are chosen to fit within the blocks as much as possible while still connecting the centroids. The series of connected centroids is the skeleton of the original character [26]. See Figure 2.29.

The idea behind skeletonization is to reduce the character glyph to its underlying form such that multiple fonts reduce to the same structure. From the literature, the only algorithm that does this reduction reliably is the method of Lakshmi et al. [26]. Unfortunately, the computational complexity of this algorithm is quite large compared to other, less reliable algorithms. More research needs to be done on this topic.

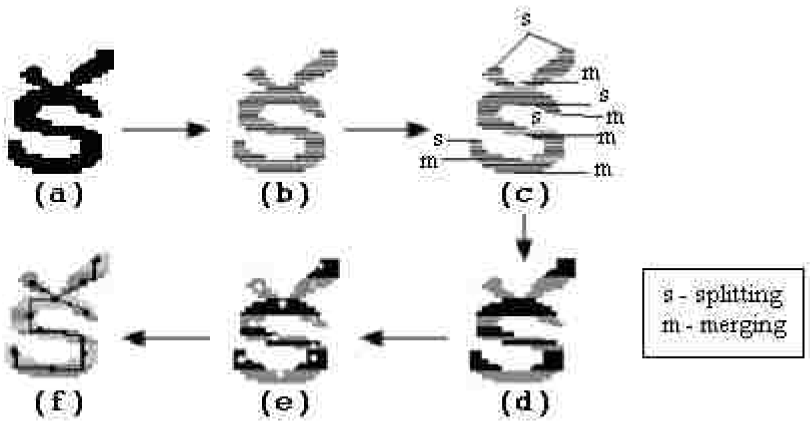

Figure 2.27: (a) the original character (b) horizontal runs (c) runs marked as splitting or merging; unmarked runs are continuous (d) blocks (e) centroid computation (f) connected centroids. Figure recreated from Lakshmi et al. [26].

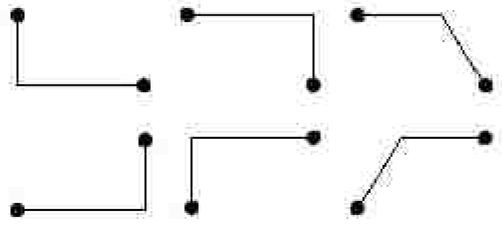

Figure 2.28: Allowed connection paths. The sizes are not relative. Figure recreated from Lakshmi et al. [26].

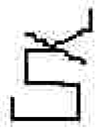

Figure 2.29: The calculated skeleton.

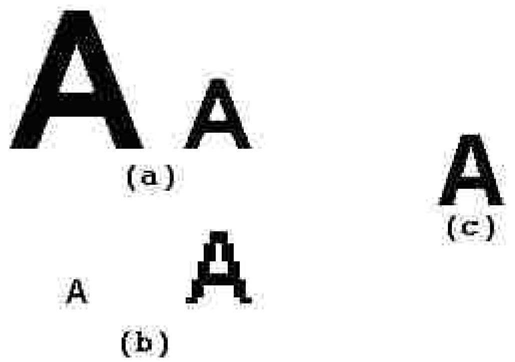

Figure 2.30: (a) a 72pt character scaled down to 36pt. (b) a 12pt character scaled up to 36pt. (c) an original 36pt character.

Character normalization

1. A simple method for character normalization is to scale the character based on the size of the bounding box. Scaling a small font up does not perform as well as scaling a large font down, due to missing pixel data (see Figure 2.30).

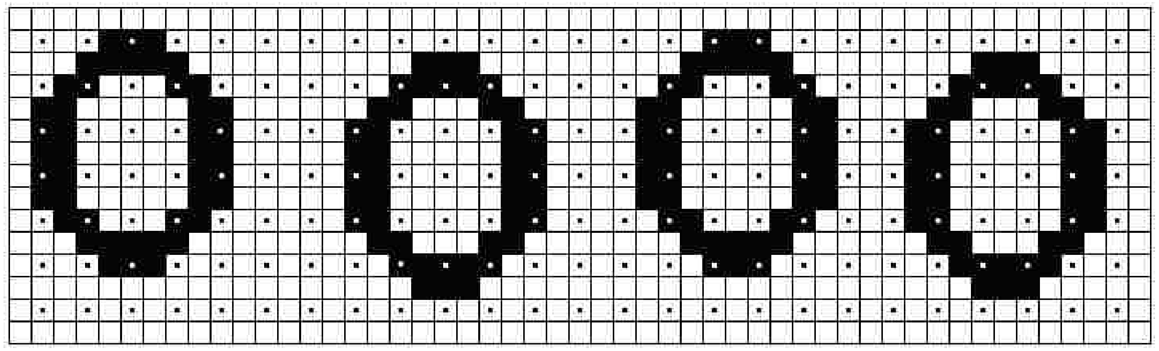

(a)

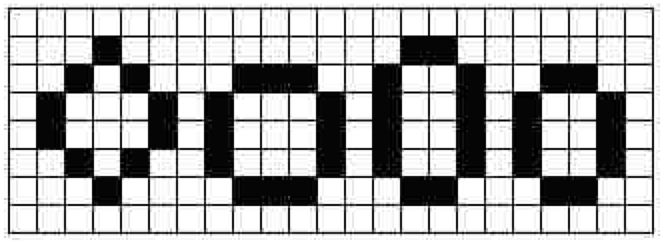

(b)

Figure 2.31: The black and white dots show the sampling positions. (a) the original characters with various orientations within the image. (b) the resultant scaled-down characters. Figure recreated from Barrera et al. [6].

a) **Sampling** is a down-scaling method that relies on sampling pixels in the horizontal and vertical directions at a rate defined by the **step**. For example, a step of 2 means that every second pixel is included in the sample, whereas a step of 3 means every third pixel is included. Each sampled pixel is included to construct the final, scaled down image. Depending on the position of a character at the start of the sampling process, this method may result in varying shapes (see Figure 2.31).

b) **Anchoring** is a variation of the sampling method that computes an anchor point for each character before sampling. The anchor point is the center of the bounding box that contains the character and serves as the starting point for the sampling process. By determining a standard starting point, the anchoring method results in more consistent shapes [6].

Data extraction

There are many techniques for extracting features from character images. Successful OCR applications combine a number of the following techniques. Rather than list them all, I present a classification[4] of the techniques and provide several examples under each heading.

Feature extraction: Templating

Templating algorithms construct a representation of each known character, called a template, and then match those templates against unknown symbols to identify them.

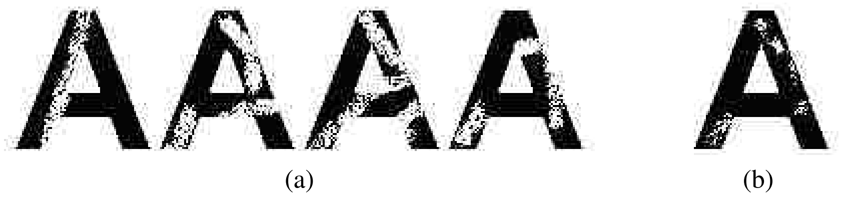

Figure 2.32: (a) the original degraded characters; (b) the combined "stamp".

1. **Edge filtering** is a templating method that provides a measure against which unknown characters can be compared. This method requires a "stamp" to serve as the idealized form of each character (see Figure 2.32). Stamp creation consists of examining multiple instances of "normal" and "degraded" characters and combining the common pixels into the stamp, discarding the rest. The selection and identification of characters that comprise the stamp is often done manually. The stamp is then matched and aligned against unknown characters and is identified based on the total overlapping area (i.e. in a bi-tonal image, the overlapping black pixels) the unknown character shares with the template. The stamp and unknown character are aligned based on an **anchor point**, typically the center of the image. The more the unknown character overlaps with the stamp, the more likely the stamp and the unknown character represent the same character [6]. Because the calculation of the anchor point might be incorrect, this method does not work very well on severely degraded characters.

2. Another method of templating by Bar-Yosef et al. [5], generally used for recognizing severely degraded historical documents, requires "shape models". The first step is to create multiple "shape priors". Each shape prior is analogous to a "stamp" from the previous technique. Because the character base can be so severely degraded that no single image contains the full character, the algorithm creates multiple shape priors. This method ensures that each portion of the character base is captured in at least one shape prior. The set of shape priors represent the character base as a whole [5].

   All shape priors are compared against one another and aligned based on the maximum normalized cross-correlation of the two images. The normalized cross-correlation method maximizes the alignment of the borders within each image to ensure the greatest amount of overlap between the two shape priors (see Figure 2.33).

   The algorithm creates a confidence map for each aligned pair of shape priors by weighting pixels included in both shape priors more heavily than those pixels only included

[4]I adopt the classification from the introduction of Shanthi et al. [48].

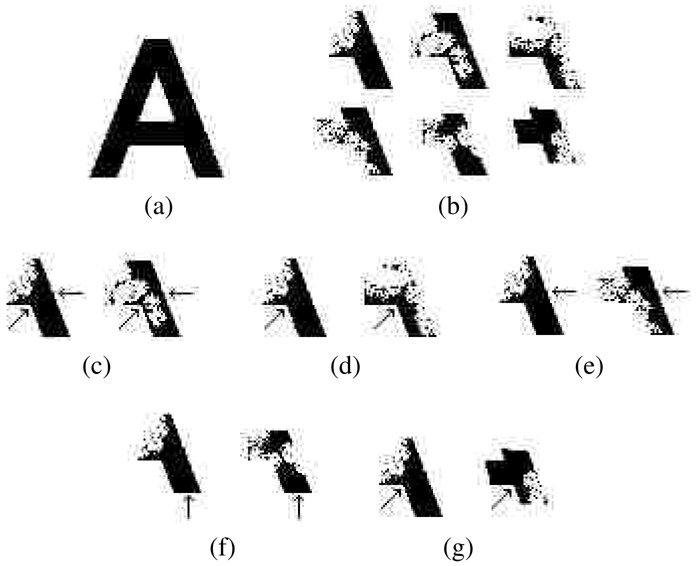
Figure 2.33: (a) the original character (b) a set of shape priors (c) – (g) shape prior border alignment; the arrow depicts the most likely border for alignment. The image degradation is intentional.

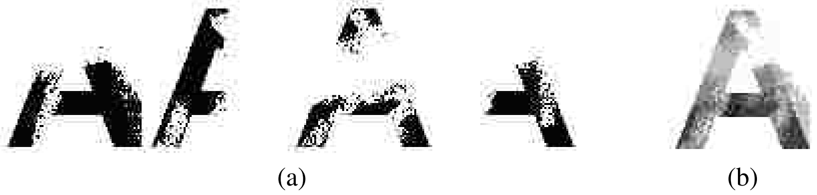
Figure 2.34: (a) shape priors and (b) the confidence map. Darker pixels are more likely to appear and are weighted more heavily during comparisons with unknown characters.

in one (see Figure 2.34). Then, for each pixel within each confidence map, the final confidence value for that pixel is the average value from all the confidence maps. The combined map of these averaged confidence values is the shape model.

The algorithm then compares the shape model against unknown character images by maximizing border alignment and calculates a confidence value. The higher the confidence value, the more likely the shape model and unknown character represent the same character [5].

The stamp model by Barrera et al. [6] has significant problems that prevent inclusion in a practical OCR engine. First, the technique relies on computing an “anchor” point — a single pixel upon which both the unknown glyph and the stamp can be aligned. This reliance is a problem because the location of this point can vary based on the width and height of the unknown glyph; severely degraded characters or very noisy edges skew the calculation and subsequent alignment. Second, there is no way to choose one stamp from the set of stamps. This selection problem, essentially, is the recognition problem; if the authors could reliably choose the correct stamp, then the glyph would already be known and no further processing would be necessary. The method by Bar-Yosef et al. [5] solves these problems. This method has a built-in alignment technique that far outperforms the simple notion of anchoring each image at its center and, rather than a single stamp, the algorithm the authors describe creates multiple stamps for the recognition phase. Further, since most of the computation occurs during training to build the shape models, the computational complexity of the recognition step is still comparable to the Barrera method.

Feature extraction: Spatial techniques

Spatial techniques rely on the pixel-based-representation of a glyph and generally rely on tallying or grouping pixels.

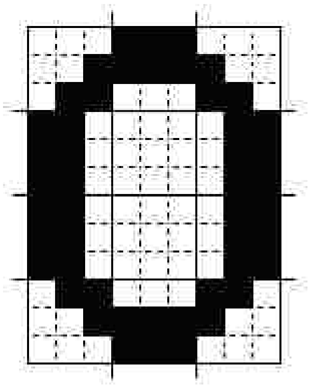

Figure 2.35: A character glyph segmented into 3×3 pixel segments.

1. The **grid-and-count** method partitions a character image into individual segments, where each segment covers roughly the same total area in the image, and then counts the black pixels in those segments. The resultant counts can be converted to a vector and used in a nearest neighbor search or in some other classifier in order to identify the glyph [7, 13]. A similar method is called **grid-and-chain**, which is the same as the previous technique, except, instead of counting the pixels in each segment, the segments are converted into chain codes [7].

2. Another method, **longest run**, projects scanlines across the character image and counts the intersections to find the longest horizontal and vertical lines within a character image. The lengths are usually used as supplemental information to another spatial extraction technique, such as grid-and-count. Stand-alone variations of this algorithm keep multiple values representing the longest horizontal and vertical lines to use in analysis. Other variants count the pixel intersections along predetermined scanline paths, such as horizontal and vertical lines through the center of the bounding box, and use these values to classify the glyph [7]. See Figure 2.36.

3. The **pattern-count** method projects an arbitrary shape on the character image at various offsets and counts the black pixels that intersect the shape [7]. Similar to the grid-and-count method, each time the pattern is overlayed on the character image, the algorithm

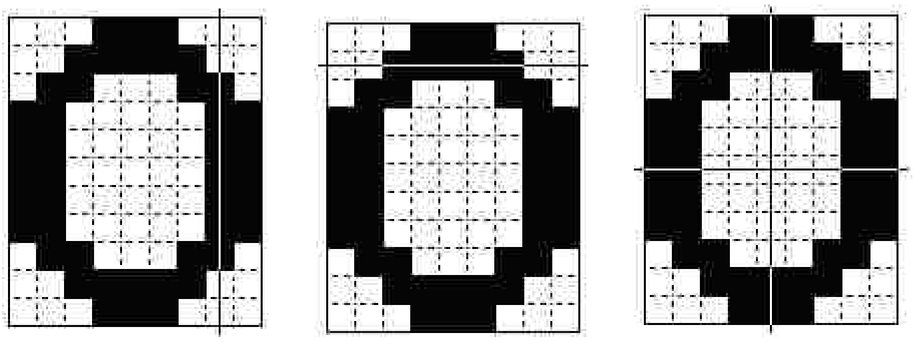
(a) (b) (c)

Figure 2.36: (a) vertical longest run (b) horizontal longest run (c) vertical and horizontal pixel intersections through the center of the bounding box.

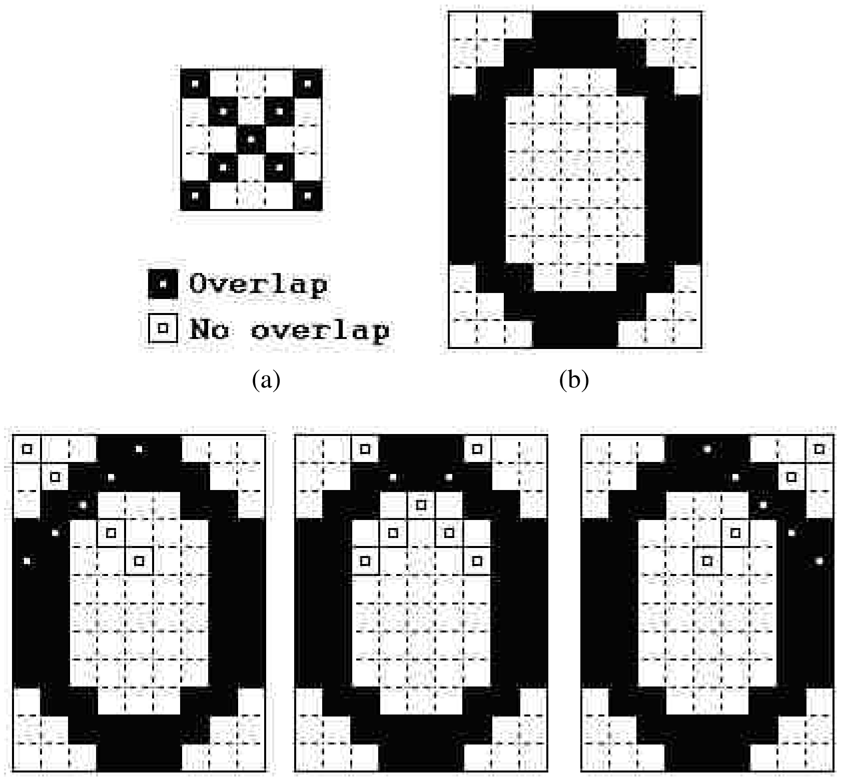

(a) (b)

(c)

Figure 2.37: (a) the pattern and legend (b) original character (c) the pattern applied across the original character image at three of the many possible positions.

counts the number of overlapping black pixels and uses these counts to identify the glyph. For example, the vector generated by the first three overlays (as seen in Figure 2.37c) of the pattern shown in 2.37a to the character shown in 2.37b is {5, 2, 5}. These values mean that the first overlay intersects 5 black pixels, the second intersects 2 pixels and the last intersects 5 pixels. This method is useful because different patterns can be implemented for different font sizes and styles, and the method works with non-rectilinear bounding boxes.

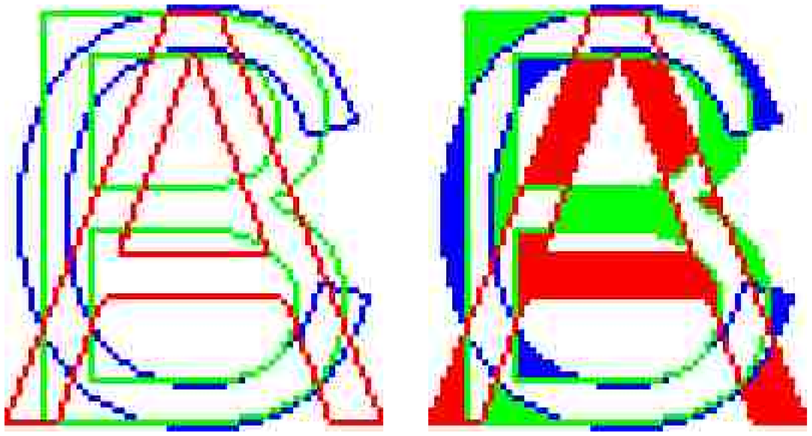

(a) (b)

Figure 2.38: (a) three 72pt Arial characters overlayed on one another (b) filled locations are unique to a single character.

I was unable to find any discussion on how to choose or design an appropriate pattern, though I have an idea about how I might create one. For a given font size and style F, a naïve approach creates a set of pixels P such that for each character in F, there exists at least one overlapping pixel in P. Further, we create P so that a non-empty subset of P uniquely identifies each character in F. For example, given the set of characters shown in Figure 2.38, we can choose three pixels (one for each character) such that each pixel both overlaps a character and uniquely identifies that character. The (x, y) coordinates of these pixels form a pattern appropriate for disambiguating one character from another.

There are many variations on spatial-feature extraction techniques. The methods mentioned are just the basic types. The grid-and-count method can be extended to be pie-shaped or have an arbitrary shape. The pattern-count method can be used with star-shaped patterns or patterns that are designed by a genetic algorithm to determine their accuracy. There is much room for research here. The best method is the one that best exploits the characteristics of the specific alphabet or font set undergoing recognition.

Feature extraction: Transformational techniques

Transformational techniques convert the character image from a pixel representation to another representation. Fourier and Wavelet transforms are examples of this type of technique [48].

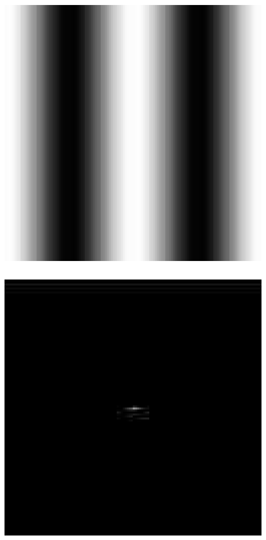
(a) 2Hz vertical sine wave

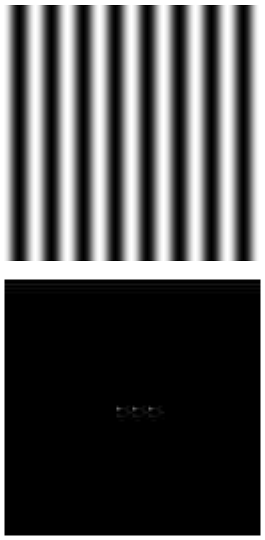
(b) 8Hz vertical sine wave

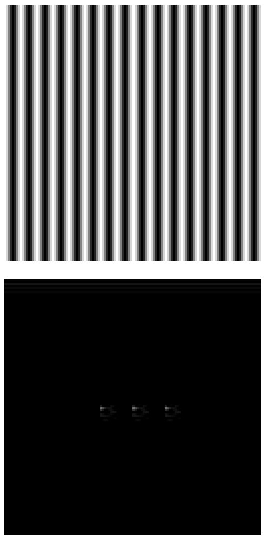
(c) 16Hz vertical sine wave

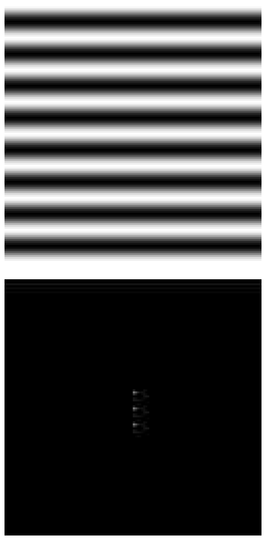
(d) 8Hz horizontal sine wave

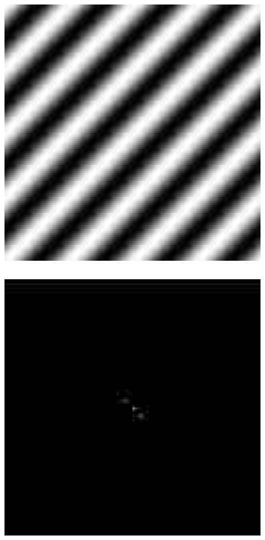
(e) 4Hz diagonal sine wave

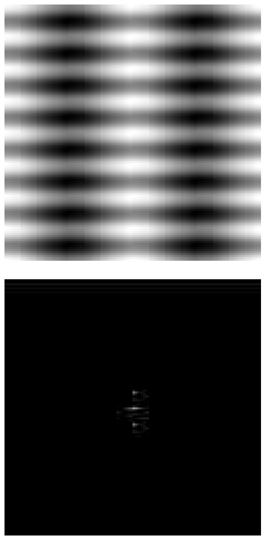
(f) 2Hz vertical sine wave plus an 8Hz horizontal sine wave

Figure 2.39: Fourier transform of sinusoidal brightness images.

1. The **Fourier transform** is generally used to analyze a closed planar curve. Since each boundary on a character is a closed curve, the sequence of (x, y) coordinates that specifies the curve is periodic, which makes conversion and analysis with a Fourier transform possible [28, 30]. The **discrete cosine transform** is a variation of the Fourier transform.

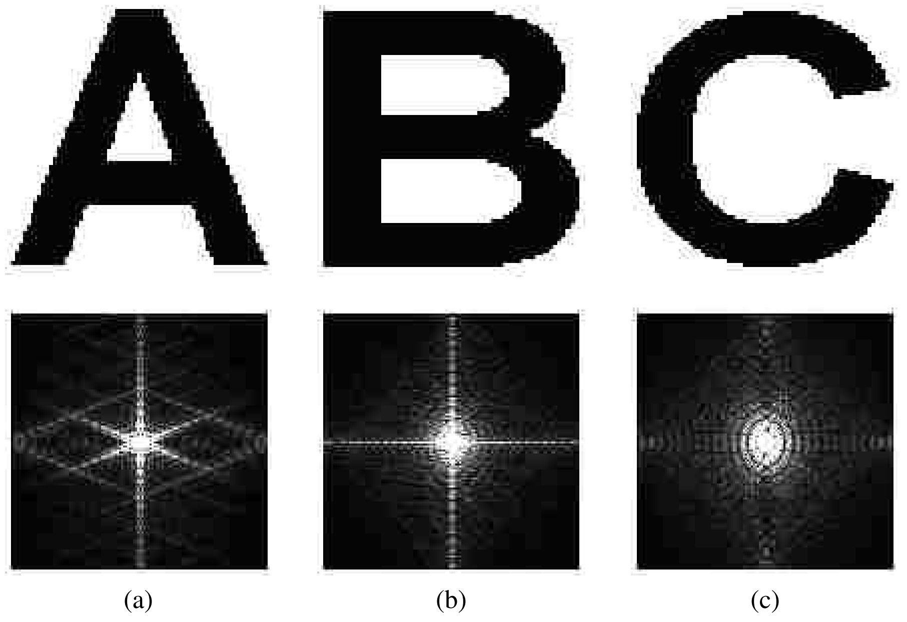

Figure 2.40: Fourier transform of 3 character images.

The idea behind the Fourier transform is that any signal can be expressed as a sum of a series of sine waves. In the case of images, the transform captures variations in brightness across the image. Each wave, or sinusoid, in the series comprising the original image is encoded in the output image of the transform by plotting the phase, the frequency and the magnitude of the wave (the three variables necessary to describe a sinusoid). Figure 2.39 on page 35 shows a series of brightness images corresponding to various sine waves and their resultant Fourier transforms.

2. The main difference between a **wavelet transform** and a Fourier transform is the **basis function** upon which the transforms rely. Whereas Fourier transforms are limited to the sine and cosine basis functions, the wavelet transform has no such limitation. The absence of this limitation means that wavelet transforms can (and do) utilize wave functions that have a defined beginning and end — that is, they are **localized in space**. Wave functions that are localized in space are referred to as **wavelets** and is where the transform gets its name [17]. See Figure 2.41.

   To help clarify, I present an example using one of the basic wavelet basis functions, called the Haar wavelet (see Figure 2.42). Suppose we are given an array of pixels, representing a 1-d image:

$$[12, 4, 6, 10, 9, 2, 5, 7]$$

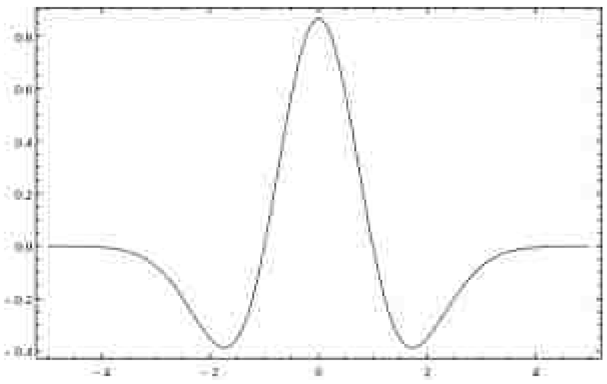
(a) Mexican Hat

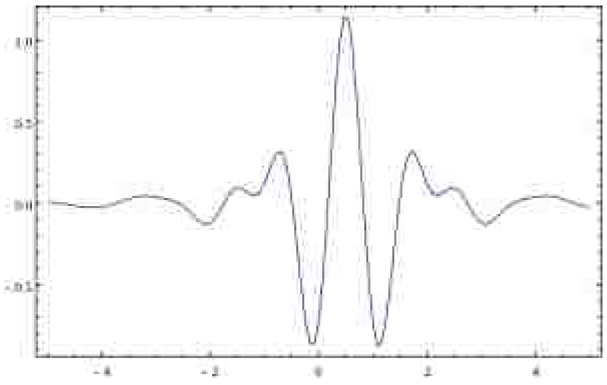
(b) Meyer

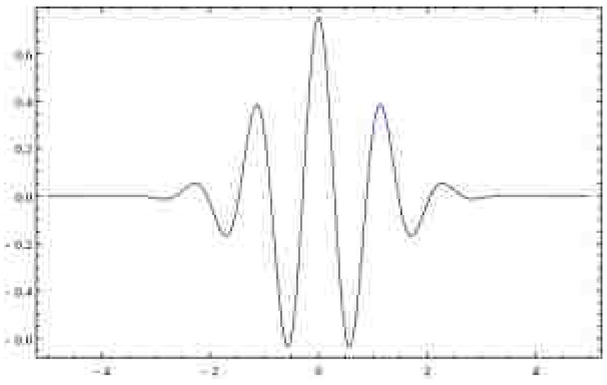
(c) Morlet

Figure 2.41: Several examples of wavelet basis functions.
Images from `http://en.wikipedia.org/wiki/Wavelet`

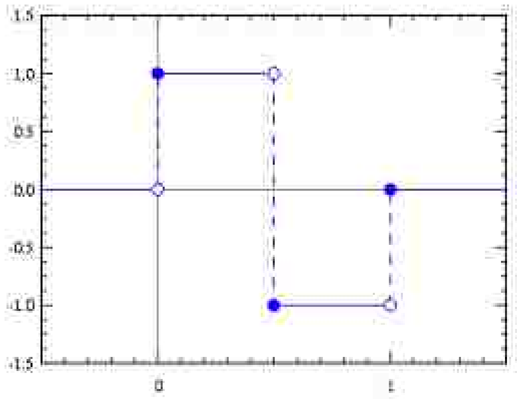

Figure 2.42: The Haar wavelet.
Image from `http://en.wikipedia.org/wiki/Haar_wavelet`

The Haar transform averages each pair of values (these are called **data coefficients**):

$$[12, 4, 6, 10, 9, 2, 5, 7] \rightarrow [8, 8, 5.5, 6]$$

It then finds the difference between the maximum value in each original pair and its average (these are called **detail coefficients**):

$$[8, 8, 5.5, 6] \rightarrow [4, 2, 3.5, 1]$$

These two sets form the entire first run of the transform, which looks like:

$$[12, 4, 6, 10, 9, 2, 5, 7] \rightarrow [8, 8, 5.5, 6, 4, 2, 3.5, 1]$$

The previous steps comprise one run of the Haar transform. Additional runs operate recursively on the set of averages from the previous step. The detail coefficients do not change and are copied through each run. When there is only one average left, no more transforms can be computed. Thus, if the transform were to carry on for another run, the result would look like:

$$[8, 8, 5.5, 6, 4, 2, 3.5, 1] \rightarrow [8, 5.75, 0, .25, 4, 2, 3.5, 1]$$

To generalize this approach to a 2-d image, the standard method is to apply the transform to each pixel row of an image and then to each column [27, 54]. See Figure 2.43.

Feature extraction: Neural networks

A neural network does not explicitly extract features from a character image, rather, during training, the network adjusts the internal pathway weights and connections within its neural layers, indirectly molding itself to the features of a given pattern. This innate behavior of the neural network, in essence, makes it a feature extraction technique, though it cannot be easily classified as transformational or spatial. There are a myriad of ways to provide image data to a neural network.

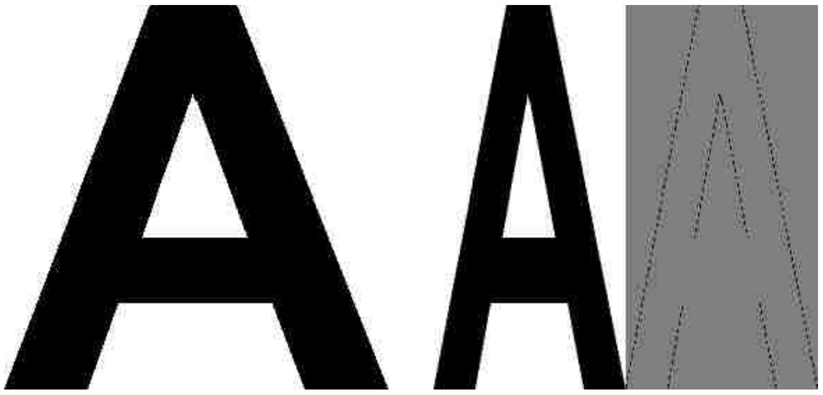
(a) The original image. (b) Haar transform applied to rows only.

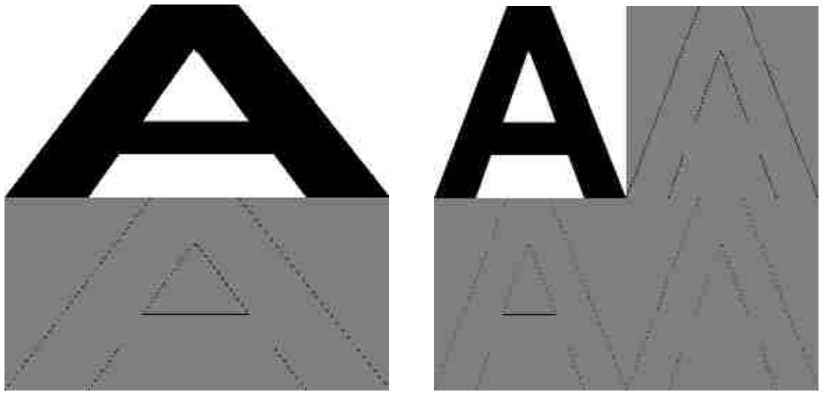
(c) Haar transform applied to columns only. (d) Transform applied to both rows and columns. The averages are a scaled down version of the original; the detail coefficients maintain detail.

Figure 2.43: The Haar transform in action.

1. One method is to normalize the character image to a standard size, then feed a 1 or 0 for each pixel, representing a black or white pixel respectively (grayscale may also work as a valued between 0 and 1), as input into the network. The output of the network identifies the character.
2. Alternatively, the output from any of the spatial feature extraction techniques described previously could also serve as input to the network.

Training data

Each of the identification methods discussed in this thesis relies on some sort of pre-existing knowledge base against which an algorithm can test unknowns. This knowledge base is called the **training data**. The construction of the training data is algorithm-specific and is usually a manual or semi-automated process. For example, building the training data for a 3×3 grid-and-count algorithm requires several steps:

1. Find appropriate "training" glyph images
2. Pair each glyph image with its correct classification
3. Process each glyph image and store the results; these results comprise the training data

Software can automate some of this process via embedding parts 2 and 3 in an interactive program (i.e the software presents the user with a glyph image and the user provides the classification). The software can also be configured to allow for manual correction of OCR output [13].

2.9 Post-processing phase: Problems

This phase typically also includes the use of language-specific dictionaries and grammar checks to help increase the overall accuracy of the OCR application.

Text reconstruction

During identification, the OCR application stores coordinates for each glyph (it can also store other data, such as a confidence value for its classification and less-likely alternatives). These coordinates correspond to the location of the glyph on the original image. During text reconstruction, the OCR application sorts the glyphs based on these coordinates and writes the characters to a text file. The difficulties lie in determining word boundaries and spacing. Complex formats, such as double/triple column layouts, are typically ignored in this stage and are not generally recreated.

Language-specific dictionaries and grammar checks

These post-processing techniques help increase the overall accuracy of the OCR application by validating the reconstructed text.

1. Dictionary validation can help determine if a word should be “the” or “thc” when the OCR engine could not.
2. If a word appears that is not in the dictionary and it contains a character from the confusing character set, other characters from the set can be substituted to see if the word becomes recognizable.
3. N-gram analysis provides another method to suggest possible corrections to a character with a low-confidence value or a misspelled word. **N-grams** are sets of consecutive items found in text or speech such as syllables, letters or words. For OCR, n-grams are typically character sequences. A naïve use of this type of n-gram is to rank the character sequences from most commonly found in a language, such as English, to least commonly or never found in language. For example, the **bigram** "ou" is ranked higher, or is more common, than the bigram "zz". Then, for misspelled words, low ranking bigrams could be iteratively replaced with high ranking bigrams that contain one of

the original letters. The word can then be rechecked against the dictionary. I highly recommend Kukich [25] for a full discussion on automatic word correction.

2.10 Conclusion

This chapter has presented a survey of both the problems that OCR engines must overcome to recognize text and the techniques programmers and researchers implement to accomplish the feat. I chose the selected references because they fulfill one of three purposes: the reference provides a complete (or at least complete enough) description of the algorithm; the reference provides an accessible introduction to a topic, or the reference is the seminal paper on the topic. Additionally, I chose survey references over the original references because they provide insight in comparing the algorithms and context for implementation.

Chapter 3: Introduction to GPUs

3.1 Virtual and physical architecture

A GPU is a device, connected to a computer's CPU via a high-speed bus, that contains on-board memory and, on current NVIDIA hardware, up to ~3000 processing elements that operate under a single instruction, multiple thread (SIMT) architecture. SIMT is similar to the single instruction, multiple data (SIMD) architecture except that instructions are issued to groups of threads (analogous to CPU processes), called **warps**. Each warp contains 32 threads and is part of a **block**, which is, itself, part of a **grid**. The thread-warp-block-grid hierarchy comprises the **virtual architecture** for GPU programming. See Figure 3.1.

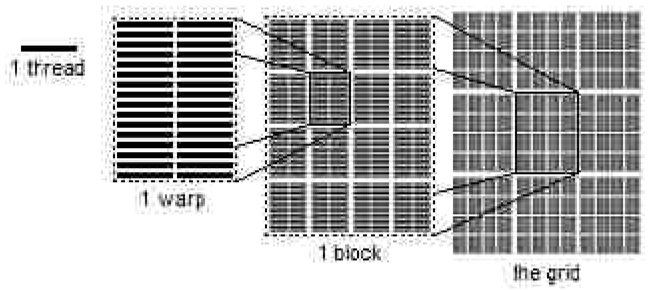

Figure 3.1: The thread-warp-block-grid hierarchy. From left to right: one thread, 32 threads inside a warp, which is inside a block of 16 warps, which is inside a grid of 9 blocks.

The **physical architecture** of a GPU is comprised of **streaming multiprocessors** (SM) and **cores**. A streaming multiprocessor is analogous to a CPU, and a core is analogous to a CPU core (as in a dual- or quad-core CPU).

3.2 Kernel execution

When a **kernel**, or function, executes on the GPU, the GPU assigns one or more blocks to an SM. The SM assigns each block to a core. On current hardware, a streaming multiprocessor may have up to 192 cores. Once assigned a block, a core partitions its block into warps and then schedules each warp for execution. When a warp executes, the core issues instructions to the warp as a whole, and each thread within the warp executes the instruction at the same time. If the threads within a warp diverge due to executing different paths of a branch (this is called **warp divergence**), threads not on the current path of execution are disabled. The core executes both paths of the branch serially until thread execution converges or execution ends. Thus, when within-warp branching occurs, execution speed is reduced. Different warps can execute different code paths without penalty. Each thread executes its own instance of the kernel. Each grid may only execute one kernel at a time.

3.3 Programming a GPU

A programmer has no direct control over how the GPU assigns blocks to cores. However, a programmer can indirectly influence block assignment by choosing the dimensions of the block and grid virtual constructs wisely. For example, given a GPU with 8 SMs, each with 8 cores, a programmer can allocate a grid of 64 total blocks where each block contains 64 threads. This design means there is a 1:1 ratio of blocks to cores, so the GPU schedules 1 block per core. Conversely, if the programmer allocates a grid of 32 blocks with 128 threads per block giving the same total number of threads as the previous grid, the GPU still schedules 1 block per core, but half the cores in the GPU go unused. Generally speaking, maximizing the **occupancy** of the GPU results in faster execution.

$$\text{occupancy} = \frac{number\ of\ active\ warps}{total\ number\ of\ warps\ the\ GPU\ can\ support}$$

A programmer codes a kernel in CUDA, a C programming language extension. OpenCL[1] is a viable alternative, but I do not discuss it here. CUDA provides several keywords, a few built-in variables and various functions that enable low-level access to the GPU. CUDA makes writing a GPU kernel very similar to writing a C program.

The code in Figure 3.2 on Page 44 illustrates a simple CUDA program. The keyword **`__global__`** signifies to the compiler that this function is a kernel. The predefined type **`dim3`** is a vector of three floats x, y and z. The predefined variables `blockIdx`, `blockDim` and `threadIdx` provide information about the current block ID, grid dimensions and current thread ID, respectively.

A block can be defined with up to three dimensions. For example, if a programmer desires a block size of 512 total threads, blocks of 512×1×1 threads, 16×32×1 threads or 8×8×8 threads are valid. The only difference among these definitions is how the GPU assigns thread IDs, which are exposed to the kernel by the predefined variable `threadIdx`.

For the first block definition, 512×1×1, the **`dim3`** vector `threadIdx` contains values such that $0 \leq threadIdx.x \leq 511$, $threadIdx.y = 0$ and $threadIdx.z = 0$. For the second definition, 16×32×1, `threadIdx` contains values such that $0 \leq threadIdx.x \leq 16$, $0 \leq threadIdx.y \leq 32$ and $threadIdx.z = 0$. For the last definition, 8×8×8, `threadIdx` contains values such that $0 \leq threadIdx.x \leq 8$, $0 \leq threadIdx.y \leq 8$ and $0 \leq threadIdx.z \leq 8$. The ability to arbitrarily define the dimensions allows a programmer to specify block sizes that result in thread IDs that map cleanly onto whatever data structure the kernel must manipulate.

A grid is defined in the same manner, and CUDA assigns block IDs in exactly the same way as for the threads. The block IDs are exposed by the **`dim3`** vector `blockIdx`, and the grid dimensions are exposed by the **`dim3`** vector `blockDim`. For example, for a grid of 8×8×8 blocks, the `blockDim` variable contains $(8, 8, 8)$.

The program in Figure 3.2 performs simple vector addition. It bases its calculation for the index i on the current block and thread IDs, which causes each thread to index a different part of each array. So, when each thread completes its single addition operation, the whole calculation is complete.

[1]The **Open Computing Language** (OpenCL) is an alternative to CUDA and is supported on a number of devices. More information can be found at `https://www.khronos.org/opencl`.

```
// define kernel
__global__ void VectorAdd(float* A, float* B, float* C, int N)
{
    int i = blockIdx.x * blockDim.x + threadIdx.x;
    if (i < N)
        C[i] = A[i] + B[i];
}

int main()
{
    // define N as total input size
    int N = ...;
    size_t size = N * sizeof(float);

    // allocate input vectors in host memory
    float* host_A = (float*)malloc(size);
    float* host_B = (float*)malloc(size);

    // initialize input vectors
    ...

    // allocate vectors in GPU memory
    float* GPU_A;
    cudaMalloc(&GPU_A, size);
    float* GPU_B;
    cudaMalloc(&GPU_B, size);
    float* GPU_C;
    cudaMalloc(&GPU_C, size);

    // copy vectors from host to GPU memory
    cudaMemcpy(GPU_A, host_A, size, cudaMemcpyHostToDevice);
    cudaMemcpy(GPU_B, host_B, size, cudaMemcpyHostToDevice);

    // execute kernel
    dim3 threadsPerBlock(256, 0, 0);
    dim3 numBlocks((N + threadsPerBlock.x - 1) / threadsPerBlock.x, 0, 0);
    VectorAdd<<<numBlocks, threadsPerBlock>>>(GPU_A, GPU_B, GPU_C, N);

    // copy results from GPU memory to host memory
    // GPU_C to host_C
    cudaMemcpy(host_C, GPU_C, size, cudaMemcpyDeviceToHost);

    // free GPU memory
    cudaFree(GPU_A);
    cudaFree(GPU_B);
    cudaFree(GPU_C);

    // free host memory, then manipulate the results
    ...
}
```

Figure 3.2: Example CUDA program modified from the NVIDIA CUDA C Programming Guide [34].

The `threadsPerBlock` and `numBlocks` variables define the grid size and shape for the kernel. Both blocks and grids can be arbitrarily sized (with some restriction). However, each GPU has limitations on the maximum number of threads in a block and the maximum number of blocks in a grid. Current GPU devices limit the size of a block to 1536 threads and a grid to $2^{31} - 1$ blocks.

Executing a kernel is the same as executing a function in C, except the dimensions of the virtual grid and block constructs are specified between "<<<" and ">>>" using a variable of type **`dim3`**, as shown in the example program in Figure 3.2.

3.4 GPU memory types

GPUs expose a variety of memory types with varying performance characteristics that a programmer must take into account when designing a program for GPU. This section gives a brief overview of the different types of GPU memory.

Register memory

Register memory is the fastest type of memory on a GPU. Variables declared in a kernel are generally stored in a register, and each thread has its own copy of these variables. However, the hardware limits each SM to 65,536 registers, and a single thread to 255 registers. If a kernel exceeds the hardware limit, the extra variables are stored in local memory. Additionally, occupancy may be reduced by kernels using a large number of registers. For example, if a kernel uses the maximum number of registers, a warp requires 8,160 registers, so that only 8 warps can be active at a time. Given 32 threads to a block, if the SM has more than 8 cores, then occupancy is reduced. Register memory accesses occur in less than one GPU clock cycle [10, 34].

Local memory

Local memory is the spill-over location for variables allocated in excess of hardware limitations for registers. Local memory is actually a part of the global memory.

Shared memory

Shared memory comprises 65,536 bytes per SM. Because the shared memory is "on-chip", it has much lower access latency than other types of memory, except register memory. Allocated shared memory is accessible by all threads in the same block and is often used for communicating between threads. When a block finishes executing, it releases its shared memory, which can then be re-allocated to other blocks. Like register memory, over-allocating shared memory reduces occupancy. Shared memory accesses occur in approximately 22 GPU clock cycles [10, 34].

Constant memory

Constant memory has global scope and is available to all threads within a grid. Constant memory shares the same performance characteristics as shared memory but is limited to

65,536 bytes [10, 34].

Texture memory

Texture memory is a read-only component of global memory accessed through dedicated hardware optimized for read operations exhibiting high 2D spatial locality (i.e. reading data elements close to one another). Texture memory is limited to the same size as global memory minus allocations for padding and texture alignment. Texture memory has global scope, is available to all threads within a grid and supports interpolated access [10, 34].

Global memory

Global memory is the largest, slowest type of memory on a GPU and is roughly 30× slower than shared memory. Global memory is available to all threads within a grid. Global memory accesses occur in approximately 600 GPU clock cycles [10, 34].

Why memory matters

The SegRec algorithm discussed in Chapter 4 is designed to process hundreds of page images concurrently. I tested SegRec Version 3 with 1000 8.5”×11” page images at 200 dpi with ~1500 characters per page. SegRec must store the images and the output data for ~1.5 million characters. There must also be memory for each thread to process the images. Memory allocation is critical for the speed of this algorithm.

Coalesced verses non-coalesced

GPU hardware tries to reduce memory reads and writes into as few transactions as possible. When a kernel takes advantage of this hardware characteristic by grouping reads or writes into consecutive memory locations, it is called a **coalesced read** or a **coalesced write**. Coalesced operations occur in the number of GPU clock cycles required for a single operation of the same type. **Non-coalesced** operations are handled serially, with each operation taking the full count of GPU clock cycles.

3.5 Programming hints

A programmer must observe several caveats when programming a GPU:

- On the device, each streaming multiprocessor (on current hardware) has up to 65,536 registers. All variables local to a kernel are stored in registers, which means these registers must be split among all active threads on a SM. If you want a high occupancy rate, the kernel must not contain a large number of local variables.

  Fortunately, the compiler for CUDA reports how many registers the kernel uses. This information allows the programmer to tweak the kernel in order to reduce the number of registers needed.

- GPU memory is persistent between kernel executions, so unused memory should be deallocated when the program no longer needs it. This persistence also means it is possible to feed the results (or original data) from one kernel into another without copying data between the host and the GPU.

- Copying data between the host and the GPU is typically the slowest step of a CUDA program. If possible, one should compress the data or avoid copying altogether by reusing earlier data.

- Registers are in short supply, but computation is cheap. Opt for recalculating over storing a temporary result.

- Define blocks in multiples of 32 threads; otherwise the GPU adds “inactive threads” to bring the block size up to the nearest multiple of 32, which can influence thread ids.

- Warp divergence increases the overall execution time of the kernel. Use **bit twiddling**[2] and **if-conversion** to avoid branching when applicable. See Appendix C on page 92 for more information.

- There is limited support for recursion in NVIDIA GPU hardware architectures $\geq$ *v*2.0. However, stack space is allocated per-thread and must be pre-allocated. Thus, memory allocation for recursive functions is difficult to predict and can be wasteful. Given that memory is extremely limited on GPUs, recursion is generally best avoided. **Dynamic Parallelism** (DP) is a viable alternative to recursion that is supported in NVIDIA GPU architectures $\geq$ *v*3.5. DP allows “parent” grids to spawn “child” grids without interacting with the host [34].

- There is no dynamic memory allocation within a kernel. A kernel cannot allocate additional space during execution. However, shared memory can be dynamically allocated when a kernel is first executed.

- Adding an “optimization” step that reduces occupancy may actually result in slower execution than the original algorithm.

3.6 Conclusion

This chapter has presented a brief introduction into the virtual and physical architecture of a graphical processing unit and the challenges in programming for such a device.

[2]Bit Twiddling Hacks: `http://graphics.stanford.edu/~seander/bithacks.html`

Chapter 4: The SegRec Algorithm

The purpose of the SegRec algorithm is to utilize GPU hardware in an effort to increase the overall speed of OCR image processing while maintaining similar accuracy ratings to existing OCR engines. In order to meet these goals, SegRec must be able to make good use of multiple threads of execution on a single scanned page, operate within the limited on-board memory, and not rely heavily on expensive, non-coalesced global memory reads/writes. The SegRec algorithm focuses on handling the isolation and identification phases. Future work will include handling the pre- and post-processing phases.

Each version of the SegRec algorithm operates on monochrome bitmap images. This image format requires 1 bit per pixel to store pixel data. The host program strips the image header, converts the raw byte data to a byte array and copies the data to the GPU. The origin of each page is the lower-left corner; X increases left to right and Y increases bottom to top. The pages themselves are stored in global memory, with each page occupying 475,200 bytes, or about 453MB total.

Upon completion, the host program copies the SegRec output from the GPU and generates an XML file that, for every glyph, contains the inferred character classification, the global density vector, and bounding box coordinates.

4.1 Version 1

I wrote the first version of SegRec as a proof of concept; it is severely limited in functionality and operates solely in GPU global memory. Version 1 requires that lines and characters be separated by white space and assumes that any marks that occur are vertically aligned to their bases.

The algorithm operates by finding the white space between lines, then between characters and, finally, by treating each glyph as a 5×5 grid to use in the grid-and-count feature-extraction method.

The first stage of the algorithm performs a horizontal pixel count on the image — counting the black pixels in each horizontal pixel row. It stores the values in an array indexed by the Y value of the line. The lines that have zero black pixels are comprised of only white space; these lines either come directly before or directly after a line. Thus, the first non-zero pixel count in ascending Y values indicates the bottom of a line and, afterwards, a zero value (assuming there are no marks outside of the bounding box for the line) indicates the top of the line. The top and bottom boundaries, along with the edge of the page, form a bounding box for the line. The output of this step is a list of bounding boxes corresponding to the lines of text in an image.

The next stage of the algorithm counts black pixels in each column within each line's bounding boxes. Version 1 stores the counts in an array indexed by the X value. As in the first stage, zero values indicate white space. Thus, starting at the left, a non-zero value indicates the left edge of a glyph, and the next zero value indicates the right edge of the glyph. The edge boundaries, combined with the top and bottom line boundaries,

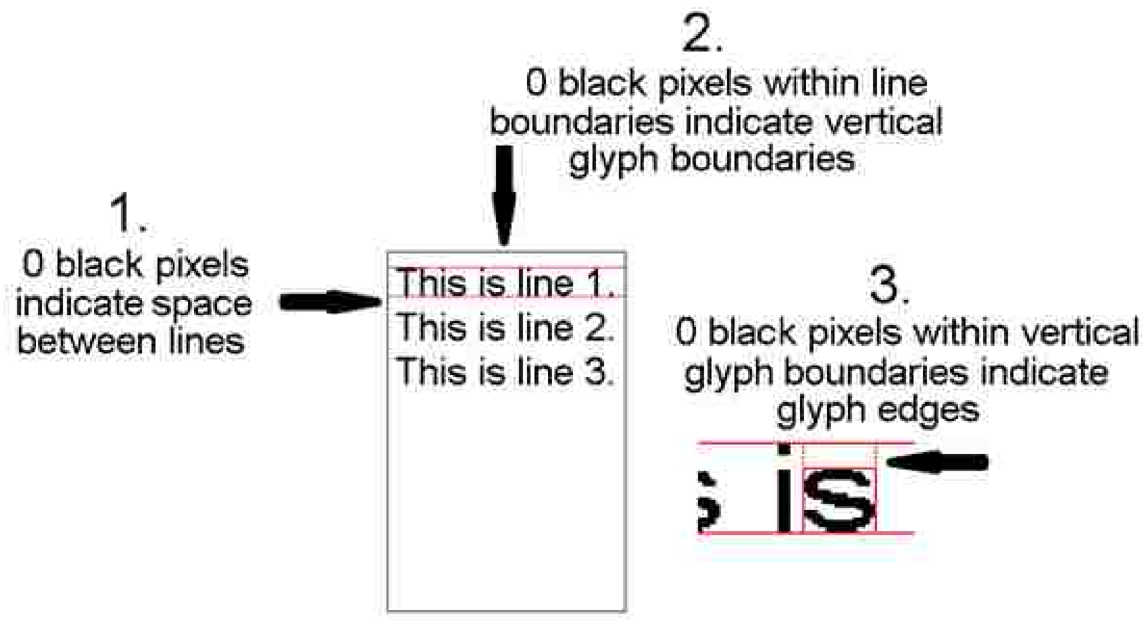
2.
0 black pixels within line boundaries indicate vertical glyph boundaries
1.
0 black pixels indicate space between lines
This is line 1.
This is line 2.
This is line 3.
3.
0 black pixels within vertical glyph boundaries indicate glyph edges
is

Figure 4.1: A graphical representation of Version 1 of the SegRec algorithm.

form a bounding box for the glyph. The output of this step is a list of bounding boxes corresponding to the glyphs in each line.

The next stage removes completely white rows from each bounding box, shrinking the box to be as compact as possible. This stage counts pixels on the rows within the glyph bounding box and removes rows with zero black pixels. The output of this step is a list of best-fit bounding boxes corresponding to the glyphs in each line.

In order to recognize each glyph, the next stage partitions each bounding box into a 5×5 grid, counts the number of black pixels in each region within the grid and computes a 25-dimensional vector containing the counts.

Figure 4.2 shows a 3×3 grid, but the idea is the same. Starting from the bottom-left, counting the black pixels in each region results in the following 9-dimensional vector:

$$(13, 1, 15, 7, 9, 11, 3, 18, 7)$$

By dividing each element of the vector by the total area of the glyph, the algorithm calculates the Global Density Vector (GDV) for the glyph:

$$(.034, .002, .039, .018, .024, .029, .008, .047, .018)$$

Version 1 finds the closest match in Euclidean 25-space for this GDV within the training data; the character associated with that match is the recognized character. The search is a brute-force comparison of the distance between the search vector against all the vectors in the training data. A more efficient method is the k-d tree nearest-neighbor search, but this search requires recursion, which has only limited support on GPUs [13].

The main flaw in this algorithm is that it can only operate on characters cleanly separated by white space. Due to the way the algorithm forms bounding boxes, at least one

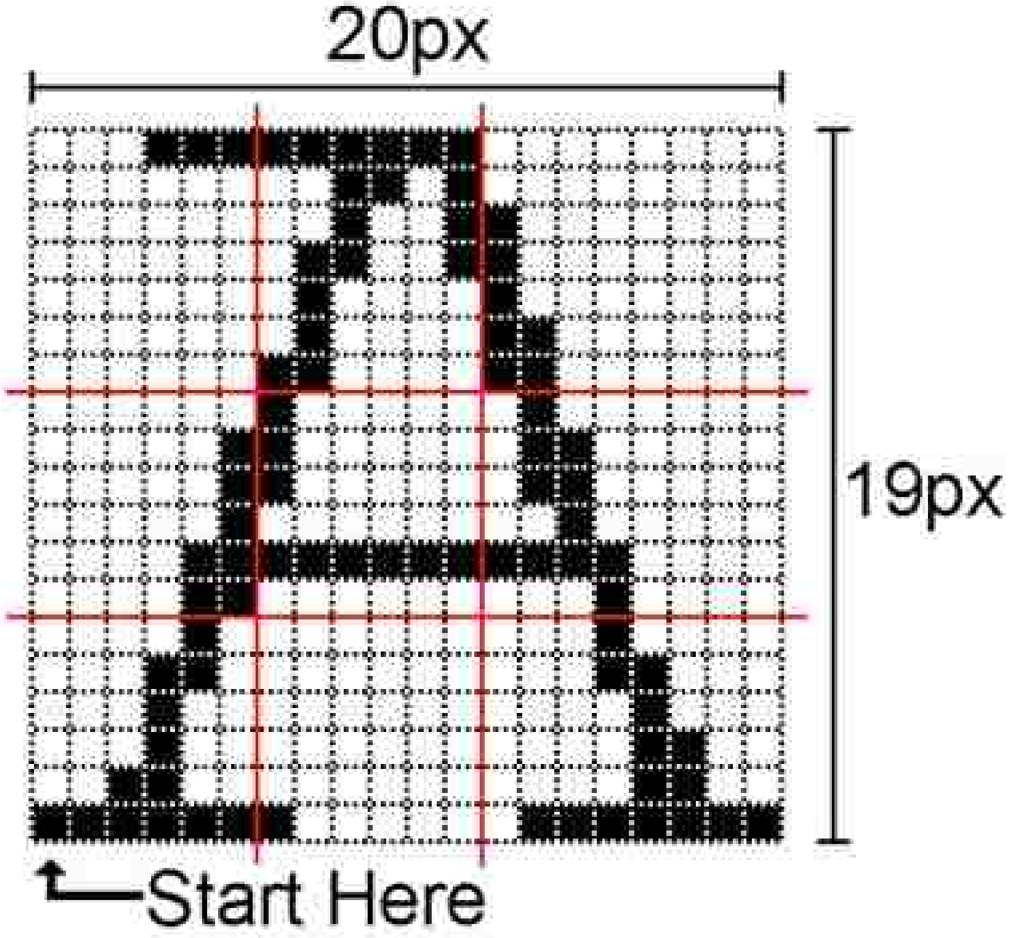

Figure 4.2: A glyph broken into a 3×3 grid

pixel of white space must surround each glyph for the algorithm to isolate it. This limitation means that the algorithm cannot handle kerning, character ligatures or fonts with characters that are too closely spaced.

There are also several minor flaws with the algorithm, such as not handling marks, not handling even simple pixel noise, and having no mechanism for handling rotation. However, these flaws can be mitigated, and perhaps even corrected, via additional pre- or post-processing phases, such as by identifying marks and bases individually and connecting them after identification, rejecting“isolated” glyphs under a certain size and gathering training data for rotated characters or pre-processing to correct rotation by employing a shear transform.

Version 1 performs extremely well on images with white-space separated characters. I performed no formal testing on Version 1, but anecdotally, runtimes average between one and three seconds for 1000 8.5”×11” pages at 200dpi[1] with ~1500 characters per page. This figure does not include time for copying to and from the GPU or reading from and writing to the hard drive.

[1]The standard unit for measuring resolution is dots per inch (dpi).

The speed is due to the manner in which the algorithm parallelizes the tasks. Multiple threads operate on a each page concurrently, counting pixels, dividing glyphs and calculating vectors. The algorithm capitalizes on the best of what GPUs have to offer — simple processing tasks performed at a massively parallel scale.

4.2 Version 2

The second version of SegRec attempts to correct the major shortcoming of the first version: its inability to handle kerning.

For each page, this version of SegRec starts at the image origin (bottom-left pixel) and inspects each pixel along the row until it finds a black pixel, which it assumes belongs to a glyph. Version 2 then walks the outer edge of the glyph in a clockwise direction, storing the leftmost and rightmost X values for each Y value it visits in a left-path bounds array and a right-path bounds array, respectively. When Version 2 reaches the pixel it started at, it has computed a bounding polygon for the glyph as represented in the left and right bounds arrays.

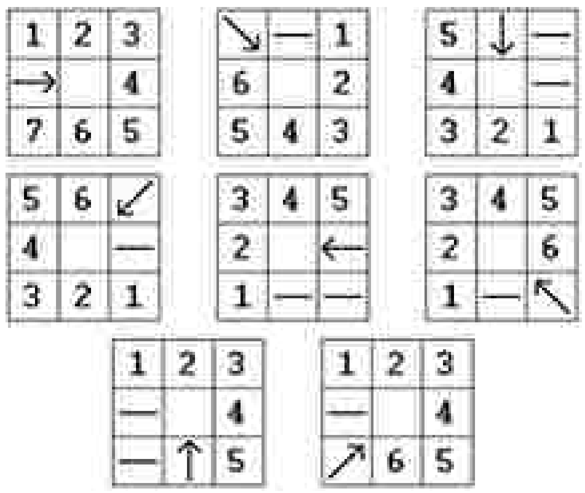

Figure 4.3: The edge-walk algorithm in the second version of SegRec.

Figure 4.3 indicates how Version 2 walks the edge of a glyph. The arrow in each grid indicates the previous position of the edge walk, and the blank region indicates the current pixel location of the edge walk. The numbers indicate the order in which the edge-walk algorithm checks the pixels for its next move. A dash in the grid indicates that the pixel location is skipped and not checked because, given the previous position, no black pixel could exist in that location. The first black pixel found is the next position for the edge walk. I invented this edge-walking algorithm and do not know if a similar version exists in the literature.

Version 2 computes the 25-vector and recognizes glyphs the same way as Version 1, but it only considers pixels within the bounding polygon, as shown in Figure 4.4.

Figure 4.4 depicts the left and right boundaries of the bounding polygon as stored by the bounds arrays. Thus, the algorithm does not inspect all the pixels within the bounding

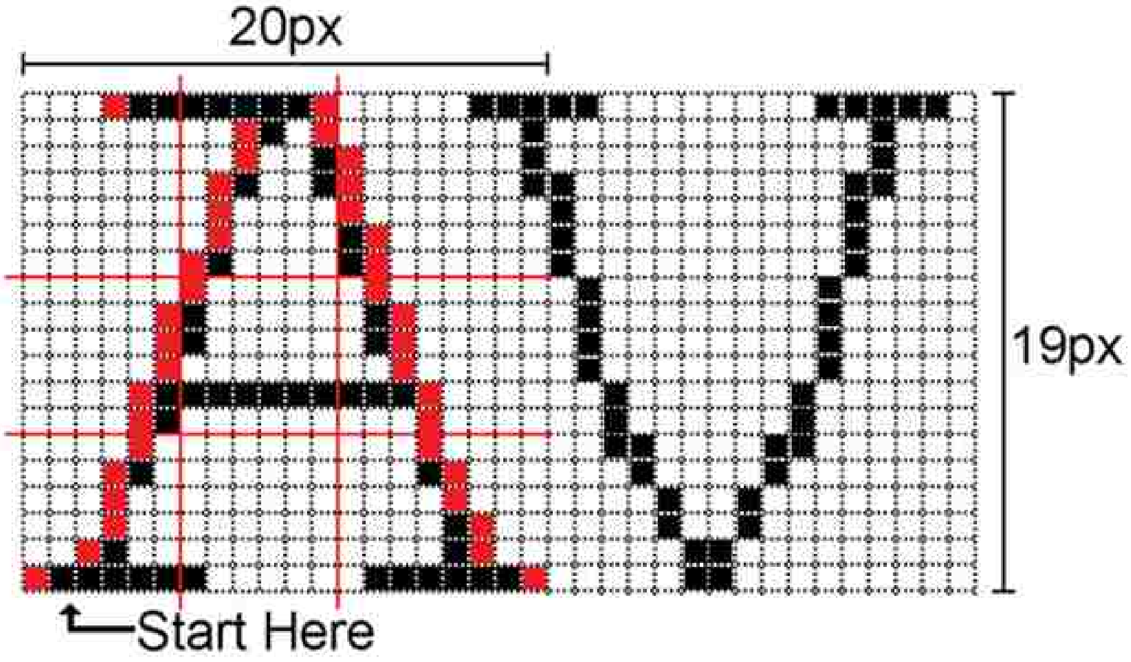

Figure 4.4: A kerned glyph with the grid-and-count grid and bounding polygon.

box during the grid-and-count process, but the same information is retrieved as in Version 1.

If the distance from the GDV to the closest match in training data exceeds some limit, the algorithm evaluates the glyph to check to see if it is a mark. The algorithm identifies the closest glyph that it has already processed and, if the midpoints between the closest glyph and this glyph are within some distance, say 15 pixels, it joins the two glyphs and then re-identifies the new glyph (i.e. the newly created glyph goes through the grid-and-count vectorization process again). The mark-joining process can be repeated for an arbitrary number of marks but, in practice for English, it typically only occurs once, when capturing the dot on ‘i’ and ‘j’.

This version of SegRec has one major shortcoming: it operates much more slowly on the GPU than Version 1. There are two reasons for the slowness. First is the way the algorithm detects and follows the edges of glyphs. On an NVIDIA GPU, the slowest operation for the hardware is a non-coalesced read from global memory. The edge walk in Version 2 makes heavy use of non-coalesced reads as it traverses the edge around a glyph. I attempted to mitigate this issue by using shared memory, but I was only able to achieve small performance gains. Second, the kernel probably exceeds the hardware limitation for registers per thread. Exceeding the limitation means that excess variables are stored in global memory, exacerbating the previous problem of too many global memory accesses. This problem could be solved by breaking Version 2 into several smaller kernels and running them separately, but I have not investigated this option.

Version 2 is unable to detect and associate marks that appear below glyphs. This flaw is a shortcoming in the design of the algorithm, because marks can only be associated with glyphs that have already been processed; since the algorithm executes on the image from the bottom up, it cannot associate marks below glyphs that it has not yet processed. Such marks exist in some alphabets, such as Hebrew.

Regarding edge walking

The edge-walk algorithm in Version 2 starts from the lowest, left-most pixel and walks the edge of the glyph clockwise until it reaches its starting point. In the general case, reaching the starting point indicates that it has surrounded the glyph.

However, there are several cases in which the edge walk returns back to the starting point without having circumnavigated the whole glyph.

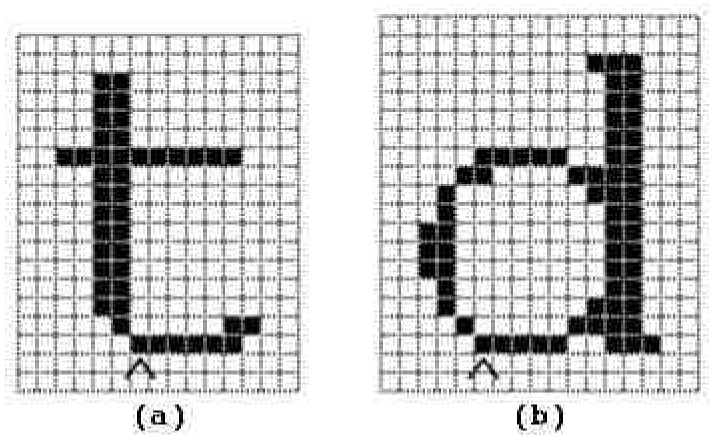

Figure 4.5: Examples of a glyph in which (a) reaching the starting point in an edge walk does not indicate being finished and (b) where the edge walk completes normally.

The letter ‘t’ shown in Figure 4.5 is one such case. The pixel indicated by the carat is the starting point. Traversing clockwise around the edge of the glyph leads back to the starting point and excludes the lower-right portion of the character, as shown in Figure 4.6. A heuristic can be used to help detect instances in which the starting point is reached prematurely, but the heuristic is imperfect in that it detects false positives, as with the letter ‘d’ shown in Figure 4.5. I believe the heuristic is only necessary for the two pixel configurations shown in Figure 4.7 — any other configuration seems to result in the appropriate behavior, because these configurations are the only ones in which the starting pixel serves as the sole pixel connecting two sections of the glyph.

4.3 Version 3

Design discussion

Version 3 of SegRec is a re-imagination of the edge-walk algorithm in Version 2. The new version is designed to significantly reduce non-coalesced global memory reads and to increase the number of threads simultaneously working on a single page. Originally, I considered assigning a thread to each X position to locate glyphs by “flooding” across adjacent black pixels. As the thread floods the glyphs, it tracks the extrema for X and

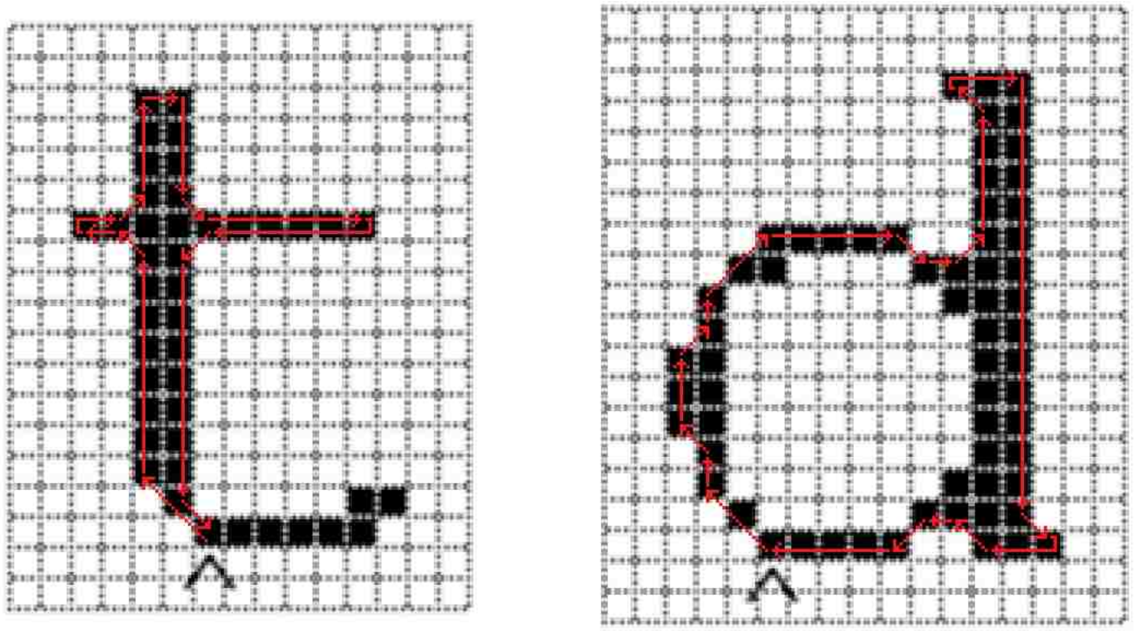

Figure 4.6: Figure 4.5 highlighting the paths the edge-walk algorithm finds.

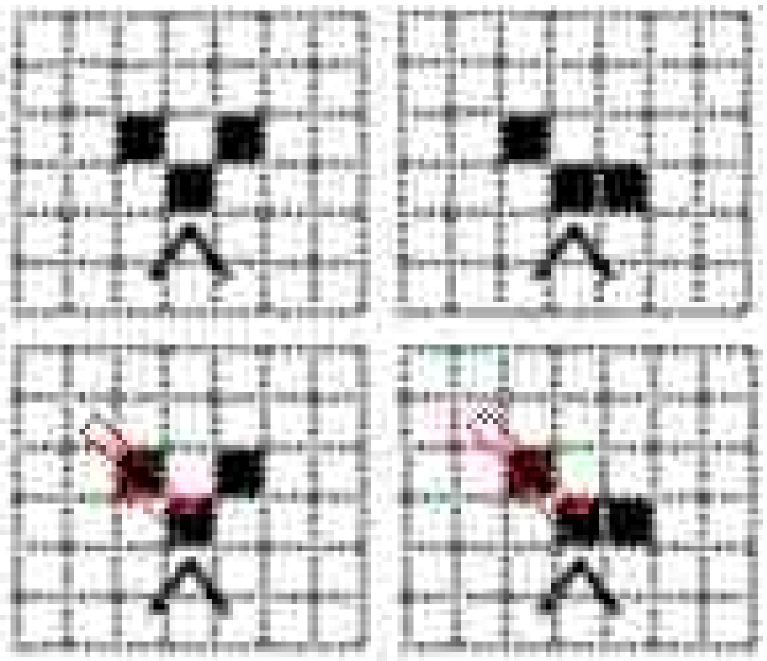

Figure 4.7: The pixel configurations fo which extra processing is necessary to detect the appropriate next step for the edge-walk algorithm.

Y and calculates a bounding box for the glyph. However, the threads would constantly be overwriting each other and duplicating work as several of them would be operating on the same glyph. In order to overcome this limitation, the threads could potentially replace black pixels with their *ThreadID* and have the highest *ThreadID* "win". Thus, if a thread were to check a pixel and find a *ThreadID* higher than its own, the thread would move to other work. However, this algorithm would require the storage for images to jump from 1 bit per pixel to 16 bits per pixel (in order to accommodate storing the *ThreadID*), which would exceed the memory capabilities of many GPUs. Additionally, there is no way to intelligently allocate memory for output from each of the threads. Because there is no way to pre-determine which thread will "win" each glyph, a huge excess of memory must be allocated for each thread, again, potentially exceeding the memory capabilities of many GPUs.

The next idea was to reduce the thread count to a maximum of 255 per image. This approach would only increase the input image size from 1 bit per pixel to 8 bits per pixel instead of 16 bits per pixel. However, it still does not solve the issue of allocating storage space for thread output, since there is still no way to pre-determine "winners".

At this point, I shifted focus to exactly what the algorithm would output. Initially, the algorithm was supposed to output the left and right boundaries associated with each glyph. However, assuming 100 boundary values per glyph, which gives us a maximum height of 50 pixels (50 boundary values for the left path and 50 values for the right path) at 64 bits per coordinate (32 bits each for X and Y) and a target throughput of 2.5 million characters, the required storage equals ~2GB — too much memory to use for output.[2] At this point, I discarded the idea of storing and outputting the full paths. Next, I considered the possibility of storing a path approximation.

The DPHull algorithm is a variation and improvement upon the Douglas-Peucker line-simplification algorithm [18]. DPHull reduces the number of vertices that comprise a closed polygon by incrementally adjusting the position of existing vertices to remove intermediate vertices. Applying DPHull has the effect of slightly altering the shape of the polygon approximation. DPHull sets a threshold for the difference and only allows cumulative changes that fall under the threshold. For a glyph, the difference can be relatively large (even up to several pixels on both sides of the glyph) while still capturing the overall shape within a reduced set of coordinates.

However, the paths need not even be stored at all. Since the eventual goal is to compute the 25-space vector to classify the glyph, we can simply store the path temporarily in order to compute the vector. The same logic could be applied to the vector, but I choose to output it, in addition to the other glyph data: bounding box coordinates and the proposed character classification.

This line of inquiry and realization led to the creation of Version 3.

[2]32 bits were required because SegRec stacks the images, thus, for 1000 pages, the y-value ranges from 0 to 2,199,999. Later, I figured out I could use 32 bits for each boundary value (16 bits per component) because the page offset is calculable and the height of a page is constant.

Version 3 of SegRec

The first part of SegRec, called the **segmentation stage**, allocates several pairs of top and bottom bounds arrays in shared memory. The number of arrays is dependent on the GPU, but generally, more is better. The minimum number of pairs required is dependent on the size, shape and other characteristics of the glyphs to be identified. The pairs of bounds arrays store the minimum and maximum Y values for the glyph parts detected in the image. A thread operates in one pair of arrays until it detects a disconnected glyph part, which causes it to move to the next pair of arrays. A disconnected glyph part is a group of pixels that is isolated by at least one pixel of white space from any other group of pixels. A group of pixels is a set of pixels such that each pixel in the group is connected to at least one other pixel contained within the group. Connected, in this case, means directly or diagonally adjacent to another pixel (this definition can be changed to tune the algorithm). For example, there are two groups of pixels in Figure 4.8. The red pixels show the divide between the two groups.

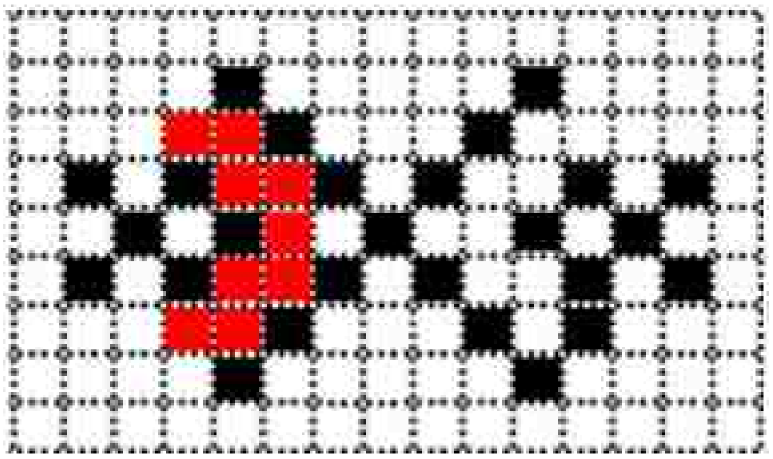

Figure 4.8: Two groups of black pixels. The red pixels show the divide between the groups.

Each thread operates on a vertical stripe of the image 8 pixels wide. The indices of the bounds arrays correspond to the X values of the stripe. The values stored in the bounds arrays correspond to the Y values (each value is 16 bits). Each array is initialized to "undefined'. The algorithm starts at the bottom-left corner of the image, assigning stripes to threads. Each thread reads[3] a byte of image data (corresponding to 8 pixels in a monochrome image) from the bottom of its assigned stripe. For each black pixel within the byte, the thread checks the top bounds array, and if the Y value of the pixel coordinate is greater than the corresponding element in the top bounds array, it overwrites the top element. If the Y value of the pixel coordinate is less than the corresponding element of the bottom bounds array, it overwrites the bottom element. (This situation only occurs when the bottom bounds array is "undefined"). Thus, after a thread finishes on the first line of its stripe, both the top and the bottom bounds arrays contain a 0 wherever it found a black

[3]That is, transfers a byte of data from global memory to register memory.

pixel. The bounds arrays represent the bounding polygon for the glyph and are comprised of the vertical paths from the pixel coordinate stored in the bottom bounds array to the pixel coordinate stored in the top bounds array. Figure 4.9 shows several glyphs with their bounding polygons highlighted in red (the paths stretch vertically from the bottom red pixel to the top red pixel), as they would be represented in a pair of bounds arrays. Figure 4.10 on page 58 presents this algorithm in pseudocode for processing a byte of data.

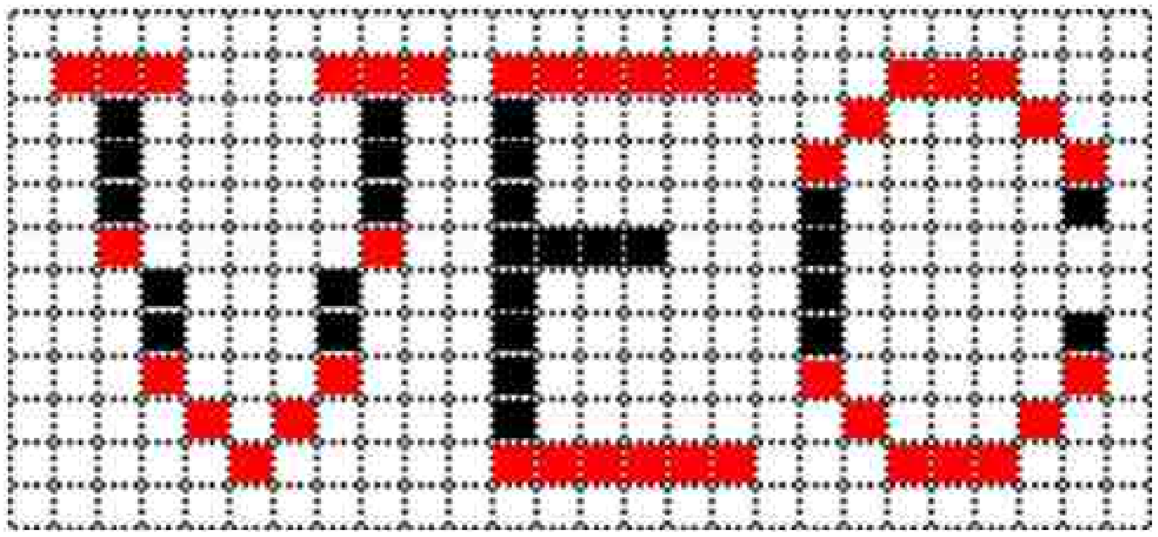
Figure 4.9: Three glyphs with their bounding polygons highlighted. The coordinates highlighted are what would be stored in the bound arrays.

To process the second line of a stripe, the thread follows same steps, but it adds a new check. If the pixel under consideration would occupy a position in the top or bottom bounds arrays that overwrites an existing value (i.e. overwrites a pixel coordinate) but is not connected to the pixel it overwrites, the thread moves to a new set of bounds arrays. The thread uses the new set of bounds arrays in exactly the same manner, starting at the pixel that initiated the move.

For example, in Figure 4.11, the blue pixels have already been processed and the red pixel is the current pixel being examined. The thread has no knowledge of anything to the left or right of its stripe (denoted by the red borders), so when it processes the pixel marked in red, it can only compare it to the values it has stored in the bounds arrays (denoted by the blue pixels). The thread finds that the red pixel is not connected to the blue pixel and starts using the next pair of bounds arrays.

When any thread fills all its available pairs of bounds arrays or the image is fully processed, the **compression stage** begins. The compression stage consolidates the bounds arrays by compressing the glyph parts contained within the pairs of top and bottom bounds arrays into larger glyph parts and, eventually, an entire glyph. A thread is assigned to a stripe within the bounds arrays (8 elements wide) and it starts at the top pair of bounds arrays, comparing the values in each pair of bounds arrays to the values in the pair of bounds arrays directly below it. If certain conditions are met (discussed in detail later), the thread merges the paths. The compression stage has the effect of extending the bounding polygon

```
//contains the current buffer count
int curBuf = 0;
//contains the current byte being processed
byte data = ...;
//contains the Y value of the current byte
short curY = ...;

for (int x = 7; x >= 0; x-=1) {
  //if the bit at position x, starting from the left, is 1
  if (((data >> x) & 1) == 1) {
    if (GetTopArrayValue(curBuf, x) == Unset) {
      //bound arrays are empty
      //set each array to the current Y value
      SetTopArrayValue(curY, curBuf, x);
      SetBottomArrayValue(curY, curBuf, x);
    } else {
      if (isConnected(x,GetTopArrayValue(curBuf, x), x, curY) == 1) {
        //this pixel is directly connected
        //to the one below it; adjust the Y value
        SetTopArrayValue(curY, curBuf, x);
      } else if ((isConnected(x - 1,GetTopArrayValue(curBuf, x - 1), x, curY) == 1)
       and (pathsOverlap(GetTopArrayValue(curBuf, x - 1), x, curY),
                         GetBottomArrayValue(curBuf, x - 1), x, curY),
                         GetTopArrayValue(curBuf, x), x, curY),
                         GetBottomArrayValue(curBuf, x), x, curY)) == 1)) {
        //the X-1th element is connected with this pixel
        //and the X-1th element overlaps with the path
        //this pixel would overwrite
        SetTopArrayValue(curY, curBuf, x);
      } else if ((isConnected(x + 1,GetTopArrayValue(curBuf, x + 1), x, curY) == 1)
       and (pathsOverlap(GetTopArrayValue(curBuf, x + 1), x, curY),
                         GetBottomArrayValue(curBuf, x + 1), x, curY),
                         GetTopArrayValue(curBuf, x), x, curY),
                         GetBottomArrayValue(curBuf, x), x, curY)) == 1)) {
        //the X+1th element is connected with this pixel
        //and the X+1th element overlaps with the path
        //this pixel would overwrite
        SetTopArrayValue(curY, curBuf, x);
      } else {
        //skip to the next buffer
        curBuf = curBuf + 1;
        //arrays are empty, so set them
        SetTopArrayValue(curY, curBuf, x);
        SetBottomArrayValue(curY, curBuf, x);
      }
    } //the value is set
  } //the pixel is black
} //each x value
```

Figure 4.10: Process a byte of image data.

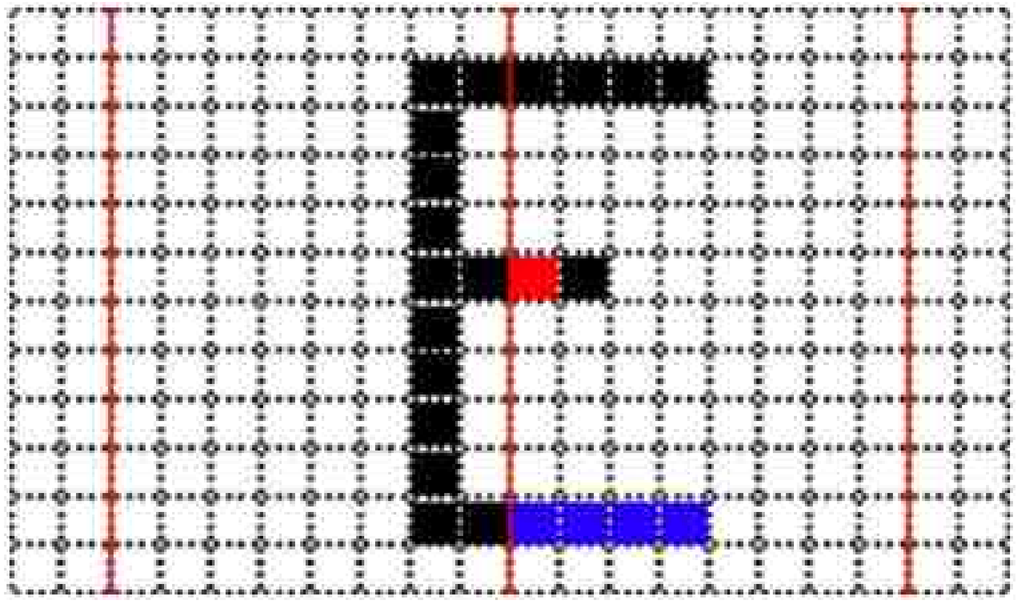

Figure 4.11: An example of a thread processing a stripe. The blue pixels have been processed and the red pixel is under consideration.

from the bottom array coordinates to the new top array coordinates, encompassing the previous top and bottom bounds array coordinates and extending the bounding polygon. Each glyph part is eventually joined to a group of glyph parts which, eventually, form an entire glyph.

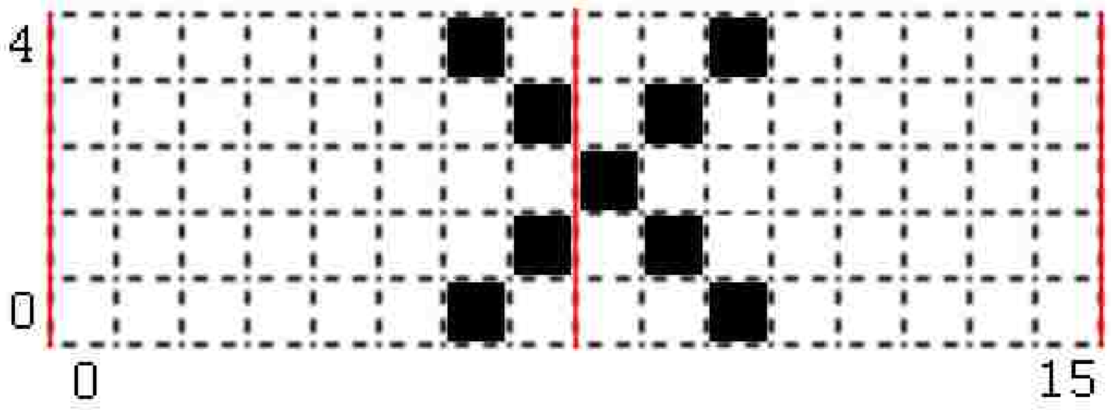

Figure 4.12: An example glyph divided into strips.

For example, assume two threads, $Thread_0$ and $Thread_1$ are executing concurrently on the stripes as shown in Figure 4.12. $Thread_0$ is operating on the left stripe and $Thread_1$ on the right stripe. After both threads process the bottom line, the active pair of top and bottom bounds arrays for each thread have values as shown below (X indicates an undefined initial value).

$After\ line\ 0:$

$$Top_0: \texttt{[X,X,X,X,X,X,0,X]} \quad \texttt{[X,X,0,X,X,X,X,X]}$$
$$Bottom_0: \texttt{[X,X,X,X,X,X,0,X]} \quad \texttt{[X,X,0,X,X,X,X,X]}$$

The bounds arrays show that $Thread_0$ sees a black pixel at $(6,0)$ and $Thread_1$ sees a black pixel at $(10,0)$. Because these pixels overwrite an unset element, they do not need to be connected to any previous entries.

$After\ line\ 1:$

$$Top_0: \texttt{[X,X,X,X,X,X,0,1]} \quad \texttt{[X,1,0,X,X,X,X,X]}$$
$$Bottom_0: \texttt{[X,X,X,X,X,X,0,1]} \quad \texttt{[X,1,0,X,X,X,X,X]}$$

The threads add an additional pixel to the bounds arrays at $(7,1)$ and $(9,1)$, respectively. Both of these pixels overwrite an unset element, so they do not need to be connected (even though: $(7,1)$ is connected to $(6,0)$ and $(9,1)$ is connected to $(10,0)$).

$After\ line\ 2:$

$$Top_0: \texttt{[X,X,X,X,X,X,0,1]} \quad \texttt{[2,1,0,X,X,X,X,X]}$$
$$Bottom_0: \texttt{[X,X,X,X,X,X,0,1]} \quad \texttt{[2,1,0,X,X,X,X,X]}$$

$Thread_0$ sees only white pixels in line 2, so it does not modify any values in the bounds arrays. $Thread_1$ sees an additional pixel at $(8,2)$. This pixel overwrites an unset element, so it does not need to be connected (even though it is: $(8,2)$ is connected to $(9,1)$).

$After\ line\ 3:$

$$Top_1: \texttt{[X,X,X,X,X,X,X,3]} \quad \texttt{[X,X,X,X,X,X,X,X]}$$
$$Bottom_1: \texttt{[X,X,X,X,X,X,X,3]} \quad \texttt{[X,X,X,X,X,X,X,X]}$$
$$Top_0: \texttt{[X,X,X,X,X,X,0,1]} \quad \texttt{[2,3,0,X,X,X,X,X]}$$
$$Bottom_0: \texttt{[X,X,X,X,X,X,0,1]} \quad \texttt{[2,1,0,X,X,X,X,X]}$$

$Thread_0$ sees a pixel at $(7,3)$, but because the pixel is not connected to any existing coordinate stored in first set of bounds arrays (the algorithm checks the $X-1th$ and Xth element for connectedness), the thread starts using the next pair of bounds arrays. $Thread_0$ adds $(7,3)$ to the new pair of bounds arrays. $Thread_1$ continues to use the first pair of bounds arrays and adds an additional pixel found at $(9,3)$. Because $(9,3)$ overwrites an existing pixel coordinate, the thread verifies that it is connected: $(9,3)$ is connected to $(8,2)$.

$After\ line\ 4:$

$$
\begin{aligned}
Top_1 &: \texttt{[X,X,X,X,X,X,4,3]} \quad \texttt{[X,X,X,X,X,X,X,X]}\\
Bottom_1 &: \texttt{[X,X,X,X,X,X,4,3]} \quad \texttt{[X,X,X,X,X,X,X,X]}\\
Top_0 &: \texttt{[X,X,X,X,X,X,0,1]} \quad \texttt{[2,3,4,X,X,X,X,X]}\\
Bottom_0 &: \texttt{[X X,X,X,X,X,0,1]} \quad \texttt{[2,1,0,X,X,X,X,X]}
\end{aligned}
$$

$Thread_0$ sees a pixel at $(6,4)$ and adds it to its current pair of bounds arrays. $Thread_1$ sees a pixel at $(10,4)$. Both pixels overwrite existing coordinates; and the threads verify that they are connected. $(6,4)$ is connected to $(7,3)$ in the second set of bounds arrays and $(10,4)$ is connected to $(9,3)$.

For the sake of the example, say that both threads have completed their entire stripes. The bounds arrays now represent a polygonal bounding box around the glyph, as shown in Figure 4.13. Each color represents a different pair of bounds arrays — the blue pixels show paths stored by S_0, a thread's first pair of bounds arrays, and the red pixels show paths stored by S_1, a thread's second pair of bounds arrays. The compression stage now begins.

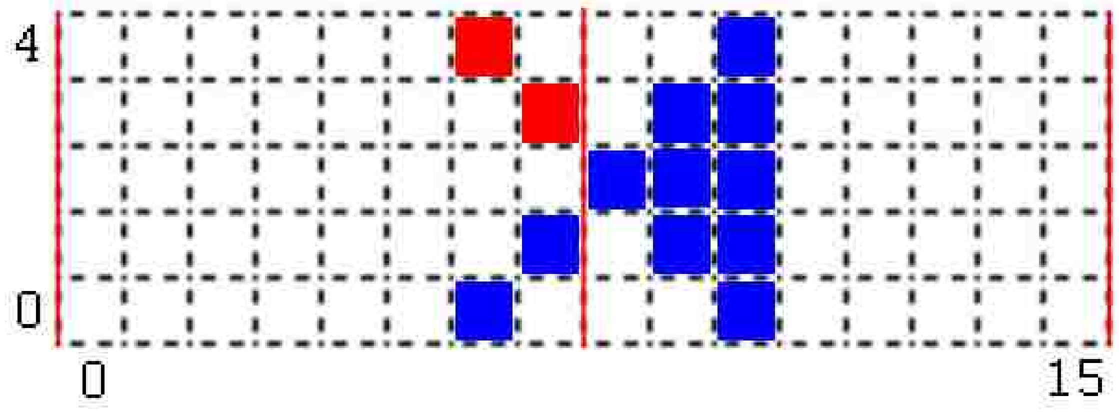

Figure 4.13: A glyph encircled by a polygonal bounding box.

I use the following conventions to refer to the pairs of bounds arrays, the positions within them and the coordinates they represent:

- S_n indicates the concatenation of the *nth* pair of bound arrays across all threads; i.e. S_0 is the first pair, S_1 is the second pair and so on.

- $S_n[T|B|A]$ refers to the top, bottom or both (all) bounds arrays in pair, S_n; i.e. S_0B refers to the bottom bounds array in the first pair and S_1T refers to the top bound array in the second pair. S_1A refers to both the top and bottom bound arrays in the second pair.

- $S_n[T|B|A]_m$ indicates stripe m in the $[T|B|A]$ bounds array in pair S_n; i.e. S_0B_0 is the first stripe in the bottom array in the first pair of bounds arrays. In this example, a stripe consists of eight indices (corresponding to the 8 pixels within the stripes on the image).

- P_q indicates a position within a given bounds array or stripe. When referring to a stripe, P_q refers to the position within the stripe with P_0 being the first (leftmost) position. When referring to a bounds array, P_q refers to the position in the array at the index q. When P_q is used in reference to a single bounds array, P_q refers to a coordinate. When P_q is used in reference to a pair of bounds arrays, P_q refers to the path formed by the vertical line drawn from the coordinate at P_q in the bottom bounds array to the coordinate at P_q in the top bounds array.

- A coordinate (x, y) means the specified bounds array at index x holds the value y.

- A **path** is the vertical line created by the coordinates $(x1, y1..y2)$ in a pair of bounds arrays where $(x1, y1)$ is the coordinate held by the bottom bounds array and $(x1, y2)$ is the coordinate held by the top bounds array.

- The term "overlap" means the paths overlap in the Y direction or the endpoints are adjacent. For example, given two paths $(x1, y1..y2)$ and $(x2, y3..y4)$ the paths are said to overlap if $(((y1 \geq max(y4 - 1, 0))$ *and* $(max(y4 - 1, 0) \geq max(y2 - 1, 0)))$ or $((y3 \geq max(y2 - 1, 0))$ *and* $(y2 \geq max(y4 - 1, 0))))$.

SegRec allocates a thread to run on each stripe. Each thread evaluates a maximum of four possibilities for each position within its stripe, starting in S_{MAX} at P_0:

1. If the path in S_n at P_q is unset, it is skipped.

2. If the path in S_n at P_q overlaps the path in S_{n-1} at P_q or the path in S_{n-1} at P_q is unset, the paths are merged. See Figure 4.14a.

3. If the path in S_n at P_q overlaps the path in S_{n-1} at P_{q-1} and the path in S_{n-1} at P_{q-1} overlaps the path in S_{n-1} at P_q, the paths S_n at P_q and S_{n-1} at P_q are merged. See Figure 4.14b.

4. If the path in S_n at P_q overlaps the path in S_{n-1} at P_{q+1} and the path in S_{n-1} at P_{q+1} overlaps the path in S_{n-1} at P_q, the paths S_n at P_q and S_{n-1} at P_q are merged. See Figure 4.14c.

Figure 4.14 displays examples of these comparisons. Each color represents a different pair of bounds arrays. The red path is the path being processed in $S_{CURRENT}$ at P_q.

- In Figure 4.14a, the red path (S_n at P_q) overlaps the blue path (S_{n-1} at P_q), so the paths can be merged.

- In Figure 4.14b, the blue path in (S_{n-1} at P_{q-1} overlaps both the red path in S_n at P_q and the blue path in S_{n-1} at P_q, so the paths S_n at P_q and S_{n-1} at P_q can be merged.

- In Figure 4.14c, the blue path in S_{n-1} at P_{q+1} overlaps both the red path in S_n at P_q and the blue path in S_{n-1} at P_q, so the paths S_n at P_q and S_{n-1} at P_q can be merged.

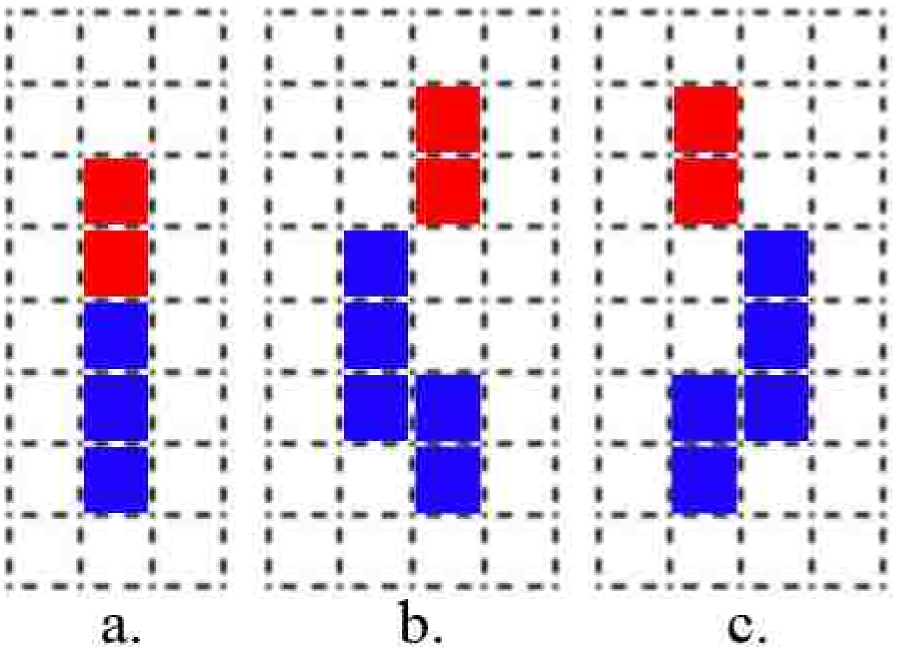

Figure 4.14: Sample paths showing the different comparison types for the compression stage.

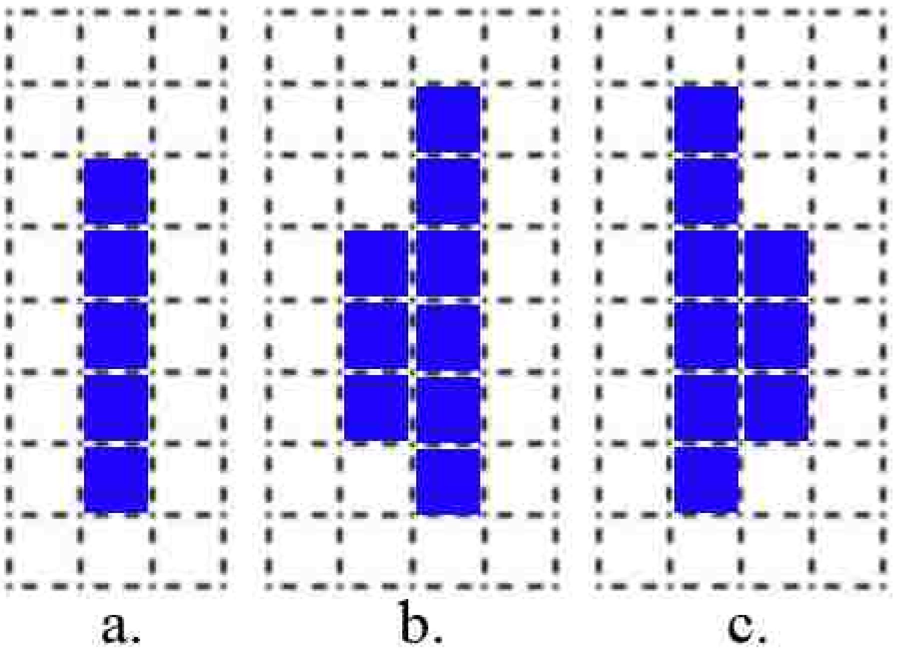

Figure 4.15: The results of merging the example paths.

Merging combines the paths by moving the value in S_nT at P_q to $S_{n-1}T$ at P_q, overwriting the previous value. If the path in S_{n-1} is unset, the value in S_nB at P_q is also moved. Merging the paths extends the boundaries of the polygonal bounding box from the bottom of the path in S_{n-1} at P_q to the top of the path in S_n at P_q, as seen in Figure 4.15.

From the example in Figure 4.13, the bounds arrays currently appear as follows:

$Start\ state$:

```
   Top1 : [X,X,X,X,X,X,4,3]  [X,X,X,X,X,X,X,X ]
Bottom1 : [X,X,X,X,X,X,4,3]  [X,X,X,X,X,X,X,X ]
   Top0 : [X,X,X,X,X,X,0,1]  [2,3,4,X,X,X,X,X ]
Bottom0 : [X,X,X,X,X,X,0,1]  [2,1,0,X,X,X,X,X ]
```

SegRec allocates two threads, $Thread_0$ and $Thread_1$ to operate on the two stripes. $Thread_0$ processes the left stripe and $Thread_1$ processes the right stripe. $Thread_0$ skips the unset positions and arrives at P_6. $Thread_0$ compares S_1 at P_6 to S_0 at P_6 and finds the paths do not overlap. $Thread_0$ then compares S_1 at P_6 to S_0 at P_5 and finds the paths do not overlap. $Thread_0$ then compares S_1 at P_6 to S_0 at P_7 and finds the paths do not overlap. $Thread_0$ is done processing P_6 in S_1. $Thread_1$ finds only unset positions and skips them all.

$Thread_0$ arrives at P_7. $Thread_0$ compares S_1 at P_7 to S_0 at P_7 and finds the paths do not overlap. $Thread_0$ then compares S_1 at P_7 to S_0 at P_6 and finds the paths do not overlap. $Thread_0$ then compares S_1 at P_7 to S_0 at P_8 (which crosses the stripe border) and finds the paths overlap. $Thread_0$ then compares S_0 at P_7 to S_0 at P_8 and finds the paths overlap. $Thread_0$ then merges P_7 in S_1 to P_7 in S_0. $Thread_0$ unsets P_7 in S_1.

$After\ pass$ 1 :

```
   Top1 : [X,X,X,X,X,X,4,X]  [X,X,X,X,X,X,X,X]
Bottom1 : [X,X,X,X,X,X,4,X]  [X,X,X,X,X,X,X,X]
   Top0 : [X,X,X,X,X,X,0,3]  [2,3,4,X,X,X,X,X]
Bottom0 : [X,X,X,X,X,X,0,1]  [2,1,0,X,X,X,X,X]
```

Since $Thread_0$ has made a change, all threads perform another compression pass. The threads repeat this process until no thread makes a change.

$Thread_0$ skips all the unset positions and arrives at P_6. $Thread_0$ compares S_1 at P_6 to S_0 at P_6 and finds the paths do not overlap. $Thread_0$ then compares S_1 at P_6 to S_0 at P_5 and finds the paths do not overlap. $Thread_0$ then compares S_1 at P_6 to S_0 at P_7 and finds the paths overlap. $Thread_0$ then compares S_0 at P_7 to S_0 at P_6 and finds the paths overlap. $Thread_0$ then merges P_6 in S_1 to P_6 in S_0. $Thread_0$ unsets P_6 in S_1. $Thread_0$ skips P_7, because it is unset. $Thread_1$ finds only unset positions and skips them all.

$After\ pass\ 2:$

$$\begin{aligned}
Top_1 &: \texttt{[X,X,X,X,X,X,}\mathbf{\texttt{X}}\texttt{,X]}\quad \texttt{[X,X,X,X,X,X,X,X]}\\
Bottom_1 &: \texttt{[X,X,X,X,X,X,}\mathbf{\texttt{X}}\texttt{,X]}\quad \texttt{[X,X,X,X,X,X,X,X]}\\
Top_0 &: \texttt{[X,X,X,X,X,X,}\mathbf{\texttt{4}}\texttt{,3]}\quad \texttt{[2,3,4,X,X,X,X,X]}\\
Bottom_0 &: \texttt{[X,X,X,X,X,X,0,1]}\quad \texttt{[2,1,0,X,X,X,X,X]}
\end{aligned}$$

Since $Thread_0$ has again made a change, all threads perform another compression pass. Pass 3 results in no changes, so the compression stage is complete. Figure 4.16 shows the final bounding polygon for this example.

$After\ pass\ 3:$

$$\begin{aligned}
Top_1 &: \texttt{[X,X,X,X,X,X,X,X]}\quad \texttt{[X,X,X,X,X,X,X,X]}\\
Bottom_1 &: \texttt{[X,X,X,X,X,X,X,X]}\quad \texttt{[X,X,X,X,X,X,X,X]}\\
Top_0 &: \texttt{[X,X,X,X,X,X,4,3]}\quad \texttt{[2,3,4,X,X,X,X,X]}\\
Bottom_0 &: \texttt{[X,X,X,X,X,X,0,1]}\quad \texttt{[2,1,0,X,X,X,X,X]}
\end{aligned}$$

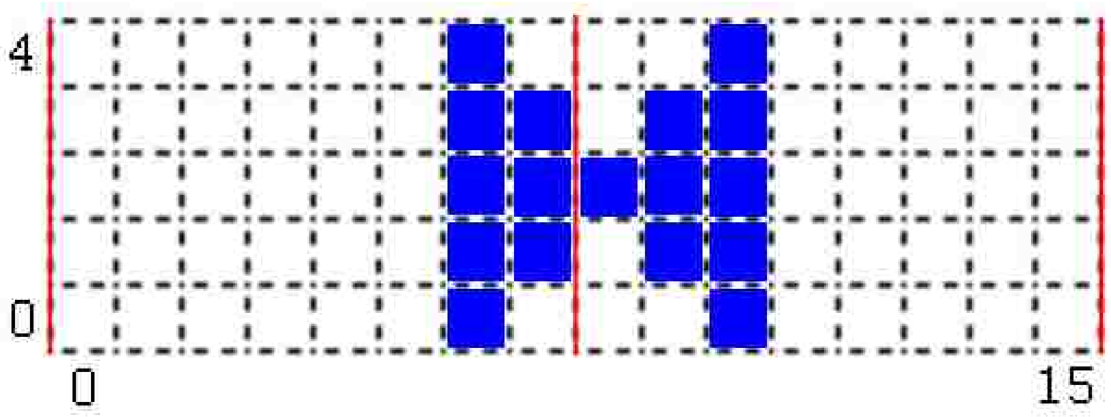

Figure 4.16: The bounding polygon for the example.

Version 3 of SegRec processes all stripes concurrently due to the mechanism by which the threads operate on the GPU, assuming we only use one warp per page. Each thread within a warp executes the same instructions at the same time; thus, each thread is at exactly the same point within the compression stage at the same time, so there is no chance the threads can directly interfere with one another. However, it is possible that a thread could run out of bounds arrays before it, or some other thread, has seen the full glyph. Thus, Version 3 could begin the compression stage with partial glyphs in the bounds arrays. Version 3 handles this case by comparing the bounding polygons in the bounds arrays with the most recently processed Y value; if the bounding polygon shares a border with the Y value, the algorithm skips the glyph.

Once the compression stage is complete, the **construction stage** begins. For the sake of the example, assume that we have two more glyphs in our example as shown in Figure 4.17.

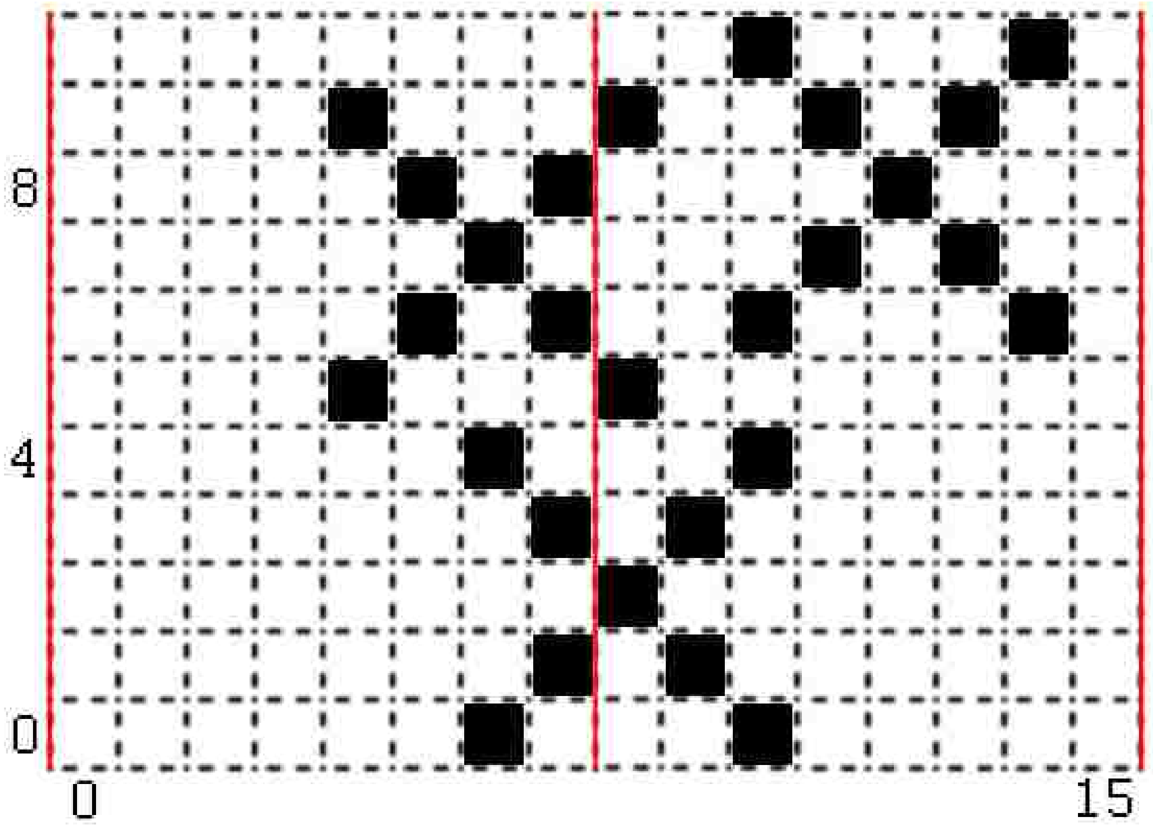

Figure 4.17: Three glyphs.

At the end of the compression stage, the bounds arrays look as follows:

With two more glyphs :

Top_1 :	[X,X,X,X,X,X,7,8]	[9,X,10,X,X,X, X,X]
$Bottom_1$:	[X,X,X,X,X,X,7,6]	[5,X, 6,X,X,X, X,X]
Top_0 :	[X,X,X,X,9,8,4,3]	[2,3, 4,9,8,9,10,X]
$Bottom_0$:	[X,X,X,X,5,6,0,1]	[2,1, 0,7,8,7, 6,X]

Figure 4.18 shows the paths stored by the bounds arrays. The blue paths are stored by S_0 and the red paths by S_1.

Once again, SegRec allocates a thread to run on each stripe. Each thread evaluates two possibilities for each position within its stripe to determine if it should process the position, starting in S_0 at P_0:

1. If the path in S_n at P_q is unset, it is skipped.

2. If any path from S_0 to S_{MAX} at P_{q-1} overlaps S_n at P_q, the position is skipped.

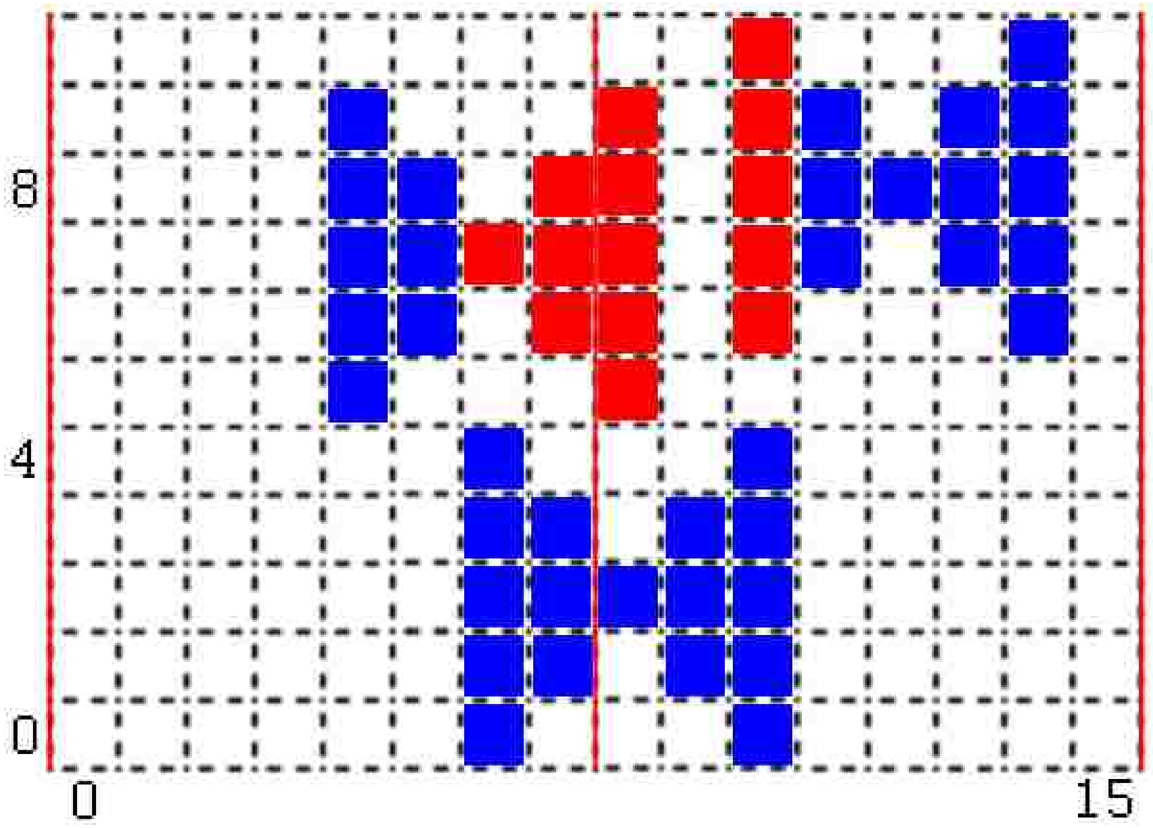

Figure 4.18: The paths stored in the bounds arrays. The red paths are stored in S_1 and the blue paths in S_0.

If the thread decides to process the position, it executes the following procedure twice: once to compute the bounding box and once to compute the 25-space vector:

1. For each position P_q, check the paths from S_0 to S_{MAX} at P_{q+1}. If it finds an overlapping path, move to that position.

2. If this is the first run, update the minimum and maximum X and Y values and continue with Step 1.

3. If this is the second run, count the black pixels within the path in $S_{CURRENT}$ at P_q and store them in a 25-space vector.

4. If no overlapping path can be found in any S_n at P_{q+1}, this glyph ready for the next step.

In the example, $Thread_0$ skips positions until it finds the path $((4,5),(4,9))$ in S_0A_0 at P_4. $Thread_0$ then checks to see if any paths in S_0A_0 or S_1A_0 at P_3 overlap. $Thread_0$ finds no overlapping paths, so the thread processes the glyph. This is the first pass through the glyph, so $Thread_0$ tracks and stores X_{min}, Y_{min}, X_{max}, and Y_{max}.

$After\ processing\ P_4:$

$$Current\ Position = S_0A_0\ at\ P_4$$
$$X_{min} = 4$$
$$Y_{min} = 5$$
$$X_{max} = 4$$
$$Y_{max} = 9$$

Next, $Thread_0$ looks for an overlapping path in S_0A_0 to S_1A_0 at P_5. $Thread_0$ finds an overlapping path in S_0A_0 at P_5: $((5,6),(5,8))$. $Thread_0$ moves to this location and checks the minima and maxima.

$After\ processing\ P_5:$

$$Current\ Position = S_0A_0\ at\ P_5$$
$$X_{min} = 4$$
$$Y_{min} = 5$$
$$X_{max} = \mathbf{5}$$
$$Y_{max} = 9$$

Next, $Thread_0$ looks for an overlapping path in S_0A_0 to S_1A_0 at P_6. $Thread_0$ finds an overlapping path in S_1A_0 at P_6: $((6,7),(6,7))$. $Thread_0$ moves to this location and checks the minima and maxima.

$After\ processing\ P_6:$

$$Current\ Position = S_1A_0\ at\ P_6$$
$$X_{min} = 4$$
$$Y_{min} = 5$$
$$X_{max} = \mathbf{6}$$
$$Y_{max} = 9$$

Next, $Thread_0$ looks for an overlapping path in S_0A_0 to S_1A_0 at P_7. $Thread_0$ finds an overlapping path in S_1A_0 at P_7: $((7,6),(7,8))$. $Thread_0$ moves to this location and checks the minima and maxima.

$After\ processing\ P_7:$

$$Current\ Position = S_1A_0\ at\ P_7$$
$$X_{min} = 4$$
$$Y_{min} = 5$$
$$X_{max} = \mathbf{7}$$
$$Y_{max} = 9$$

Next, $Thread_0$ looks for an overlapping path in S_0A_0 to S_1A_0 at P_8. $Thread_0$ finds an overlapping path in S_1A_0 at P_8: $((8,5),(8,9))$. $Thread_0$ moves to this location and checks the minima and maxima.

$After\ processing\ P_8:$

$$\begin{aligned} Current\ Position &= S_1A_0\ at\ P_8 \\ X_{min} &= 4 \\ Y_{min} &= 5 \\ X_{max} &= \mathbf{8} \\ Y_{max} &= 9 \end{aligned}$$

Next, $Thread_0$ looks for an overlapping path in S_0A_0 to S_1A_0 at P_9. $Thread_0$ is unable to find an overlapping path, so this pass is complete. $Thread_0$ goes back to the starting position, S_0A_0 at P_4 and iterates through the glyph again in the same manner. During the second pass, $Thread_0$ counts the black pixels in the paths at each position it processes and computes a 25-space vector. The vector computed for the first glyph $Thread_0$ finds is:

$$(1, 0, 0, 0, 1, 0, 1, 0, 1, 0, 0, 0, 1, 0, 0, 0, 1, 0, 1, 0, 1, 0, 0, 0, 1)$$

As $Thread_0$ counts pixels, it unsets the processed paths. When $Thread_0$ has finished processing the first glyph, the bounds arrays look as follows (not taking into account changes by $Thread_1$):

$After\ Thread_0\ processes\ the\ first\ glyph:$

$$\begin{aligned} Top_1 &: \texttt{[X,X,X,X,X,X,\textbf{X},\textbf{X}]}\quad \texttt{[\textbf{X},X,10,X,X,X, X,X]} \\ Bottom_1 &: \texttt{[X,X,X,X,X,X,\textbf{X},\textbf{X}]}\quad \texttt{[\textbf{X},X, 6,X,X,X, X,X]} \\ Top_0 &: \texttt{[X,X,X,X,\textbf{X},\textbf{X},4,3]}\quad \texttt{[2,3, 4,9,8,9,10,X]} \\ Bottom_0 &: \texttt{[X,X,X,X,\textbf{X},\textbf{X},0,1]}\quad \texttt{[2,1, 0,7,8,7, 6,X]} \end{aligned}$$

$Thread_0$ is not finished processing S_0A_0, so it resumes from where it left off and finds another path in S_0A_0 at P_6, which indicates a new glyph. $Thread_0$ follows the same procedure to process the new glyph.

$Thread_1$ is operating concurrently with $Thread_0$. The following outlines the actions $Thread_1$ takes while $Thread_0$ is processing:

1. $Thread_1$ finds the path $((8, 2), (8, 2))$ in S_0A_1 at P_0. $Thread_1$ then checks to see if any paths in S_0A_1 or S_1A_1 at P_{-1} overlap. $Thread_1$ finds an overlapping path $((7, 1,), (7, 3))$ in S_0A_1 at P_{-1}, so $Thread_1$ skips P_0.

2. $Thread_1$ finds that S_1A_1 at P_0 is empty, so the position is skipped.

3. $Thread_1$ finds the path $((9, 1), (9, 3))$ in S_0A_1 at P_1. $Thread_1$ then checks to see if any paths in S_0A_1 or S_1A_1 at P_0 overlap. $Thread_1$ finds an overlapping path $((8, 2,), (8, 2))$ in S_0A_1 at P_0, so $Thread_1$ skips P_1.

4. $Thread_1$ finds that S_1A_1 at P_1 is empty, so the position is skipped.

5. $Thread_1$ finds the path $((10, 0), (10, 4))$ in S_0A_1 at P_2. $Thread_1$ then checks to see if any paths in S_0A_1 or S_1A_1 at P_1 overlap. $Thread_1$ finds an overlapping path $((9, 1,), (9, 3))$ in S_0A_1 at P_1, so $Thread_1$ skips P_2.

6. $Thread_1$ finds the path $((10,6),(10,10))$ in S_1A_1 at P_2. $Thread_1$ then checks to see if any paths in S_0A_1 or S_1A_1 at P_1 overlap. $Thread_1$ finds no overlapping paths, so $Thread_1$ processes the glyph using the same procedure already described. The bounds arrays look as follows (not taking into account changes by $Thread_0$):

   $After\ Thread_1\ processes\ the\ glyph:$

$$\begin{aligned}
Top_1 &: \texttt{[X,X,X,X,X,X,X,X]} \quad \texttt{[X,X,}\mathbf{X}\texttt{,X,X,X,X,X]} \\
Bottom_1 &: \texttt{[X,X,X,X,X,X,X,X]} \quad \texttt{[X,X,}\mathbf{X}\texttt{,X,X,X,X,X]} \\
Top_0 &: \texttt{[X,X,X,X,X,X,4,3]} \quad \texttt{[2,3,4,}\mathbf{X}\texttt{,}\mathbf{X}\texttt{,}\mathbf{X}\texttt{,}\mathbf{X}\texttt{,X]} \\
Bottom_0 &: \texttt{[X,X,X,X,X,X,}\mathbf{0}\texttt{,1]} \quad \texttt{[2,1,}\mathbf{0}\texttt{,}\mathbf{X}\texttt{,}\mathbf{X}\texttt{,}\mathbf{X}\texttt{,}\mathbf{X}\texttt{,X]}
\end{aligned}$$

7. $Thread_1$ continues processing at the next position. $Thread_1$ finds that S_0A_1 at P_3 is empty, so the position is skipped.
8. $Thread_1$ finds that S_1A_1 at P_3 is empty, so the position is skipped.
9. $Thread_1$ finds that S_0A_1 at P_4 is empty, so the position is skipped.
10. $Thread_1$ finds that S_1A_1 at P_4 is empty, so the position is skipped.
11. $Thread_1$ finds that S_0A_1 at P_5 is empty, so the position is skipped.
12. $Thread_1$ finds that S_1A_1 at P_5 is empty, so the position is skipped.
13. $Thread_1$ finds that S_0A_1 at P_6 is empty, so the position is skipped.
14. $Thread_1$ finds that S_1A_1 at P_6 is empty, so the position is skipped.
15. $Thread_1$ finds that S_0A_1 at P_7 is empty, so the position is skipped.
16. $Thread_1$ finds that S_1A_1 at P_7 is empty, so the position is skipped.
17. At this point, $Thread_1$ has completed processing.

The output of this step of the construction stage is a list of best-fit bounding box coordinates and 25-space vectors. Each bounding box and 25-space vector corresponds to a glyph that was calculated from the bounding polygon of a glyph in the bounds arrays.

The final step of the construction stage is a search of the training data to classify each glyph. This step searches in the same manner as Version 1 and Version 2.

4.4 Output

The output of the construction stage, stored in global memory, is a list of best-fit bounding box coordinates, 25-space vectors, and the character classification. The output is downloaded from the GPU into host memory and converted to XML. See Figure 4.19 on page 71 for sample XML output.

```xml
<GlyphContainer>
  <Glyphs>
    <Glyph>
      <ID>0</ID>
      <Page>0</Page>
      <BoundingBox>
        <Left>839</Left>
        <Bottom>904</Bottom>
        <Top>918</Top>
        <Right>853</Right>
      </BoundingBox>
      <Vector>2,4,5,4,4,0,6,3,0,3,0,6,3,0,0,0,6,3,0,0,2,6,5,0,0</Vector>
      <Distance>0</Distance>
      <Character>L</Character>
    </Glyph>
    <Glyph>
      <ID>1</ID>
      <Page>0</Page>
      <BoundingBox>
        <Left>301</Left>
        <Bottom>905</Bottom>
        <Top>919</Top>
        <Right>317</Right>
      </BoundingBox>
      <Vector>0,0,6,0,0,0,2,11,0,0,0,6,7,3,0,1,9,2,6,0,6,9,1,7,4</Vector>
      <Distance>0</Distance>
      <Character>V</Character>
    </Glyph>
  </Glyphs>
</GlyphContainer>
```

Figure 4.19: Sample XML output.

Chapter 5: Findings and Results

5.1 OCR engines

I test SegRec v3 against Tesseract v3.04.01, ABBYY FineReader Professional 12 and OmniPage Ultimate 19. Brief descriptions of each engine can be found below.

Tesseract

Tesseract is an open-source, command-line driven OCR engine that was developed by Hewlett-Packard and presented at the 1995 UNLV Annual Test of OCR Accuracy [53]. Entered as "HP Labs OCR", Tesseract consistently scored in the top three (out of eight) for character recognition accuracy [44]. The version I test against is Tesseract v3.04.01[1].

ABBYY FineReader

ABBYY FineReader is a commercial OCR engine by ABBYY. ABBYY was founded in 1989 and ABBYY FineReader debuted in 1993 [2]. According to ABBYY, the ABBYY FineReader software is used by over 30 million people world-wide. The version I test against is ABBYY FineReader 12 Professional[2].

OmniPage Ultimate

OmniPage Ultimate is a commercial OCR engine by Nuance. Nuance's products are in use by over 22 million users [33]. The version I test against is OmniPage Ultimate 19[3].

5.2 Image set creation

Normal set

I programatically generated one thousand 8.5"×11" page images of "lorem ipsum"[4] using a 12pt "Courier New" font. These page images are flawless and should be easily recognizable by all engines. This set of page images is the "normal" set. See Figure B.1 in Appendix B on page 86 for a sample page.

[1]Tesseract can be downloaded from `https://github.com/tesseract-ocr`

[2]A trial version of ABBYY FineReader can be downloaded from `https://www.abbyy.com/en-us/finereader/professional/`

[3]A trial version of OmniPage Ultimate can be downloaded from `http://www.nuance.com/for-business/by-product/omnipage/ultimate/index.htm`.

[4]**Lorem Ipsum** is the printing and typesetting industry standard dummy text. See `http://www.lipsum.com/` for more information.

Noisy set

Next, I programmatically add noise to the characters on each page. The algorithm I use to add noise is as follows:

```
//~15% chance to add a pixel to the
//end of a left-to-right run of pixels
int lastPixelBlack;
for (int x = 0; x < image_width; x++)  {
  lastPixelBlack = 0;
  for (int y = 0; y < image_height; y++) {
    if (getPixel(x,y) == Black) {
      lastPixelBlack = 1;
    } else if (lastPixelBlack == 1) {
      lastPixelBlack = 0;
      if (Random.Next(0,1000000) > 850000) {
         setPixel(x,y,Black);
      }
    }
  }
}
```

The noise algorithm as shown has a ~15% chance of adding a pixel to the end of a left-to-right run of pixels. I run a variation of this algorithm for top-to-bottom, bottom-to-top and right-to-left pixel runs, each with a ~15% chance to add a black pixel. The algorithm simulates the noise that appears from repeated photocopying. After adding noise, the characters will look similar to Figure B.4. This set of page images is the "noisy" set. See Figure B.2 in Appendix B on page 87 for a sample page.

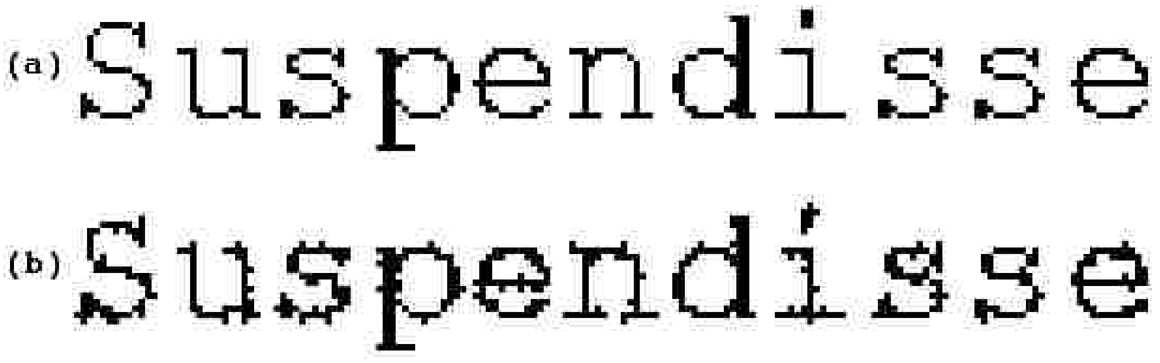

Figure 5.1: (a) Original characters. (b) Characters with added noise.

Scan1 set

Next, I printed 100 pages of the original set and then scanned them back into digital form. This set of page images is the "scan1" set. See Figure B.4 in Appendix B on page 89 for a sample page.

Scan2 set

For the last set of images, I printed the scan1 set and then scanned the physical pages. This set of page images is the "scan2" set. See Figure B.5 in Appendix B on page 90 for a sample page.

5.3 Results

The results are the averaged run speeds and accuracy ratings of each OCR engine as tested against each set of images. All engines were tested with their respective default settings on a machine running Windows 2008 R2 (64 bit) with 32GB of RAM, a 1TB Western Digital Blue 7200 RPM hard drive (model WD10EZEX-00BN5A0) and a quad-core Intel i7-4771 CPU running at 3.5GHz. The GPU used to test SegRec is a NVIDIA Tesla K40 running the NVIDIA development driver v353.90 and CUDA v7.5.17. The results are shown in Table 5.1. Graphs depicting the results are show in Figures 5.2, 5.3, and 5.4. Additional results are shown in Figures 5.5, 5.6, and 5.7.

Table 5.1: Each OCR engine versus each set of images averaged over 5 runs. "PC" signifies that SegRec used the pixel count vector for classification whereas "GDV" signifies SegRec used the global density vector for classification. For speed comparison purposes, each page within image sets Scan1 and Scan2 was duplicated ten times to give 1000 total pages.

Image Set	Statistic	SegRec w/PC	SegRec w/GDV	Tesseract	OmniPage	ABBYY
Normal (1000 Images)	Run Time	31.6s	35.6s	2,767s	225s	574s
	Macro-F	0.948	0.850	0.841	0.828	0.960
	Micro-F	0.998	0.941	0.966	0.999	0.988
Noisy (1000 Images)	Run Time	35.1s	38.4s	3,606s	633s	1,864s
	Macro-F	0.415	0.430	0.539	0.546	0.575
	Micro-F	0.676	0.765	0.990	0.993	0.989
Scan1 (1000 Images)	Run Time	38.1s	41.6s	5,696s	831s	2,205s
	Macro-F	0.200	0.174	0.373	0.537	0.554
	Micro-F	0.336	0.358	0.935	0.974	0.978
Scan2 (100 Images)	Run Time	34.4s	37.6s	5,459s	950s	1,719s
	Macro-F	0.178	0.168	0.372	0.594	0.591
	Micro-F	0.332	0.358	0.956	0.982	0.985

5.4 Metrics

The macro-f score is an average of how well the engine recognizes each individual character. For example, a macro-f score of 0.75 means that, on average, the engine is correctly recognizing 75% of each individual character. A high macro-f score indicates the engine is recognizing each character well. A low or mid-range macro-f score indicates the engine

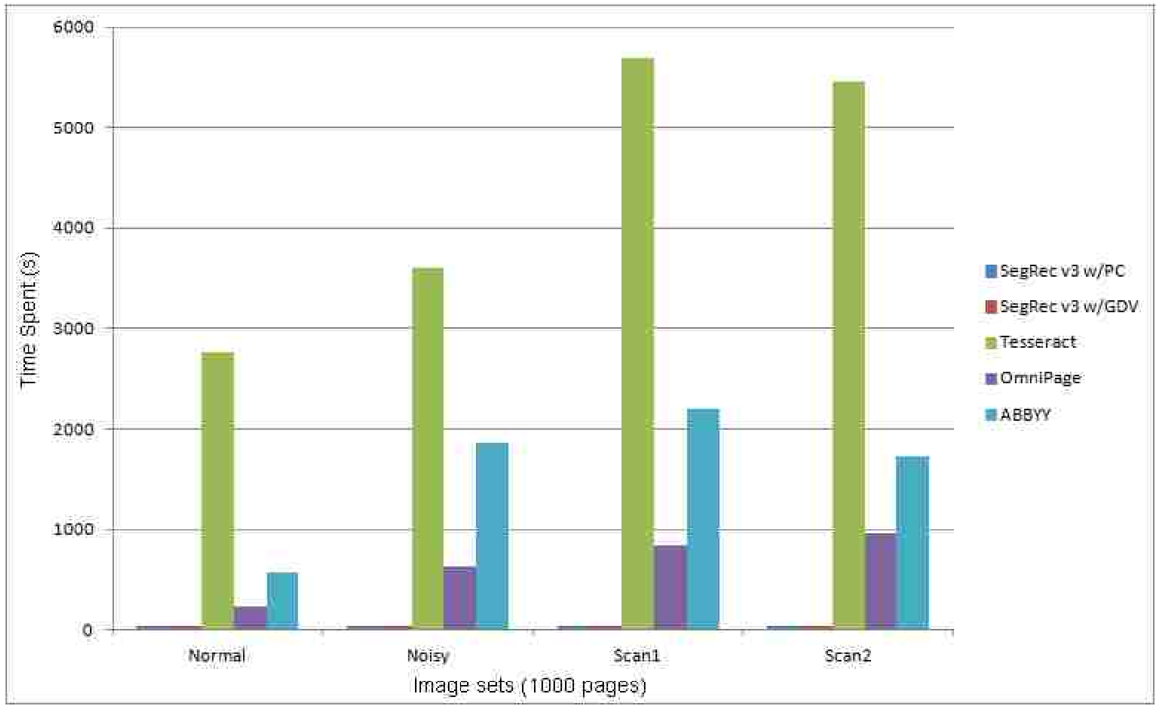

Figure 5.2: A graph of the total time each engine spent per number of pages in seconds. These metrics include time for reading the images from the hard drive and copying data to and from the GPU.

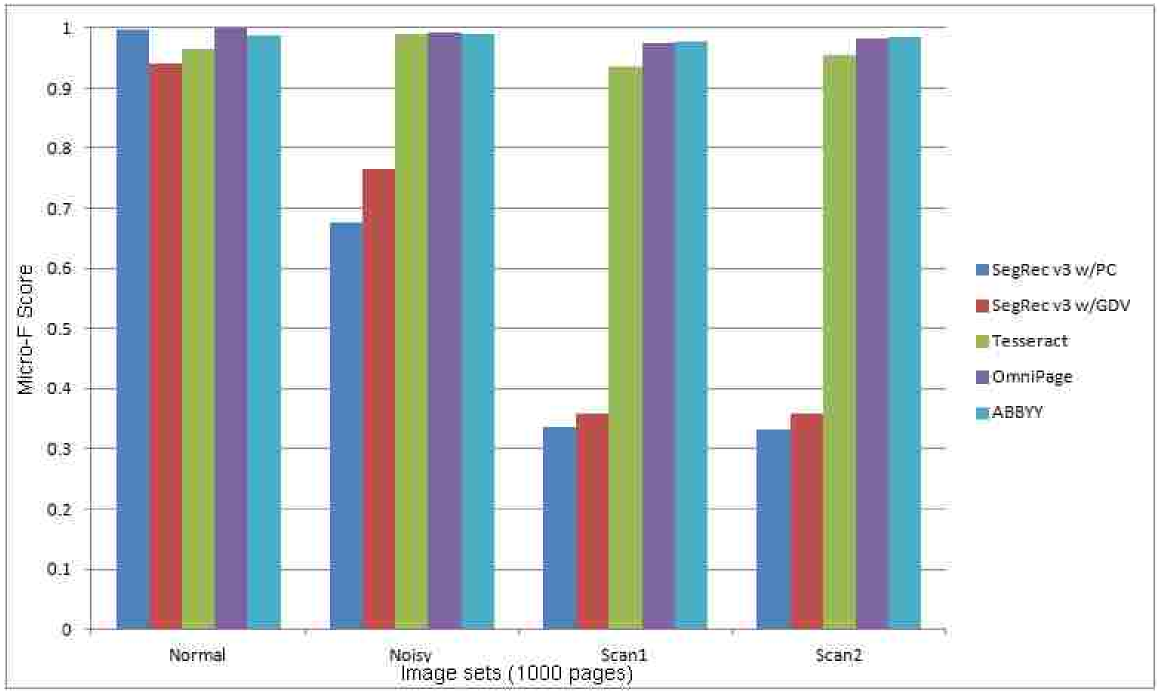

Figure 5.3: A graph of the micro-f score for each engine versus each set of images.

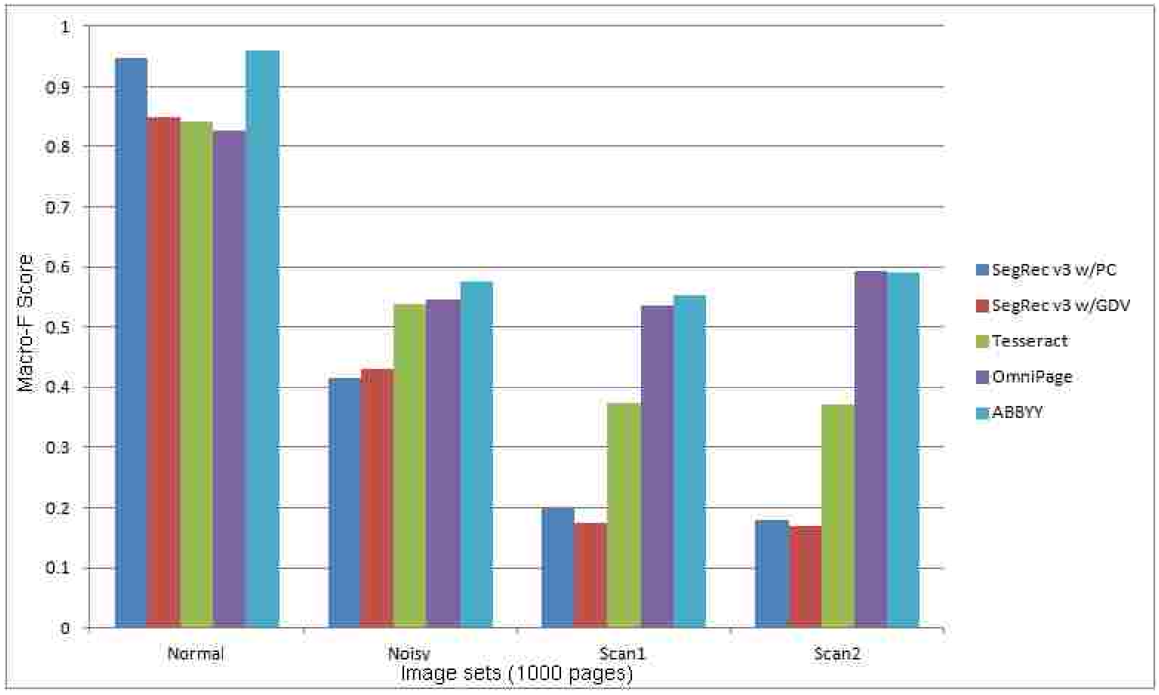

Figure 5.4: A graph of the macro-f score for each engine versus each set of images.

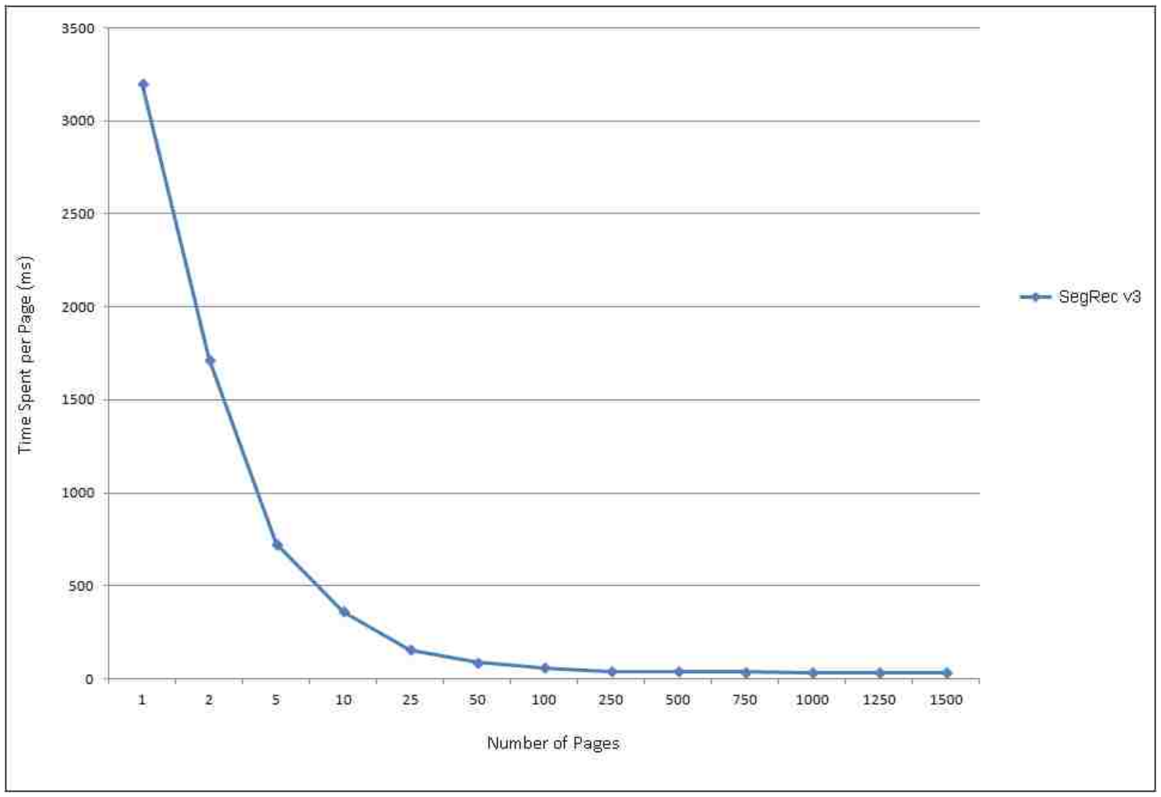

Figure 5.5: A graph of the time SegRec v3 spent per page in milliseconds versus number of pages. These metrics include time for reading the images from the hard drive and copying data to and from the GPU.

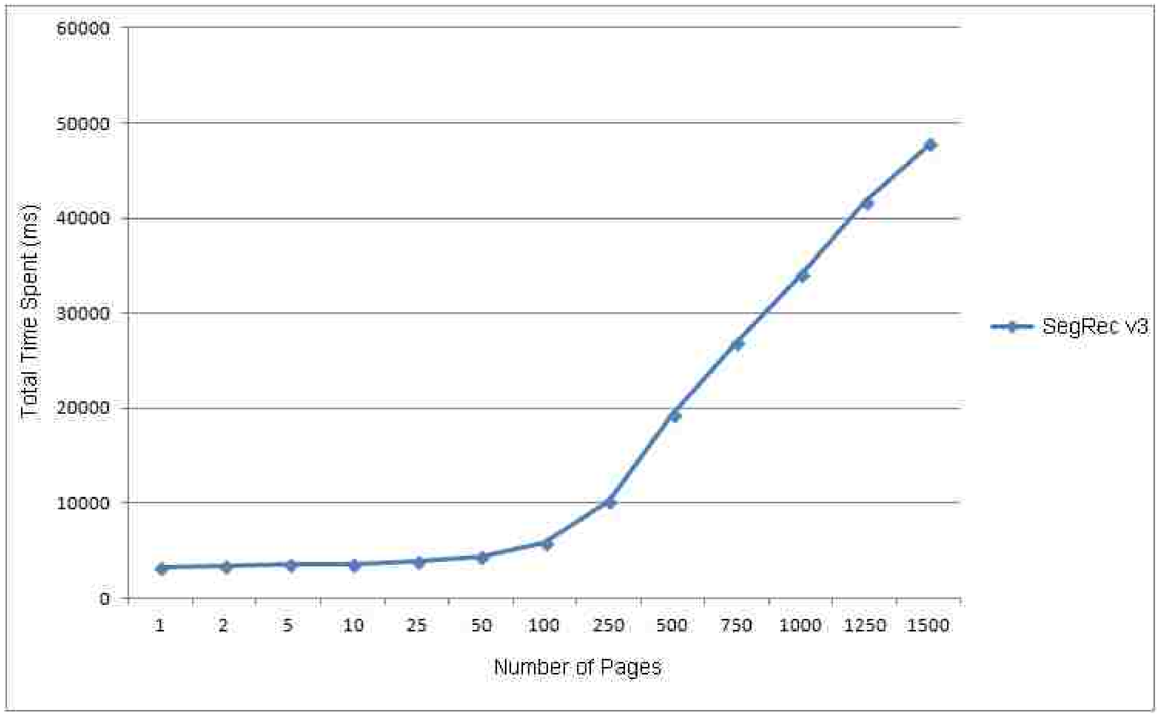

Figure 5.6: A graph of the total time SegRec v3 spent per number of pages in milliseconds. These metrics include time for reading the images from the hard drive and copying data to and from the GPU.

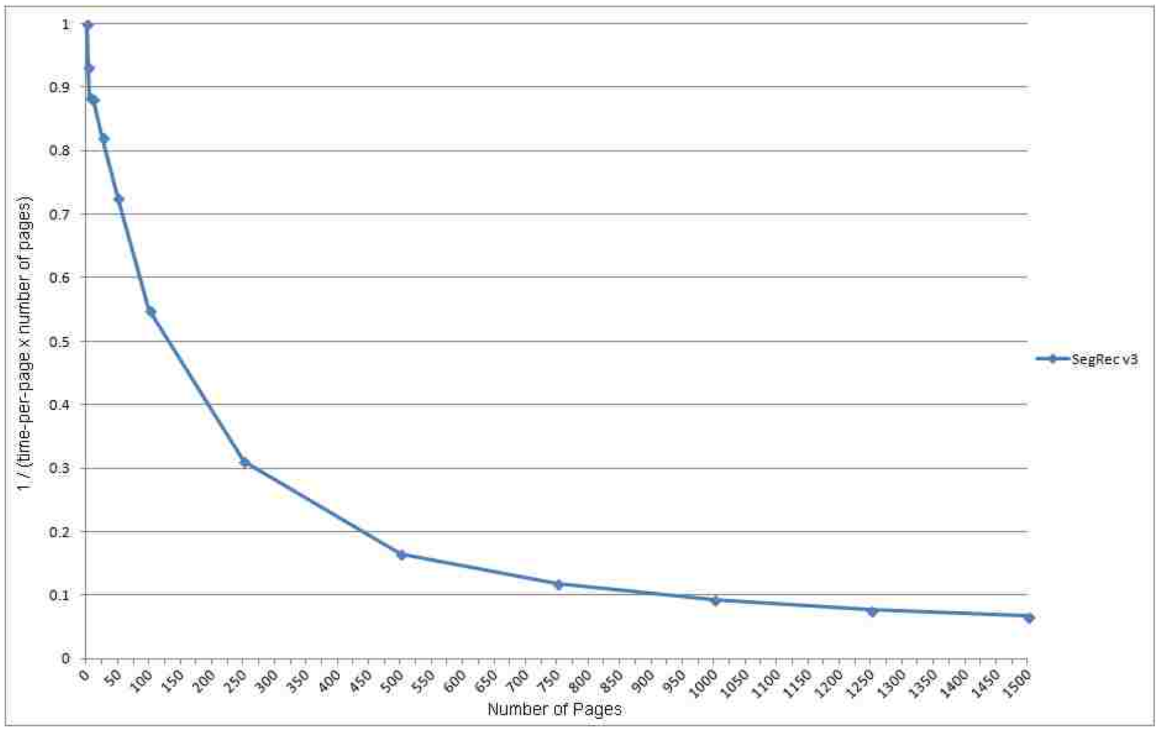

Figure 5.7: A graph of efficiency for SegRec v3 normalized to 1.

is recognizing at least some of the characters poorly. The micro-f score is the weighted average of how well the engine recognizes each character, with the weight of each character reflecting how many times the character appears in the text. For example, a micro-f score of 0.75 means that the engine is correctly recognizing 75% of the total character count, regardless of the type of character. A high micro-f score indicates that the engine is recognizing the vast majority of characters correctly and vice versa for a low or mid-range micro-f score. See Appendix A for a more in-depth discussion on the macro-f and micro-f metrics.

5.5 Discussion: Software limitations

I chose to implement SegRec v3 in C#.NET, which interfaces with CUDA via a third-party library called Cudafy.NET. Unfortunately, .NET has a ~2GB file limit size, which limits the amount of data I can read and push to the GPU in a single interaction. This limit is reached at approximately 1500 pages of text, which is why SegRec v3 test results only include results up to 1500 pages. The Tesla K40 GPU I test on is capable of supporting up to 12GB of data, which should hold approximately 9000 pages of text, given SegRec v3's current memory requirements. I plan to rewrite the .NET portion of SegRec v3 in a language that does not have such file size limitations in the future.

5.6 Discussion: Speed

Figure 5.5 shows the speed per page for SegRec v3 when running various numbers of pages. Figure 5.6 shows the total time taken by SegRec v3 when running various numbers of pages. The data shows that as SegRec v3 processes more pages, the time spent per page decreases in a non-linear fashion. In my experience, this decrease is typical of GPU processing. The reason for that is because the GPU tries to hide the latency of I/O operations. The GPU has been optimized so that context switching between threads costs almost nothing. So, when a thread warp issues an I/O operation and is idle while waiting for the instruction to complete, such as a global memory read or write (SegRec v3 uses global memory to store image and output data), the GPU will switch to a thread warp that is ready to execute instructions. In other words, the GPU pipelines I/O and takes advantage of nearly free context switches to minimize time spent actively executing idle warps and to maximize instruction execution throughput [34].

5.7 Discussion: Image sets

Normal image set

SegRec is significantly faster than any other engine, with a speedup of ×88 over Tesseract, ×7 over OmniPage Ultimate, and ×18 over ABBYY FineReader. All engines have high micro-f measures, meaning each engine recognizes the majority of characters correctly. The relatively low macro-f scores for SegRec w/GDC, Tesseract and Omnipage combined with the high micro-f scores indicate these engines struggle to recognize several character types. Examining the full character result tables in D, we see that SegRec w/GDC struggles to recognize the character “l”, mistaking it for an “i”, and Tesseract consistently mistakes the character “s” for “5” and the character “v“ for “V” (See Table 5.2). OmniPage recognizes each character type consistently well, but also recognizes extra characters that were not present which reduces the overall average for macro-f.

Table 5.2: The reason for the relatively low macro-f scores for SegRec w/GDC and Tesseract. A subset of the confusing character set for each engine.

Engine	ASCII/Unicode	Character	False Negatives	False Positives	True Positives	Actual Total
SegRec w/GDV	105	i	311	78,299	131,464	131,775
	108	l	78,508	2	6	78,514
Tesseract	53	5	0	25,734	0	0
	115	s	26,423	19	83,288	109,711
	86	V	0	10,180	2,131	2,131
	118	v	10,181	1	10,427	20,608

Noisy image set

Again, SegRec is significantly faster, with a speedup of ×103 over Tesseract, ×18 over OmniPage Ultimate, and ×53 over ABBYY FineReader. However, SegRec has significantly worse micro-f scores. The pixel count classification does the worst, which is expected, since the Noisy image set randomly adds connected pixels to the glyphs. The global density classification does better, but still far worse than the other three engines. SegRec struggles to recognize characters with the additional noise added — the pixel count and global density classification methods are unable to handle the additional noise. Additional training on noisy images may improve this result; however, more research should be conducted to find additional classification methods that fit the massively parallel nature of GPUs. The macro-f scores of each engine are significantly closer, but it turns out that the remaining engines recognize extra characters that are not present, which reduces their respective averages.

Scan1 and Scan2 image sets

Once again, SegRec is significantly faster, with a speedup of ×150 and ×159 over Tesseract, ×22 and ×38 over OmniPage Ultimate, and ×58 and ×50 over ABBYY FineReader for image sets Scan1 and Scan2, respectively. The accuracy metrics for SegRec are abysmal, but this result is expected for SegRec v3. The glyphs in sets Scan1 and Scan2, in most instances, are significantly degraded from their original, pristine state, upon which SegRec was trained. Additionally, many glyphs broke apart (see Figure 5.8) and SegRec treats each piece as a separate glyph — SegRec, in its current form, does not attempt to reconstruct a glyph.

5.8 Discussion: SegRec

Figure 5.9 shows the breakdown of the time spent by SegRec for each stage of the algorithm using pixel count classification, and Table 5.3 shows the actual time spent. The vast

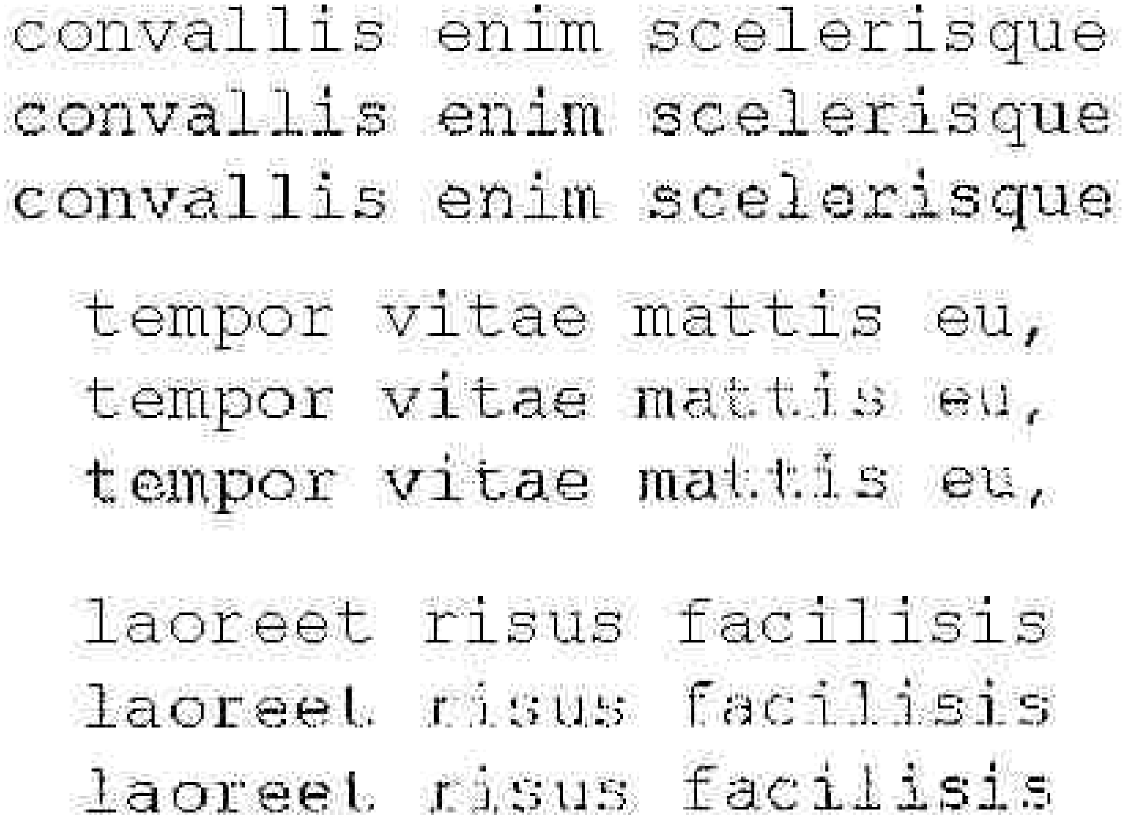

convallis enim scelerisque
convallis enim scelerisque
convallis enim scelerisque

tempor vitae mattis eu,
tempor vitae mattis eu,
tempor vitae mattis eu,

laoreet risus facilisis
laoreet risus facilisis
laoreet risus facilisis

Figure 5.8: A comparison of lines from the original image, the Scan1 image and the Scan2 image.

majority of execution time is spent in the compression stage because each successful compression sparks an additional run. There are, more than likely, optimizations that can be implemented to reduce the computational complexity of this stage.

The main focus of future work should be in additional and/or better classification methods and in reconstructing glyphs. The pixel count and global density classification methods served fine as prototypes, but it is clear, given the data, that there are better options — such as the methods implemented by Tesseract, OmniPage and ABBYY. Glyph reconstruction and, by proxy, assigning marks to their bases, should increase the effectiveness of SegRec as a whole.

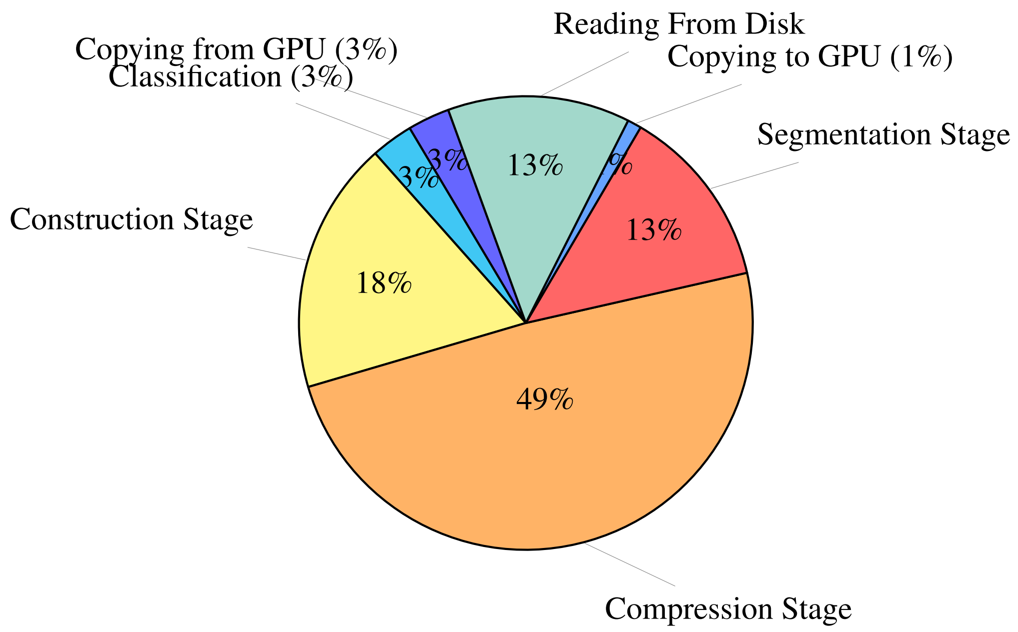

Figure 5.9: Breakdown of time spent for SegRec v3 using pixel count classification across all image sets. SegRec v3 using global density classification is similar, but with more time spent in the classification.

Table 5.3: Actual times for SegRec v3, averaged over 5 runs. “PC” signifies that SegRec used the pixel count vector for classification whereas “GDV” signifies SegRec used the global density vector for classification.

Image Set	**Reading From Disk**	**Copying to and from the GPU**	**Segmentation**	**Compression**	**Construction**	**Classification**
Normal w/PC (1000 images)	4,032ms	1,189ms	4,020ms	15,654ms	5,622ms	1,085ms
Normal w/GDC (1000 images)	3,975ms	1,253ms	3,994ms	15,756ms	5,518ms	5,145ms
Noisy w/PC (1000 images)	4,053ms	1,317ms	4,402ms	17,318ms	6,346ms	1,634ms
Noisy w/GDC (1000 images)	3,778ms	1,239ms	4,414ms	17,389ms	6,357ms	5,196ms
Scan1 w/PC (100 images)	561ms	157ms	1,071ms	2,982ms	3,451ms	410ms
Scan1 w/GDC (100 images)	595ms	174ms	1,069ms	2,992ms	3,448ms	1,018ms
Scan2 w/PC (100 images)	573ms	258ms	925ms	2,775ms	2,110ms	342ms
Scan2 w/GDC (100 images)	557ms	240ms	956ms	2,777ms	2,106ms	1,026ms

Chapter 6: Moving Forward

6.1 Improving SegRec

SegRec v3 is intentionally modularized to support easy modification within stages for the purposes of enhancing or altering existing functionality. For example, SegRec v3 employs the grid-and-count feature extraction method but could easily support other (or additional) methods such as longest run (page 32) or pattern-count (page 32). The grid-and-count method was chosen because it performs well, is easy to understand and is easy to implement. More research is necessary to determine the best feature-extraction algorithm for a GPU.

The classification algorithm employed by SegRec v3 is finding the closest training data match in Euclidean 25-space. This is a simple, brute-force classifier. More efficient and more complex classifiers are available and should be investigated for implementation on the GPU (such as a k-d tree). Research on improving feature extraction and identification should probably be conducted in tandem, as various classifiers may work better or worse depending on the type, quality and quantity of features extracted.

6.2 Towards a full-featured OCR engine

SegRec v3 provides an effective means for segmenting and identifying glyphs, but for a fully-featured OCR engine, that is not enough. SegRec v3, by itself, handles none of the pre- or post-processing tasks necessary for a full-fledged engine. Additionally, there are tasks that OCR engines must do to handle real-life data, such as splitting or joining glyphs and connecting marks with their base, that SegRec v3 does not currently handle. These tasks are part of a normal OCR engine and were simply omitted due to focusing primarily on the SegRec algorithms.

Pre-processing

For page or character rotation and skew, SegRec v3 can be trained on text that exhibits these flaws and, therefore, should be able to identify characters that are skewed or rotated. However, severely skewed or rotated text may still present a problem, and training will need to include various degrees of rotation and skew. Additionally, corrective algorithms can be implemented to fix rotated or skewed pages and lines, rather than simply training around them.

For pixel noise, SegRec v3 treats the noise as a glyph and outputs a XML record that can be discarded during the post-processing phase.

For all other pre-processing problems (degrees of contrast, bleed-through text and multiple colors of text) additional functionality must be added. The desired functionality varies depending on the intended use of the OCR engine. For example, severely degraded texts may have high contrast between various sections of text as well as sections of bleed-through. An adaptive thresholding algorithm might work best. For general purposes, global thresholding will work well.

Post-processing

SegRec v3 handles none of the typical post-processing tasks and, since SegRec v3 ignores character spacing within the original image, the task of grouping characters into words, paragraphs, columns and pages is pushed from the isolation phase to this phase. The output of SegRec v3 is a XML file containing the bounding box dimensions and original image coordinates for each glyph, so this phase must take this information, determine the original page layout and reconstruct the text appropriately (accounting for multiple columns, etc.).

Once the text is reconstructed, other post-processing steps can occur, such as performing language-specific dictionary checks to help identify and correct commonly miss-OCRed letters (such as "thc" instead of "the").

SegRec v3 is a promising step towards a fully functional OCR engine on the GPU.

Appendix A: Measures of accuracy and precision for OCR

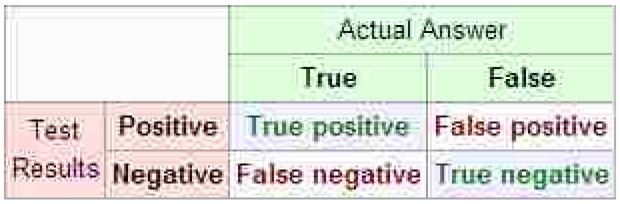

		Actual Answer	
		True	False
Test Results	Positive	True positive	False positive
	Negative	False negative	True negative

Figure A.1: Table for binary classification.
Adapted from `http://en.wikipedia.org/wiki/Accuracy_and_precision`

For a binary decision, the definitions of accuracy and precision are defined as follows:

- Accuracy:

$$\frac{true\ positives + true\ negatives}{true\ positives + true\ negatives + false\ positives + false\ negatives}$$

- Precision:

$$\frac{true\ positives}{true\ positives + false\ positives}$$

Additional useful statistical measures:

- Recall:

$$\frac{true\ positives}{true\ positives + false\ negatives}$$

- F-measure:

$$2 \cdot \frac{\text{Precision} \cdot \text{Recall}}{\text{Precision} + \text{Recall}}$$

For OCR, the notion of "true negative" is removed because it no longer applies — the OCR engine can only reply with an answer from the alphabet, it cannot respond "not-A", for example. The key concept for multinary classification, as relevant to OCR engines, is that an incorrect answer by the OCR engine counts as both a "false positive" and a "false negative". The answer counts as a false positive for the incorrect character presented as the answer and as a false negative for the answer that should have been presented. For example, if the answer is "A" and the engine responds with a "B", the response counts as a false positive for B and a false negative for A. A full classification table for the alphabet $[A, B, C]$ is shown in Figure A.2.

The statistical measures for multinary classification are called **micro** and **macro averaging** of F-measures. Macro averaging incorporates the base formulae for precision, recall and F-measure to calculate a value for an entire system. For a given alphabet, A, the equation for macro averaging is as follows:

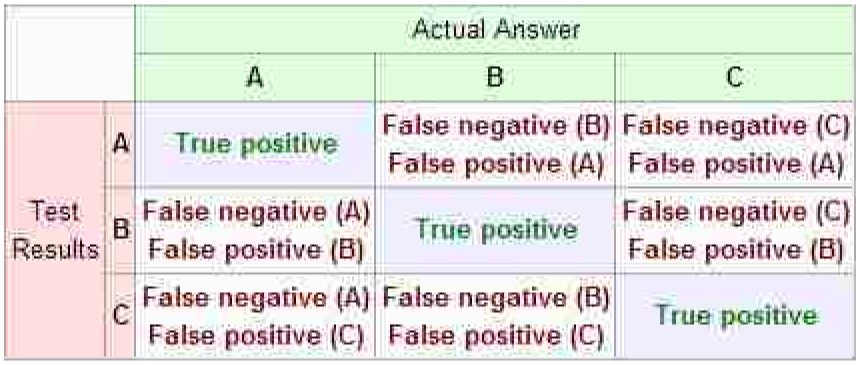

		Actual Answer		
		A	B	C
Test Results	A	True positive	False negative (B) False positive (A)	False negative (C) False positive (A)
	B	False negative (A) False positive (B)	True positive	False negative (C) False positive (B)
	C	False negative (A) False positive (C)	False negative (B) False positive (C)	True positive

Figure A.2: Table for multinary classification. The value in parenthesis denotes to which character the classification applies.
Adapted from `http://en.wikipedia.org/wiki/Accuracy_and_precision`

$$\text{Macro-F Average} = \frac{\sum_{i=1}^{|A|} \text{F-measure}(A_i)}{|A|}$$

The Macro-F equation has the effect of weighting each character within the alphabet the same. Conversely, micro averaging tends to assign heavier weights to more frequently used characters over less frequently used characters. For micro averaging, the base measures for precision and recall are modified as follows:

$$\text{Precision}^{micro} = \frac{\sum_{i=1}^{|A|} true\ positives_i}{\sum_{i=1}^{|A|}(true\ positives_i + false\ positives_i)}$$

$$\text{Recall}^{micro} = \frac{\sum_{i=1}^{|A|} true\ positives_i}{\sum_{i=1}^{|A|}(true\ positives_i + false\ negatives_i)}$$

Which gives the micro averaging F-measure equation:

$$\text{Micro-F} = 2 \cdot \frac{\text{Precision}^{micro} \cdot \text{Recall}^{micro}}{\text{Precision}^{micro} + \text{Recall}^{micro}}$$

Appendix B: Sample pages

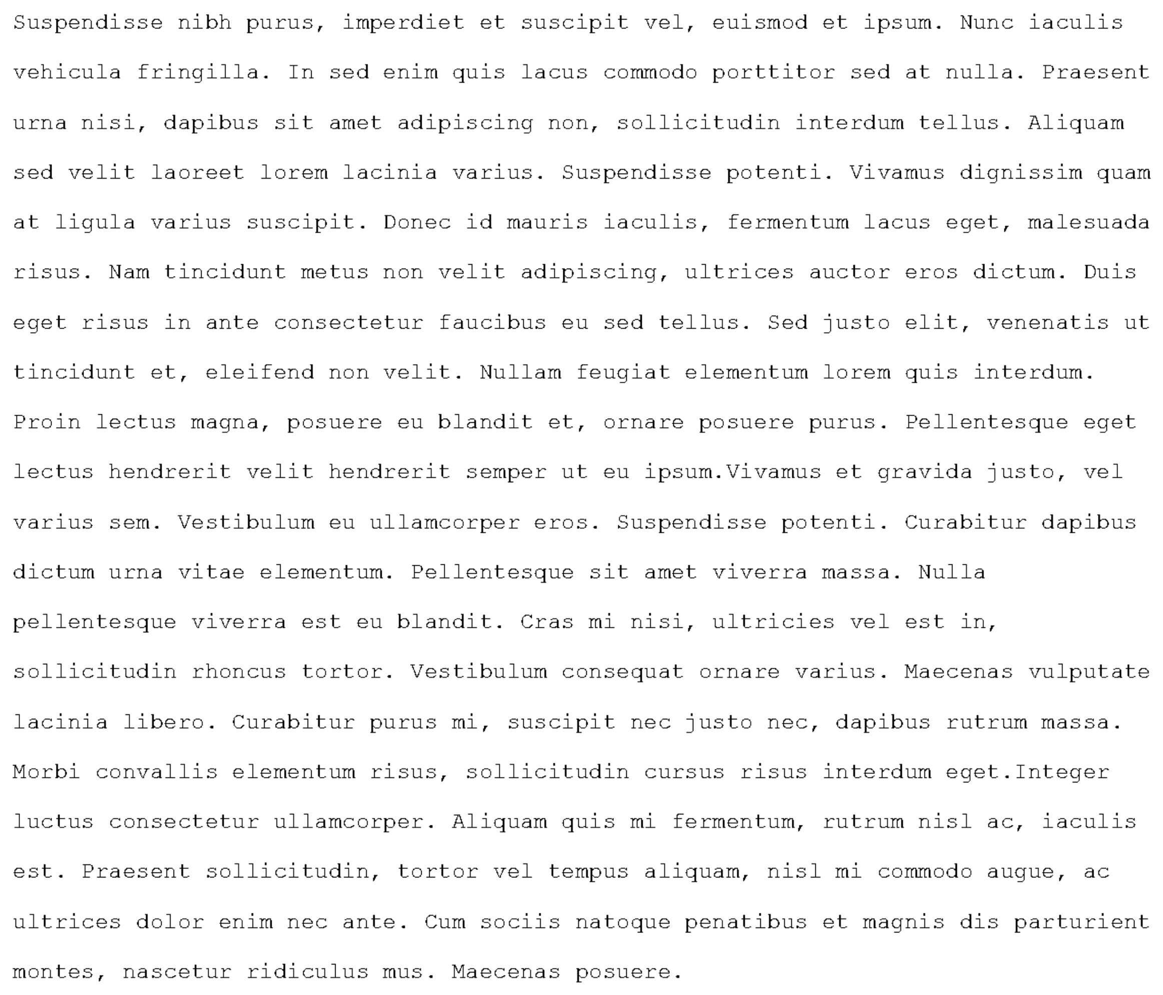

Suspendisse nibh purus, imperdiet et suscipit vel, euismod et ipsum. Nunc iaculis vehicula fringilla. In sed enim quis lacus commodo porttitor sed at nulla. Praesent urna nisi, dapibus sit amet adipiscing non, sollicitudin interdum tellus. Aliquam sed velit laoreet lorem lacinia varius. Suspendisse potenti. Vivamus dignissim quam at ligula varius suscipit. Donec id mauris iaculis, fermentum lacus eget, malesuada risus. Nam tincidunt metus non velit adipiscing, ultrices auctor eros dictum. Duis eget risus in ante consectetur faucibus eu sed tellus. Sed justo elit, venenatis ut tincidunt et, eleifend non velit. Nullam feugiat elementum lorem quis interdum. Proin lectus magna, posuere eu blandit et, ornare posuere purus. Pellentesque eget lectus hendrerit velit hendrerit semper ut eu ipsum.Vivamus et gravida justo, vel varius sem. Vestibulum eu ullamcorper eros. Suspendisse potenti. Curabitur dapibus dictum urna vitae elementum. Pellentesque sit amet viverra massa. Nulla pellentesque viverra est eu blandit. Cras mi nisi, ultricies vel est in, sollicitudin rhoncus tortor. Vestibulum consequat ornare varius. Maecenas vulputate lacinia libero. Curabitur purus mi, suscipit nec justo nec, dapibus rutrum massa. Morbi convallis elementum risus, sollicitudin cursus risus interdum eget.Integer luctus consectetur ullamcorper. Aliquam quis mi fermentum, rutrum nisl ac, iaculis est. Praesent sollicitudin, tortor vel tempus aliquam, nisl mi commodo augue, ac ultrices dolor enim nec ante. Cum sociis natoque penatibus et magnis dis parturient montes, nascetur ridiculus mus. Maecenas posuere.

Figure B.1: The original, perfect page.

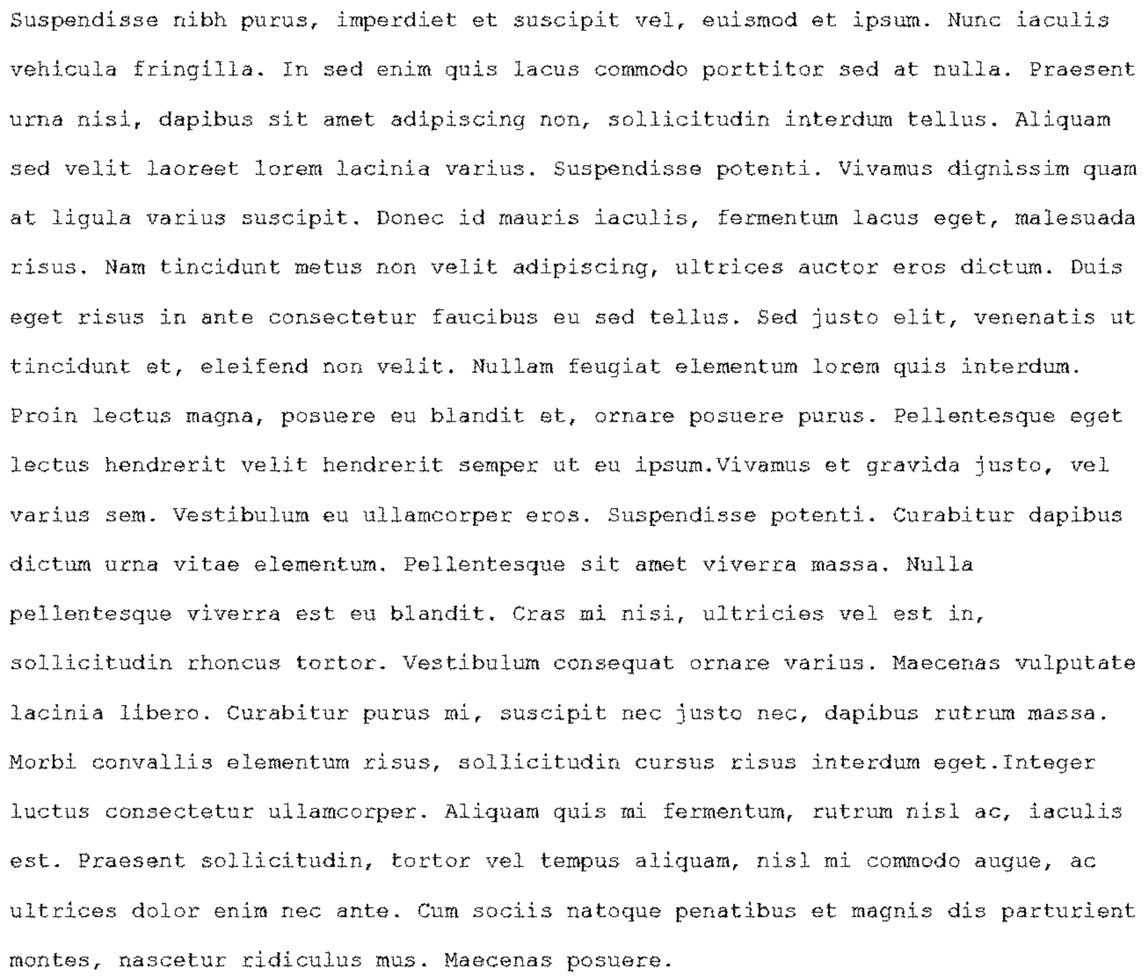

Suspendisse nibh purus, imperdiet et suscipit vel, euismod et ipsum. Nunc iaculis vehicula fringilla. In sed enim quis lacus commodo porttitor sed at nulla. Praesent urna nisi, dapibus sit amet adipiscing non, sollicitudin interdum tellus. Aliquam sed velit laoreet lorem lacinia varius. Suspendisse potenti. Vivamus dignissim quam at ligula varius suscipit. Donec id mauris iaculis, fermentum lacus eget, malesuada risus. Nam tincidunt metus non velit adipiscing, ultrices auctor eros dictum. Duis eget risus in ante consectetur faucibus eu sed tellus. Sed justo elit, venenatis ut tincidunt et, eleifend non velit. Nullam feugiat elementum lorem quis interdum. Proin lectus magna, posuere eu blandit et, ornare posuere purus. Pellentesque eget lectus hendrerit velit hendrerit semper ut eu ipsum.Vivamus et gravida justo, vel varius sem. Vestibulum eu ullamcorper eros. Suspendisse potenti. Curabitur dapibus dictum urna vitae elementum. Pellentesque sit amet viverra massa. Nulla pellentesque viverra est eu blandit. Cras mi nisi, ultricies vel est in, sollicitudin rhoncus tortor. Vestibulum consequat ornare varius. Maecenas vulputate lacinia libero. Curabitur purus mi, suscipit nec justo nec, dapibus rutrum massa. Morbi convallis elementum risus, sollicitudin cursus risus interdum eget.Integer luctus consectetur ullamcorper. Aliquam quis mi fermentum, rutrum nisl ac, iaculis est. Praesent sollicitudin, tortor vel tempus aliquam, nisl mi commodo augue, ac ultrices dolor enim nec ante. Cum sociis natoque penatibus et magnis dis parturient montes, nascetur ridiculus mus. Maecenas posuere.

Figure B.2: The same page with noise added.

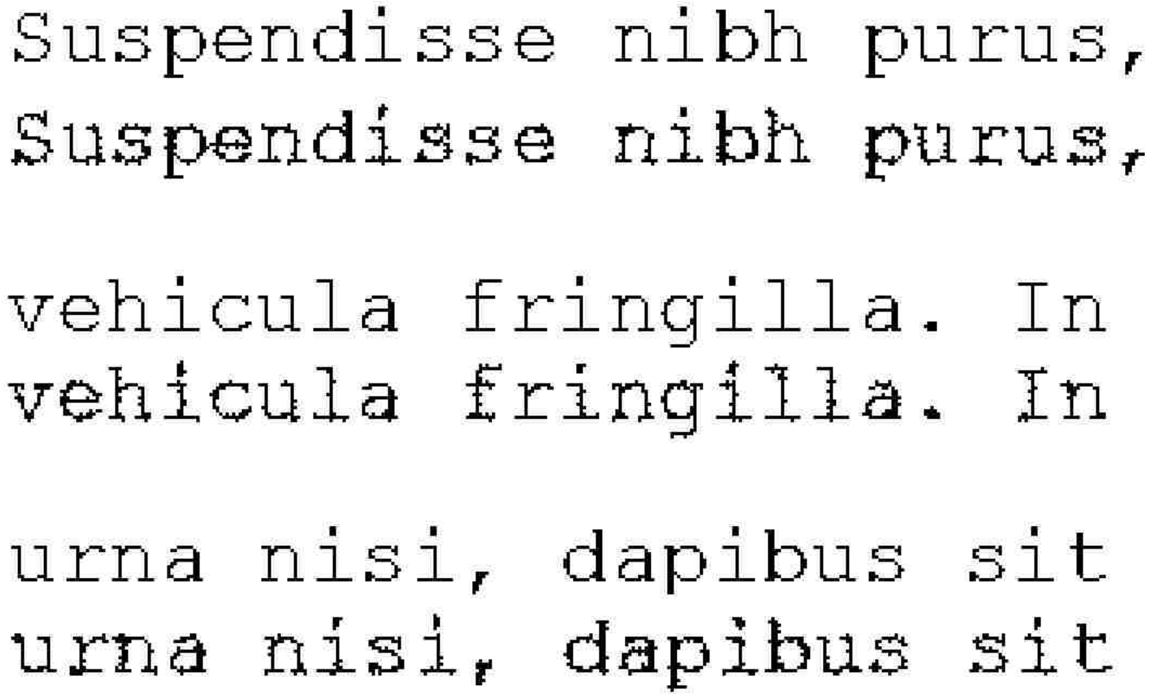
Suspendisse nibh purus,
Suspendisse nibh purus,

vehicula fringilla. In
vehicula fringilla. In

urna nisi, dapibus sit
urna nisi, dapibus sit

Figure B.3: A comparison of lines from the original image and the noise-added image.

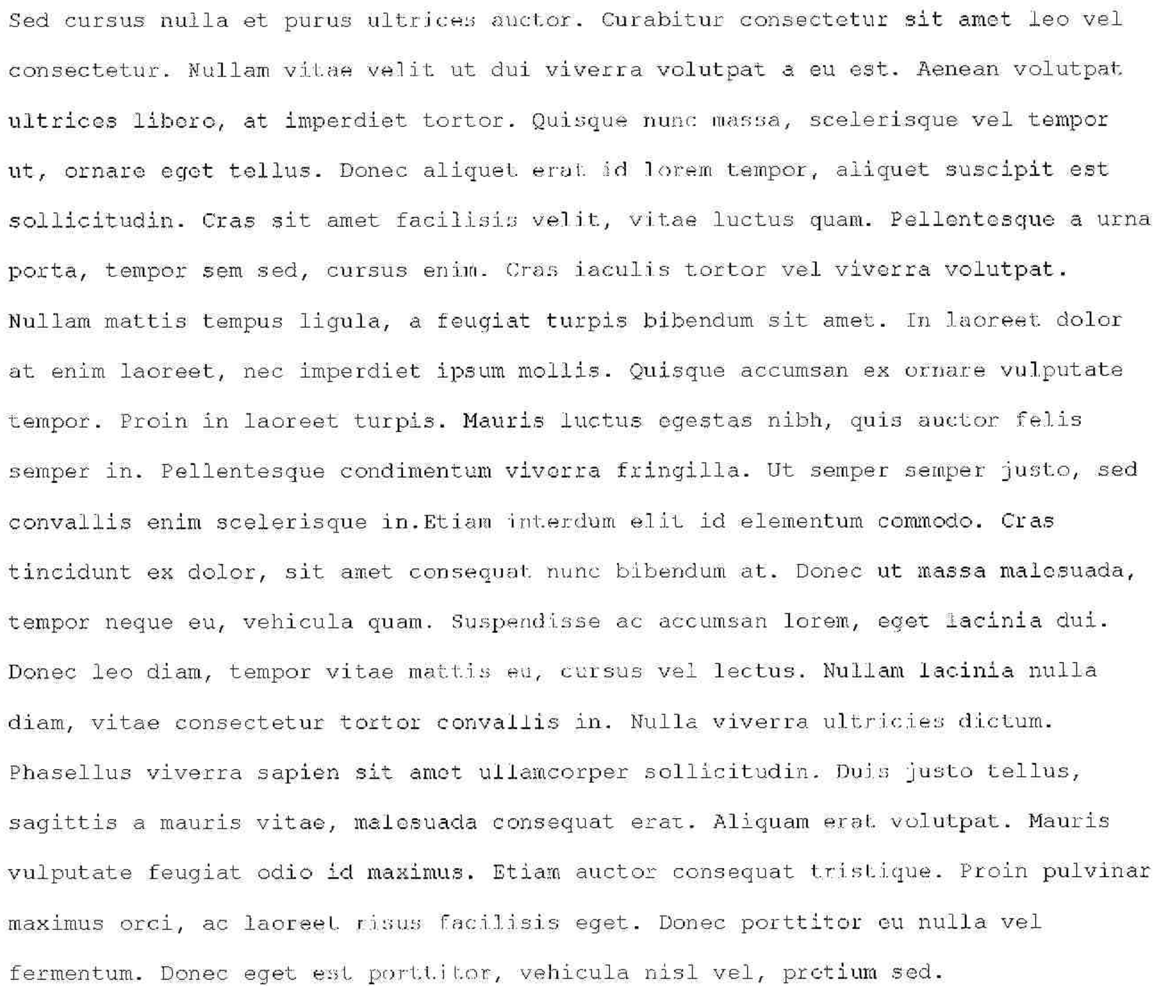
Sed cursus nulla et purus ultrices auctor. Curabitur consectetur sit amet leo vel consectetur. Nullam vitae velit ut dui viverra volutpat a eu est. Aenean volutpat ultrices libero, at imperdiet tortor. Quisque nunc massa, scelerisque vel tempor ut, ornare eget tellus. Donec aliquet erat id lorem tempor, aliquet suscipit est sollicitudin. Cras sit amet facilisis velit, vitae luctus quam. Pellentesque a urna porta, tempor sem sed, cursus enim. Cras iaculis tortor vel viverra volutpat. Nullam mattis tempus ligula, a feugiat turpis bibendum sit amet. In laoreet dolor at enim laoreet, nec imperdiet ipsum mollis. Quisque accumsan ex ornare vulputate tempor. Proin in laoreet turpis. Mauris luctus egestas nibh, quis auctor felis semper in. Pellentesque condimentum viverra fringilla. Ut semper semper justo, sed convallis enim scelerisque in.Etiam interdum elit id elementum commodo. Cras tincidunt ex dolor, sit amet consequat nunc bibendum at. Donec ut massa malesuada, tempor neque eu, vehicula quam. Suspendisse ac accumsan lorem, eget lacinia dui. Donec leo diam, tempor vitae mattis eu, cursus vel lectus. Nullam lacinia nulla diam, vitae consectetur tortor convallis in. Nulla viverra ultricies dictum. Phasellus viverra sapien sit amet ullamcorper sollicitudin. Duis justo tellus, sagittis a mauris vitae, malesuada consequat erat. Aliquam erat volutpat. Mauris vulputate feugiat odio id maximus. Etiam auctor consequat tristique. Proin pulvinar maximus orci, ac laoreet risus facilisis eget. Donec porttitor eu nulla vel fermentum. Donec eget est porttitor, vehicula nisl vel, pretium sed.

Figure B.4: A page printed and then scanned.

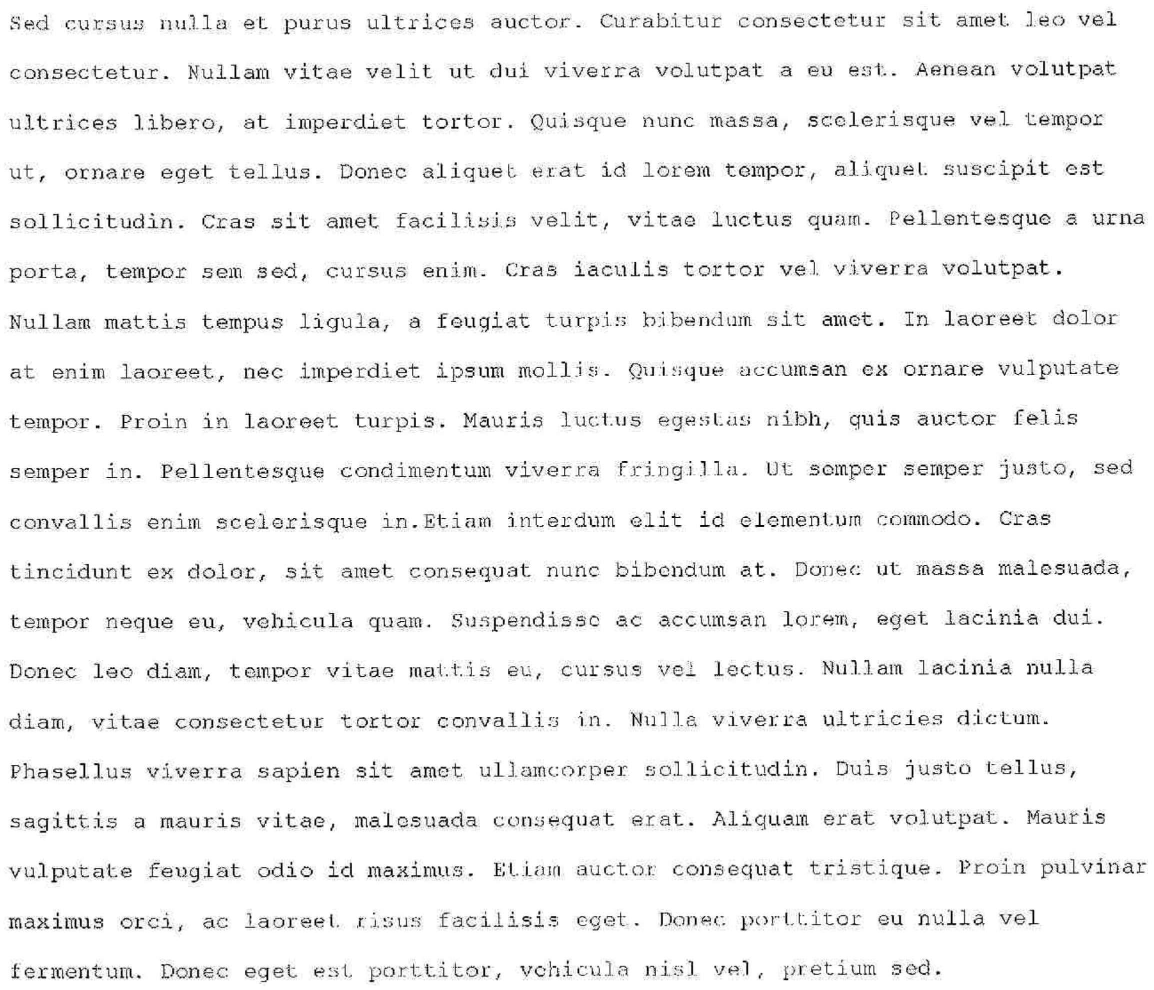

Sed cursus nulla et purus ultrices auctor. Curabitur consectetur sit amet leo vel consectetur. Nullam vitae velit ut dui viverra volutpat a eu est. Aenean volutpat ultrices libero, at imperdiet tortor. Quisque nunc massa, scelerisque vel tempor ut, ornare eget tellus. Donec aliquet erat id lorem tempor, aliquet suscipit est sollicitudin. Cras sit amet facilisis velit, vitae luctus quam. Pellentesque a urna porta, tempor sem sed, cursus enim. Cras iaculis tortor vel viverra volutpat. Nullam mattis tempus ligula, a feugiat turpis bibendum sit amet. In laoreet dolor at enim laoreet, nec imperdiet ipsum mollis. Quisque accumsan ex ornare vulputate tempor. Proin in laoreet turpis. Mauris luctus egestas nibh, quis auctor felis semper in. Pellentesque condimentum viverra fringilla. Ut semper semper justo, sed convallis enim scelerisque in.Etiam interdum elit id elementum commodo. Cras tincidunt ex dolor, sit amet consequat nunc bibendum at. Donec ut massa malesuada, tempor neque eu, vehicula quam. Suspendisse ac accumsan lorem, eget lacinia dui. Donec leo diam, tempor vitae mattis eu, cursus vel lectus. Nullam lacinia nulla diam, vitae consectetur tortor convallis in. Nulla viverra ultricies dictum. Phasellus viverra sapien sit amet ullamcorper sollicitudin. Duis justo tellus, sagittis a mauris vitae, malesuada consequat erat. Aliquam erat volutpat. Mauris vulputate feugiat odio id maximus. Etiam auctor consequat tristique. Proin pulvinar maximus orci, ac laoreet risus facilisis eget. Donec porttitor eu nulla vel fermentum. Donec eget est porttitor, vehicula nisl vel, pretium sed.

Figure B.5: The same page printed, scanned, re-printed and re-scanned.

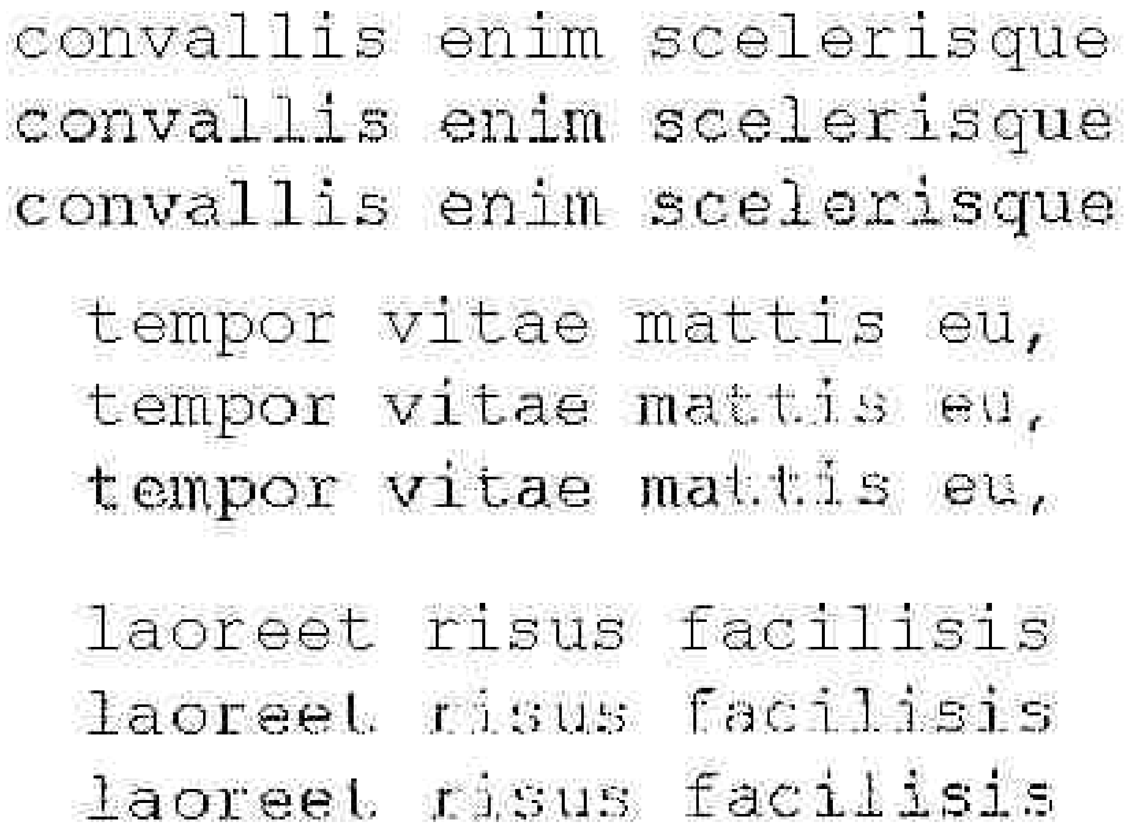
convallis enim scelerisque
convallis enim scelerisque
convallis enim scelerisque

tempor vitae mattis eu,
tempor vitae mattis eu,
tempor vitae mattis eu,

laoreet risus facilisis
laoreet risus facilisis
laoreet risus facilisis

Figure B.6: A comparison of lines from the original image, the scan1 image and the scan2 image.

Appendix C: Avoiding branching with inline Boolean expressions

This section addresses the question of whether inline Boolean expressions avoid branching on NVIDIA hardware. In CUDA C, inline Boolean expressions evaluate to 1 for *true* and 0 for $false$. A shrewd programmer can take advantage of this fact.

The two functions, `example1` and `example2`, written in CUDA C and shown in Figures C.1 and C.2, respectively, are functionally identical. Function `example1` contains several nested **if** statements, and function `example2` implements the same functionality with inline Boolean statements. The compiled **PTX**[1] code for `example1` is in Figure C.3 and C.4. The branching instructions in the figures are highlighted in red, and the labels, which serve as jump targets, are highlighted in purple. Figure C.5 contains the code for `example2`. It contains no branch instructions or jump targets. Clearly, using inline Boolean expressions avoids branching.

However, threads running `example2` might execute many more instructions overall, so whether avoiding branching actually helps increase execution speed remains unclear. Benchmarking and testing can determine which function will perform the best given real-world data. The tests and results that follow were conducted and gathered using a GTX 480.

A grid of 65,535 blocks each containing 1,024 threads executes each function — a total of 67,107,840 executions per function — and Table C.1 provides the results given by the NVIDIA command-line profiler, **nvprov**[2]. **Branch efficiency**, the ratio of non-divergent branches to total branches, is controlled by altering the input data to force `example1` to execute a specific code path out of the four alternatives[3]. Table C.1 compares the execution time of `example1` and `example2` at several different **branch efficiencies**. As branch efficiency decreases, the run-time of `example1` increases, while the run-time of `example2` remains relatively constant. This is the predicted behavior. Unexpectedly, the run-time for `example1` at 100% branch efficiency is about 1ms slower than `example2`.

Table C.2 is a subset of the metrics available from nvprof (full list shown in Table C.3) and contains metrics where the values gathered by nvprof for each function differ by a significant amount. The first metric shown, "Executed Instructs Per Cycle", provides a reason for the difference in speed. Even at 100% branch efficiency, the function `example1` had a much lower executed instruction throughput than `example2`. I hypothesize that the reason for the difference in throughput is the additional number of control-flow instructions[4] executed by `example1`. The data in Table C.2 seems to support this hypothesis. Over the course of the ~67M function executions, `example1` issues and executes 4× more control-flow instructions than `example2`[5] (8,388,840 to 2,097,120). This metric is the only instruc-

[1]PTX is an assembly-like language generated by the NVIDIA CUDA compiler and is used by NVIDIA's GPUs [34, 35].

[2]NVIDIA's command-line profiler, nvprov, provides information such as run-time, occupancy, and throughput among a myriad of other metrics [36].

[3]The code paths are labeled via comments — see Figure C.1.

[4]**Control-flow** instructions are PTX instructions related to **if**, **switch**, **do**, **for**, and **while** statements [34].

[5]Remember that NVIDIA GPUs operate with the SIMT (Single Instruction, Multiple Threads) architec-

tion that `example1` executes more than `example2`. For all others — integer instructions, load/store instructions, miscellaneous instructions, etc. — `example2` executes more.

Table C.1: Run-time vs. branch efficiency averaged over 5 runs

Branch Efficiency	**`example1`**	**`example2`**	**Execution Percentages**			
			Path 1	Path 2	Path 3	Path 4
100%	11.281ms	10.176ms	100%	0%	0%	0%
83.3%	12.009ms	10.179ms	75%	25%	0%	0%
75.0%	13.591ms	10.180ms	50%	25%	25%	0%
70.0%	14.282ms	10.180ms	25%	25%	25%	25%

Table C.2: Subset of the metrics from Table C.3 depicting significant differences.

Metric Name	**Description**	**`example1`**	**`example2`**
ipc	Executed Instructions Per Cycle (IPC)	0.664111	0.758048
issued_ipc	Issued Instructions Per Cycle	0.664146	0.795211
inst_per_warp	Instructions per warp	30.000000	33.000000
eligible_warps_per_cycle	Eligible Warps Per Active Cycle	2.567671	2.868818
inst_issued	Instructions Issued	62,916,912	72,597,662
inst_executed	Instructions Executed	62,913,600	69,204,960
cf_issued	Issued Control-Flow Instructions	8,388,480	2,097,120
cf_executed	Executed Control-Flow Instructions	8,388,480	2,097,120
inst_integer	Integer Instructions	1,140,833,280	1,476,372,480
inst_control	Control-Flow Instructions	134,215,680	67,107,840
inst_compute_ld_st	Load/Store Instructions	268,431,360	268,431,360
inst_misc	Misc Instructions	335,539,200	402,647,040
ldst_issued	Issued Load/Store Instructions	8,389,470	11,778,315
inst_replay_overhead	Instruction Replay Overhead	0.000053	0.049024
alu_fu_utilization	Arithmetic Function Unit Utilization	Low (3)	Mid (4)
issue_slots	Issue Slots	62,916,912	72,597,662
issue_slot_utilization	Issue Slot Utilization	33.21%	39.76%

ture which means that 1 instruction is issued to a full warp of 32 threads. The warp executes the instruction as a group, unless there is warp divergence. See "Introduction to GPUs" on page 42.

```
__global__  void check1(int* a, int* b, int* c, int* d) {
  //  calculate global thread ID
  int gID = blockIdx.x * blockDim.x + threadIdx.x;
  if (a[gID] < b[gID]) {
    if (((b[gID] - a[gID]) * 2 + 1) <= (c[gID] % 5))
      d[gID] = 1; // path 1
    else
      d[gID] = 0; // path 2
  } else if (a[gID] >= b[gID]) {
    if (((a[gID] - b[gID]) * 2) <= (c[gID] % 5))
      d[gID] = 1; // path 3
    else
      d[gID] = 0; // path 4
    }
}
```

Figure C.1: CUDA C version of function `example1`.

```
__global__ void check2(int* a, int* b, int* c, int* d) {
  //  calculate global thread ID
  int gID = blockIdx.x * blockDim.x + threadIdx.x;
  d[gID] = (a[gID] < b[gID]) * (((b[gID] - a[gID]) * 2 + 1) <= (c[gID] % 5))
         + (a[gID] >= b[gID]) * (((a[gID] - b[gID]) * 2) <= (c[gID] % 5));
}
```

Figure C.2: CUDA C version of function `example2`.

```
.version 4.2
.target sm_20
.address_size 64

.visible .entry _example1(
  .param .u64 _example1_param_0,
  .param .u64 _example1_param_1,
  .param .u64 _example1_param_2,
  .param .u64 _example1_param_3
)
{
  .reg .pred              %p<5>;
  .reg .s32               %r<29>;
  .reg .s64               %rd<14>;

  ld.param.u64            %rd3, [_example1_param_0];
  ld.param.u64            %rd4, [_example1_param_1];
  ld.param.u64            %rd5, [_example1_param_2];
  ld.param.u64            %rd6, [_example1_param_3];
  cvta.to.global.u64      %rd7, %rd6;
  mov.u32                 %r3, %ntid.x;
  mov.u32                 %r4, %ctaid.x;
  mov.u32                 %r5, %tid.x;
  mad.lo.s32              %r6, %r3, %r4, %r5;
  cvta.to.global.u64      %rd8, %rd3;
  mul.wide.s32            %rd9, %r6, 4;
  add.s64                 %rd10, %rd8, %rd9;
  cvta.to.global.u64      %rd11, %rd4;
  add.s64                 %rd12, %rd11, %rd9;
  ld.global.u32           %r1, [%rd12];
  ld.global.u32           %r2, [%rd10];
  setp.lt.s32             %p1, %r2, %r1;
  cvta.to.global.u64      %rd13, %rd5;
  add.s64                 %rd1, %rd13, %rd9;
  add.s64                 %rd2, %rd7, %rd9;
  @%p1 bra                BB0_4;
  bra.uni                 BB0_1;

BB0_4:
  sub.s32                 %r18, %r1, %r2;
  shl.b32                 %r19, %r18, 1;
  ld.global.u32           %r20, [%rd1];
  mul.hi.s32              %r21, %r20, 1717986919;
  shr.u32                 %r22, %r21, 31;
  shr.s32                 %r23, %r21, 1;
  add.s32                 %r24, %r23, %r22;
  mul.lo.s32              %r25, %r24, 5;
  sub.s32                 %r26, %r20, %r25;
  setp.lt.s32             %p3, %r19, %r26;
  @%p3 bra                BB0_6;
  bra.uni                 BB0_5;

BB0_6:
  mov.u32                 %r28, 1;
  st.global.u32           [%rd2], %r28;
  bra.uni                 BB0_7;


```

Figure C.3: PTX version of function `example1`.

```
BB0_1:
  sub.s32                  %r7, %r2, %r1;
  shl.b32                  %r8, %r7, 1;
  ld.global.u32            %r9, [%rd1];
  mul.hi.s32               %r10, %r9, 1717986919;
  shr.u32                  %r11, %r10, 31;
  shr.s32                  %r12, %r10, 1;
  add.s32                  %r13, %r12, %r11;
  mul.lo.s32               %r14, %r13, 5;
  sub.s32                  %r15, %r9, %r14;
  setp.gt.s32              %p2, %r8, %r15;
  @%p2 bra                 BB0_3;
  bra.uni                  BB0_2;

BB0_3:
  mov.u32                  %r17, 0;
  st.global.u32            [%rd2], %r17;
  bra.uni                  BB0_7;

BB0_5:
  mov.u32                  %r27, 0;
  st.global.u32            [%rd2], %r27;
  bra.uni                  BB0_7;

BB0_2:
  mov.u32                  %r16, 1;
  st.global.u32            [%rd2], %r16;

BB0_7:
  ret;
}
```

Figure C.4: PTX version of function `example1` continued.

```
.version 4.2
.target sm_20
.address_size 64

// .globl        _example2

.visible .entry _example2(
  .param .u64 _example2_param_0,
  .param .u64 _example2_param_1,
  .param .u64 _example2_param_2,
  .param .u64 _example2_param_3
)
{
  .reg .pred                %p<7>;
  .reg .s32                 %r<21>;
  .reg .s64                 %rd<14>;

  ld.param.u64              %rd1, [_example2_param_0];
  ld.param.u64              %rd2, [_example2_param_1];
  ld.param.u64              %rd3, [_example2_param_2];
  ld.param.u64              %rd4, [_example2_param_3];
  cvta.to.global.u64        %rd5, %rd4;
  cvta.to.global.u64        %rd6, %rd3;
  cvta.to.global.u64        %rd7, %rd2;
  cvta.to.global.u64        %rd8, %rd1;
  mov.u32                   %r1, %ctaid.x;
  mov.u32                   %r2, %ntid.x;
  mov.u32                   %r3, %tid.x;
  mad.lo.s32                %r4, %r2, %r1, %r3;
  mul.wide.s32              %rd9, %r4, 4;
  add.s64                   %rd10, %rd8, %rd9;
  ld.global.u32             %r5, [%rd10];
  add.s64                   %rd11, %rd7, %rd9;
  ld.global.u32             %r6, [%rd11];
  setp.gt.s32               %p1, %r6, %r5;
  sub.s32                   %r7, %r6, %r5;
  shl.b32                   %r8, %r7, 1;
  add.s64                   %rd12, %rd6, %rd9;
  ld.global.u32             %r9, [%rd12];
  mul.hi.s32                %r10, %r9, 1717986919;
  shr.u32                   %r11, %r10, 31;
  shr.s32                   %r12, %r10, 1;
  add.s32                   %r13, %r12, %r11;
  mul.lo.s32                %r14, %r13, 5;
  sub.s32                   %r15, %r9, %r14;
  setp.lt.s32               %p2, %r8, %r15;
  and.pred                  %p3, %p2, %p1;
  selp.u32                  %r16, 1, 0, %p3;
  setp.gt.s32               %p4, %r5, %r6;
  sub.s32                   %r17, %r5, %r6;
  shl.b32                   %r18, %r17, 1;
  setp.le.s32               %p5, %r18, %r15;
  and.pred                  %p6, %p5, %p4;
  selp.u32                  %r19, 1, 0, %p6;
  add.s32                   %r20, %r19, %r16;
  add.s64                   %rd13, %rd5, %rd9;
  st.global.u32             [%rd13], %r20;
  ret;
}
```

Figure C.5: PTX version of function `example2`.

Table C.3: Nvprof output for `example1` and `example2` (excluding metrics reporting no activity).

Metric Name	Description	`example1`	`example2`
achieved_occupancy	Achieved Occupancy	0.586682	0.572264
branch_efficiency	Branch Efficiency	100.00%	100.00%
warp_execution_efficiency	Warp Execution Efficiency	100.00%	100.00%
sm_efficiency	Multiprocessor Activity	93.48%	92.33%
ipc	Executed Instructions Per Cycle (IPC)	0.664111	0.758048
issued_ipc	Issued Instructions Per Cycle	0.664146	0.795211
inst_per_warp	Instructions per warp	30.000000	33.000000
eligible_warps_per_cycle	Eligible Warps Per Active Cycle	2.567671	2.868818
inst_issued	Instructions Issued	62,916,912	72,597,662
inst_executed	Instructions Executed	62,913,600	69,204,960
cf_issued	Issued Control-Flow Instructions	8,388,480	2,097,120
cf_executed	Executed Control-Flow Instructions	8,388,480	2,097,120
inst_integer	Integer Instructions	1,140,833,280	1,476,372,480
inst_control	Control-Flow Instructions	134,215,680	67,107,840
inst_compute_ld_st	Load/Store Instructions	268,431,360	268,431,360
inst_misc	Misc Instructions	335,539,200	402,647,040
ldst_issued	Issued Load/Store Instructions	8,389,470	11,778,315
ldst_executed	Executed Load/Store Instructions	8,388,480	8,388,480
inst_replay_overhead	Instruction Replay Overhead	0.000053	0.049024
gld_requested_throughput	Requested Global Load Throughput	83.735GB/s	85.950GB/s
gst_requested_throughput	Requested Global Store Throughput	27.912GB/s	28.650GB/s
gld_transactions	Global Load Transactions	6,297,840	6,294,240
gst_transactions	Global Store Transactions	2,099,400	2,100,120
gld_transactions_per_request	Global Load Transactions Per Request	1.001030	1.000458
gst_transactions_per_request	Global Store Transactions Per Request	1.001087	1.001431
gst_throughput	Global Store Throughput	27.912GB/s	28.650GB/s
gld_throughput	Global Load Throughput	83.821GB/s	85.989GB/s
gst_efficiency	Global Memory Store Efficiency	100.00%	100.00%
gld_efficiency	Global Memory Load Efficiency	99.90%	99.95%
stall_inst_fetch	Issue Stall Reasons (Instructions Fetch)	5.35%	3.03%
stall_exec_dependency	Issue Stall Reasons (Input Not Available)	12.39%	13.15%
stall_memory_dependency	Issue Stall Reasons (Data Request)	74.42%	76.33%
stall_other	Issue Stall Reasons (Other)	2.51%	2.81%
stall_pipe_busy	Issue Stall Reasons (Pipe Busy)	5.33%	4.68%
stall_memory_throttle	Issue Stall Reasons (Memory Throttle)	0.00%	0.02%
global_cache_replay_overhead	Global Memory Cache Replay Overhead	0.100149	0.091029
dram_read_transactions	Device Memory Read Transactions	25,457,261	25,459,065
dram_write_transactions	Device Memory Write Transactions	8,389,014	8,388,499
dram_read_throughput	Device Memory Read Throughput	84.706GB/s	86.952GB/s
dram_write_throughput	Device Memory Write Throughput	27.914GB/s	28.650GB/s
dram_utilization	Device Memory Utilization	High (7)	High (7)
l2_l1_read_throughput	L2 Cache Throughput (L1 Reads)	83.735GB/s	85.950GB/s
l2_read_transactions	L2 Cache Read Transactions	25,466,315	25,461,201
l2_write_transactions	L2 Cache Write Transactions	8,388,885	8,388,499
l2_read_throughput	L2 Cache Throughput (Reads)	84.736GB/s	86.960GB/s
l2_write_throughput	L2 Cache Throughput (Writes)	27.913GB/s	28.650GB/s
l2_l1_read_transactions	L2 Read Transactions (L1 read requests)	25,165,440	25,165,440
l2_l1_write_transactions	L2 Write Transactions (L1 write requests	8,388,480	8,388,480
l2_l1_write_throughput	L2 Throughput (L1 Writes)	27.912GB/s	28.650GB/s
l2_utilization	L2 Cache Utilization	Mid (5)	Mid (5)
l1_shared_utilization	L1/Shared Memory Utilization	Low (1)	Low (1)
ldst_fu_utilization	Load/Store Function Unit Utilization	Low (1)	Low (1)
alu_fu_utilization	Arithmetic Function Unit Utilization	Low (3)	Mid (4)
cf_fu_utilization	Control-Flow Function Unit Utilization	Low (1)	Low (1)
issue_slots	Issue Slots	62,916,912	72,597,662
issue_slot_utilization	Issue Slot Utilization	33.21%	39.76%

Appendix D: Full character results from testing

Table D.1: Character results from SegRec v3 versus the Normal image set using pixel count classification.

ASCII/Unicode	Character	False Negatives	False Positives	True Positives	Actual Total
44	,	44	135	21,067	21,111
46	.	7	928	30,636	30,643
59	;	135	0	0	135
65	A	7	0	2,210	2,217
67	C	4	0	2,515	2,519
68	D	8	0	3,037	3,045
69	E	10	0	1,030	1,040
70	F	4	0	1,003	1,007
73	I	8	3	2,246	2,254
74	J	0	3	0	0
76	L	3	0	146	149
77	M	13	0	3,048	3,061
78	N	11	0	4,120	4,131
80	P	11	0	4,137	4,148
81	Q	4	0	1,038	1,042
83	S	20	0	3,119	3,139
85	U	3	0	1,027	1,030
86	V	8	0	2,123	2,131
97	a	226	0	105,378	105,604
98	b	49	0	15,835	15,884
99	c	120	34	53,487	53,607
100	d	103	4	35,982	36,085
101	e	338	0	149,384	149,722
102	f	39	0	11,926	11,965
103	g	30	0	16,432	16,462
104	h	14	0	7,412	7,426
105	i	306	0	131,469	131,775
106	j	2	4	1,461	1,463
108	l	197	9	78,317	78,514
109	m	143	0	60,434	60,577
110	n	171	0	77,024	77,195
111	o	127	0	56,542	56,669
112	p	57	0	28,379	28,436
113	q	45	3	16,571	16,616
114	r	149	0	73,854	74,003
115	s	240	9	109,471	109,711
116	t	273	0	108,641	108,914
117	u	255	0	119,065	119,320
118	v	40	0	20,568	20,608
120	x	5	0	2,527	2,532
				Total Characters in Image Set	1,365,890

Table D.2: Character results from SegRec v3 versus the Normal image set using global density classification.

ASCII/Unicode	Character	False Negatives	False Positives	True Positives	Actual Total
44	,	46	135	21,065	21,111
46	.	14	226	30,629	30,643
59	;	135	0	0	135
65	A	7	178	2,210	2,217
67	C	4	6	2,515	2,519
68	D	8	2	3,037	3,045
69	E	11	0	1,029	1,040
70	F	4	0	1,003	1,007
71	G	0	1	0	0
73	I	8	5	2,246	2,254
74	J	0	1	0	0
76	L	3	4	146	149
77	M	13	3	3,048	3,061
78	N	11	1	4,120	4,131
80	P	10	1	4,138	4,148
81	Q	4	0	1,038	1,042
83	S	13	5	3,126	3,139
84	T	0	1	0	0
85	U	4	0	1,026	1,030
86	V	8	381	2,123	2,131
97	a	229	9	105,375	105,604
98	b	50	4	15,834	15,884
99	c	125	30	53,482	53,607
100	d	109	33	35,976	36,085
101	e	348	5	149,374	149,722
102	f	38	0	11,927	11,965
103	g	32	3	16,430	16,462
104	h	15	1	7,411	7,426
105	i	311	78,299	131,464	131,775
106	j	2	1	1,461	1,463
108	l	78,508	2	6	78,514
109	m	147	29	60,430	60,577
110	n	180	48	77,015	77,195
111	o	130	19	56,539	56,669
112	p	58	15	28,378	28,436
113	q	43	5	16,573	16,616
114	r	153	1	73,850	74,003
115	s	258	4	109,453	109,711
116	t	283	53	108,631	108,914
117	u	266	61	119,054	119,320
118	v	45	9	20,563	20,608
120	x	5	1	2,527	2,532
122	z	0	5	0	0
				Total Characters in Image Set	1,365,890

Table D.3: Character results from SegRec v3 versus the Noisy image set using pixel count classification.

(Continued on next page.)

ASCII/Unicode	Character	False Negatives	False Positives	True Positives	Actual Total
44	,	24	199	21,130	21,154
46	.	32	1,265	30,345	30,377
59	;	162	0	0	162
65	A	805	44	1,299	2,104
66	B	0	58,786	0	0
67	C	1,782	25,125	689	2,471
68	D	246	27,788	2,791	3,037
69	E	804	1,362	179	983
70	F	370	4,655	615	985
71	G	0	16,062	0	0
72	H	0	543	0	0
73	I	182	4,475	2,193	2,375
74	J	0	11,002	0	0
75	K	0	603	0	0
76	L	20	669	131	151
77	M	610	15,420	2,439	3,049
78	N	1,269	854	2,924	4,193
79	O	0	18,083	0	0
80	P	1,306	3,440	2,800	4,106
81	Q	11	17,105	999	1,010
82	R	0	941	0	0
83	S	1,772	27,384	1,322	3,094
84	T	0	14	0	0
85	U	613	21,881	350	963
86	V	162	1,250	2,018	2,180
87	W	0	76	0	0
88	X	0	203	0	0
89	Y	0	311	0	0
97	a	33,786	11,745	73,425	107,211
98	b	135	8,022	15,068	15,203
99	c	34,405	46	19,905	54,310
100	d	12,149	8,928	25,600	37,749
101	e	34,853	14,864	113,937	148,790
102	f	1,966	30,440	7,036	9,002
103	g	2,419	1,544	15,415	17,834
104	h	1,769	150	5,707	7,476
105	i	95,884	66	35,676	131,560
106	j	2	668	1,516	1,518
107	k	0	27	0	0

Table D.3: Character results from SegRec v3 versus the Noisy image set using pixel count classification.

(Continued from previous page.)

ASCII/Unicode	**Character**	**False Negatives**	**False Positives**	**True Positives**	**Actual Total**
108	l	278	93,907	79,327	79,605
109	m	28,055	3,378	31,441	59,496
110	n	19,326	1,272	59,692	79,018
111	o	26,673	6,936	30,505	57,178
112	p	3,769	445	26,506	30,275
113	q	2,052	13	14,650	16,702
114	r	27,067	307	47,037	74,104
115	s	88,576	176	21,260	109,836
116	t	1,089	557	107,952	109,041
117	u	16,541	583	101,437	117,978
118	v	2,492	141	18,177	20,669
119	w	0	1	0	0
120	x	0	20	0	0
121	y	0	101	0	0
				Total Characters in Image Set	1,366,949

Table D.4: Character results from SegRec v3 versus the Noisy image set using global density classification.

(Continued on next page.)

ASCII/Unicode	Character	False Negatives	False Positives	True Positives	Actual Total
44	,	18	5,581	21,136	21,154
46	.	6,189	81	24,188	30,377
59	;	162	0	0	162
65	A	1,199	125	905	2,104
66	B	0	56,059	0	0
67	C	2,456	9	15	2,471
68	D	305	31,543	2,732	3,037
69	E	336	825	647	983
70	F	305	950	680	985
71	G	0	746	0	0
72	H	0	462	0	0
73	I	8	3,854	2,367	2,375
74	J	0	3,096	0	0
75	K	0	163	0	0
76	L	20	403	131	151
77	M	999	296	2,050	3,049
78	N	1,266	3,248	2,927	4,193
79	O	0	703	0	0
80	P	71	5,357	4,035	4,106
81	Q	6	19,526	1,004	1,010
82	R	0	628	0	0
83	S	3,072	15	22	3,094
84	T	0	1	0	0
85	U	630	10,444	333	963
86	V	1,550	977	630	2,180
87	W	0	385	0	0
88	X	0	480	0	0
89	Y	0	187	0	0
97	a	30,405	12,811	76,806	107,211
98	b	140	2,280	15,063	15,203
99	c	9,860	1,911	44,450	54,310
100	d	12,401	1,327	25,348	37,749
101	e	26,446	29,080	122,344	148,790
102	f	2,101	11,427	6,901	9,002
103	g	2,573	451	15,261	17,834
104	h	1,769	163	5,707	7,476
105	i	908	64,238	130,652	131,560
106	j	2	14,382	1,516	1,518
107	k	0	31	0	0

Table D.4: Character results from SegRec v3 versus the Noisy image set using global density classification.

(Continued from previous page.)

ASCII/Unicode	Character	False Negatives	False Positives	True Positives	Actual Total
108	l	64,962	78	14,643	79,605
109	m	9,370	40,808	50,126	59,496
110	n	18,886	1,805	60,132	79,018
111	o	13,567	2,154	43,611	57,178
112	p	5,689	421	24,586	30,275
113	q	2,154	12	14,548	16,702
114	r	9,886	203	64,218	74,104
115	s	63,436	1,851	46,400	109,836
116	t	793	137	108,248	109,041
117	u	16,444	584	101,534	117,978
118	v	1,363	1,601	19,306	20,669
119	w	0	61	0	0
120	x	0	689	0	0
121	y	0	193	0	0
122	z	0	2	0	0
				Total Characters in Image Set	1,366,949

Table D.5: Character results from SegRec v3 versus the Scan1 image set using pixel count classification.

(Continued on next page.)

ASCII/Unicode	Character	False Negatives	False Positives	True Positives	Actual Total
44	,	1,430	1,074	641	2,071
46	.	695	23,080	2,372	3,067
59	;	16	0	0	16
65	A	168	27	52	220
66	B	0	72	0	0
67	C	206	249	48	254
68	D	220	388	65	285
69	E	90	35	22	112
70	F	81	35	12	93
71	G	0	526	0	0
72	H	0	15	0	0
73	I	169	567	51	220
74	J	0	255	0	0
75	K	0	21	0	0
76	L	16	25	3	19
77	M	246	35	68	314
78	N	329	21	62	391
79	O	0	1,895	0	0
80	P	335	209	107	442
81	Q	100	165	27	127
82	R	0	76	0	0
83	S	264	125	51	315
84	T	0	6	0	0
85	U	89	251	17	106
86	V	161	56	40	201
87	W	0	4	0	0
88	X	0	17	0	0
89	Y	0	1	0	0
97	a	7,287	748	3,212	10,499
98	b	1,269	137	334	1,603
99	c	3,738	696	1,623	5,361
100	d	2,781	245	800	3,581
101	e	10,050	546	4,992	15,042
102	f	888	129	233	1,121
103	g	1,365	84	277	1,642
104	h	645	25	99	744
105	i	9,627	2,131	3,530	13,157
106	j	78	1,424	60	138
107	k	0	7	0	0

Table D.5: Character results from SegRec v3 versus the Scan1 image set using pixel count classification.

(Continued from previous page.)

ASCII/Unicode	Character	False Negatives	False Positives	True Positives	Actual Total
108	l	4,975	2,172	2,942	7,917
109	m	5,144	158	919	6,063
110	n	6,285	456	1,423	7,708
111	o	4,982	511	711	5,693
112	p	2,176	135	597	2,773
113	q	1,374	216	392	1,766
114	r	5,815	600	1,540	7,355
115	s	8,678	174	2,423	11,101
116	t	7,651	599	3,181	10,832
117	u	9,699	151	2,281	11,980
118	v	1,488	121	543	2,031
119	w	0	11	0	0
120	x	208	36	52	260
121	y	0	1	0	0
122	z	0	7	0	0
				Total Characters in Image Set	136,620

Table D.6: Character results from SegRec v3 versus the Scan1 image set using global density classification.

(Continued on next page.)

ASCII/Unicode	Character	False Negatives	False Positives	True Positives	Actual Total
44	,	1,397	1,534	674	2,071
46	.	1,062	9,608	2,005	3,067
59	;	16	0	0	16
65	A	118	3,460	102	220
66	B	0	352	0	0
67	C	236	227	18	254
68	D	212	621	73	285
69	E	87	208	25	112
70	F	80	197	13	93
71	G	0	299	0	0
72	H	0	41	0	0
73	I	136	3,475	84	220
74	J	0	85	0	0
75	K	0	79	0	0
76	L	16	619	3	19
77	M	249	134	65	314
78	N	321	191	70	391
79	O	0	28	0	0
80	P	321	797	121	442
81	Q	101	634	26	127
82	R	0	117	0	0
83	S	279	43	36	315
84	T	0	107	0	0
85	U	90	287	16	106
86	V	171	75	30	201
87	W	0	71	0	0
88	X	0	55	0	0
89	Y	0	28	0	0
90	Z	0	22	0	0
97	a	6,038	2,904	4,461	10,499
98	b	1,248	263	355	1,603
99	c	3,320	1,536	2,041	5,361
100	d	2,689	566	892	3,581
101	e	9,248	1,741	5,794	15,042
102	f	839	755	282	1,121
103	g	1,361	349	281	1,642
104	h	644	63	100	744
105	i	7,685	3,744	5,472	13,157
106	j	81	2,057	57	138

Table D.6: Character results from SegRec v3 versus the Scan1 image set using global density classification.

(Continued from previous page.)

ASCII/Unicode	Character	False Negatives	False Positives	True Positives	Actual Total
107	k	0	539	0	0
108	l	7,558	184	359	7,917
109	m	4,721	906	1,342	6,063
110	n	6,267	603	1,441	7,708
111	o	3,759	1,301	1,934	5,693
112	p	2,157	340	616	2,773
113	q	1,303	836	463	1,766
114	r	5,583	1,238	1,772	7,355
115	s	8,354	429	2,747	11,101
116	t	7,732	495	3,100	10,832
117	u	9,786	285	2,194	11,980
118	v	1,489	207	542	2,031
119	w	0	62	0	0
120	x	202	208	58	260
121	y	0	128	0	0
122	z	0	8	0	0
				Total Characters in Image Set	136,620

Table D.7: Character results from SegRec v3 versus the Scan2 image set using pixel count classification.

(Continued on next page.)

ASCII/Unicode	Character	False Negatives	False Positives	True Positives	Actual Total
44	,	1,517	1,016	554	2,071
46	.	1,205	13,770	1,862	3,067
59	;	16	0	0	16
65	A	170	32	50	220
66	B	0	236	0	0
67	C	204	295	50	254
68	D	228	618	57	285
69	E	101	49	11	112
70	F	82	25	11	93
71	G	0	828	0	0
72	H	0	21	0	0
73	I	180	548	40	220
74	J	0	281	0	0
75	K	0	39	0	0
76	L	15	577	4	19
77	M	253	37	61	314
78	N	345	10	46	391
79	O	0	2,180	0	0
80	P	340	226	102	442
81	Q	101	375	26	127
82	R	0	36	0	0
83	S	281	125	34	315
84	T	0	2	0	0
85	U	93	449	13	106
86	V	155	117	46	201
87	W	0	18	0	0
88	X	0	23	0	0
89	Y	0	2	0	0
97	a	7,418	1,013	3,081	10,499
98	b	1,291	230	312	1,603
99	c	3,908	583	1,453	5,361
100	d	2,801	291	780	3,581
101	e	10,004	792	5,038	15,042
102	f	883	258	238	1,121
103	g	1,377	130	265	1,642
104	h	678	33	66	744
105	i	8,998	2,333	4,159	13,157
106	j	86	1,731	52	138

Table D.7: Character results from SegRec v3 versus the Scan2 image set using pixel count classification.

(Continued from previous page.)

ASCII/Unicode	Character	False Negatives	False Positives	True Positives	Actual Total
107	k	0	14	0	0
108	l	5,009	2,559	2,908	7,917
109	m	5,394	194	669	6,063
110	n	6,405	565	1,303	7,708
111	o	5,225	467	468	5,693
112	p	2,204	188	569	2,773
113	q	1,423	214	343	1,766
114	r	5,856	572	1,499	7,355
115	s	9,037	226	2,064	11,101
116	t	7,615	576	3,217	10,832
117	u	9,695	240	2,285	11,980
118	v	1,586	187	445	2,031
119	w	0	22	0	0
120	x	215	36	45	260
121	y	0	1	0	0
122	z	0	11	0	0
				Total Characters in Image Set	136,620

Table D.8: Character results from SegRec v3 versus the Scan2 image set using global density count classification.

(Continued on next page.)

ASCII/Unicode	Character	False Negatives	False Positives	True Positives	Actual Total
44	,	1,479	1,263	592	2,071
46	.	1,335	6,481	1,732	3,067
59	;	16	0	0	16
65	A	128	2,317	92	220
66	B	0	631	0	0
67	C	244	113	10	254
68	D	217	854	68	285
69	E	89	310	23	112
70	F	81	124	12	93
71	G	0	333	0	0
72	H	0	61	0	0
73	I	132	2,763	88	220
74	J	0	73	0	0
75	K	0	103	0	0
76	L	18	391	1	19
77	M	246	120	68	314
78	N	345	89	46	391
79	O	0	38	0	0
80	P	324	620	118	442
81	Q	98	365	29	127
82	R	0	96	0	0
83	S	303	36	12	315
84	T	0	60	0	0
85	U	95	342	11	106
86	V	171	44	30	201
87	W	0	71	0	0
88	X	0	110	0	0
89	Y	0	19	0	0
90	Z	0	25	0	0
97	a	6,168	3,178	4,331	10,499
98	b	1,239	283	364	1,603
99	c	3,526	1,046	1,835	5,361
100	d	2,725	480	856	3,581
101	e	9,075	1,589	5,967	15,042
102	f	833	670	288	1,121
103	g	1,359	278	283	1,642
104	h	669	55	75	744
105	i	7,799	3,157	5,358	13,157
106	j	86	1,951	52	138

Table D.8: Character results from SegRec v3 versus the Scan2 image set using global density classification.

(Continued from previous page.)

ASCII/Unicode	Character	False Negatives	False Positives	True Positives	Actual Total
107	k	0	586	0	0
108	l	7,655	171	262	7,917
109	m	5,008	839	1,055	6,063
110	n	6,386	562	1,322	7,708
111	o	3,807	968	1,886	5,693
112	p	2,241	224	532	2,773
113	q	1,332	643	434	1,766
114	r	5,679	891	1,676	7,355
115	s	8,579	419	2,522	11,101
116	t	7,704	482	3,128	10,832
117	u	9,882	187	2,098	11,980
118	v	1,514	237	517	2,031
119	w	0	55	0	0
120	x	218	130	42	260
121	y	0	37	0	0
122	z	0	11	0	0
				Total Characters in Image Set	136,620

Table D.9: Character results from Tesseract versus the Normal image set.

ASCII/Unicode	Character	False Negatives	False Positives	True Positives	Actual Total
44	,	3	3	21,108	21,111
46	.	7	7	30,636	30,643
48	0	0	3	0	0
49	1	0	10	0	0
53	5	0	25,734	0	0
59	;	0	0	135	135
65	A	0	0	2,217	2,217
66	B	0	40	0	0
67	C	0	0	2,519	2,519
68	D	2	383	3,043	3,045
69	E	0	0	1,040	1,040
70	F	0	0	1,007	1,007
73	I	39	3,245	2,215	2,254
76	L	0	0	149	149
77	M	1	1	3,060	3,061
78	N	0	0	4,131	4,131
79	O	0	1	0	0
80	P	1	1	4,147	4,148
81	Q	0	0	1,042	1,042
83	S	1	631	3,138	3,139
85	U	0	0	1,030	1,030
86	V	0	10,180	2,131	2,131
97	a	20	20	105,584	105,604
98	b	1	1	15,883	15,884
99	c	10	10	53,597	53,607
100	d	7	7	36,078	36,085
101	e	27	251	149,695	149,722
102	f	2	2	11,963	11,965
103	g	3	3,556	16,459	16,462
104	h	1	1	7,425	7,426
105	i	32	106	131,743	131,775
106	j	0	0	1,463	1,463
108	l	3,381	57	75,133	78,514
109	m	13	1,400	60,564	60,577
110	n	1,787	19	75,408	77,195
111	o	242	14	56,427	56,669
112	p	6	6	28,430	28,436
113	q	3,556	19	13,060	16,616
114	r	11	11	73,992	74,003
115	s	26,423	19	83,288	109,711
116	t	18	18	108,896	108,914
117	u	30	23	119,290	119,320
118	v	10,181	1	10,427	20,608
120	x	0	0	2,532	2,532
				Total Characters in Image Set	1,365,890

Table D.10: Character results from Tesseract versus the Noisy image set.

(Continued on next page.)

ASCII/Unicode	Character	False Negatives	False Positives	True Positives	Actual Total
36	$	0	9	0	0
38	&	0	3	0	0
39	’	0	4	0	0
40	(	0	1	0	0
44	,	85	205	21,069	21,154
46	.	3,139	66	27,238	30,377
48	0	0	54	0	0
49	1	0	98	0	0
51	3	0	154	0	0
52	4	0	28	0	0
53	5	0	158	0	0
54	6	0	5	0	0
56	8	0	19	0	0
57	9	0	60	0	0
58	:	0	150	0	0
59	;	13	62	149	162
60	<	0	192	0	0
65	A	0	363	2,104	2,104
66	B	0	82	0	0
67	C	7	103	2,464	2,471
68	D	0	77	3,037	3,037
69	E	2	21	981	983
70	F	0	0	985	985
72	H	0	5	0	0
73	I	101	23	2,274	2,375
76	L	0	1	151	151
77	M	1	0	3,048	3,049
78	N	0	0	4,193	4,193
79	O	0	153	0	0
80	P	6	0	4,100	4,106
81	Q	0	0	1,010	1,010
83	S	91	346	3,003	3,094
85	U	2	8	961	963
86	V	22	836	2,158	2,180
87	W	0	2	0	0
90	Z	0	1	0	0
95	_	0	4	0	0
97	a	198	1,546	107,013	107,211
98	b	8	4	15,195	15,203
99	c	704	192	53,606	54,310
100	d	3	16	37,746	37,749
101	e	789	2,732	148,001	148,790
102	f	1	1	9,001	9,002
103	g	334	57	17,500	17,834
104	h	2	32	7,474	7,476

Table D.10: Character results from Tesseract versus the Noisy image set.

(Continued from previous page.)

ASCII/Unicode	Character	False Negatives	False Positives	True Positives	Actual Total
105	i	10	328	131,550	131,560
106	j	0	0	1,518	1,518
107	k	0	2	0	0
108	l	116	262	79,489	79,605
109	m	4	1,361	59,492	59,496
110	n	1,474	334	77,544	79,018
111	o	3,872	311	53,306	57,178
112	p	5	0	30,270	30,275
113	q	8	333	16,694	16,702
114	r	482	47	73,622	74,104
115	s	905	581	108,931	109,836
116	t	35	475	109,006	109,041
117	u	406	101	117,572	117,978
118	v	698	31	19,971	20,669
119	w	0	9	0	0
120	x	0	22	0	0
122	z	0	29	0	0
123	{	0	2	0	0
162	¢	0	1	0	0
233	é	0	9	0	0
8216	‘	0	1,337	0	0
8364	€	0	3	0	0
64257	ﬁ	0	21	0	0
64258	ﬂ	0	2	0	0
				Total Characters in Image Set	1,366,949

Table D.11: Character results from Tesseract versus the Scan1 image set.

(Continued on next page.)

ASCII/Unicode	Character	False Negatives	False Positives	True Positives	Actual Total
33	!	0	2	0	0
34	"	0	6	0	0
38	&	0	1	0	0
39	’	0	55	0	0
40	(	0	16	0	0
41	)	0	6	0	0
44	,	41	55	2,030	2,071
45	-	0	5	0	0
46	.	193	79	2,874	3,067
47	/	0	4	0	0
48	0	0	95	0	0
49	1	0	357	0	0
50	2	0	3	0	0
51	3	0	21	0	0
53	5	0	188	0	0
54	6	0	3	0	0
55	7	0	5	0	0
56	8	0	5	0	0
57	9	0	39	0	0
58	:	0	133	0	0
59	;	1	37	15	16
60	<	0	8	0	0
63	?	0	4	0	0
65	A	4	13	216	220
66	B	0	24	0	0
67	C	8	58	246	254
68	D	6	28	279	285
69	E	13	18	99	112
70	F	4	60	89	93
71	G	0	9	0	0
72	H	0	31	0	0
73	I	45	43	175	220
74	J	0	95	0	0
75	K	0	2	0	0
76	L	2	1,193	17	19
77	M	6	6	308	314
78	N	1	2	390	391
79	O	0	48	0	0
80	P	11	8	431	442
81	Q	1	10	126	127
82	R	0	3	0	0
83	S	22	199	293	315
84	T	0	20	0	0
85	U	1	60	105	106
86	V	7	217	194	201
87	W	0	47	0	0

Table D.11: Character results from Tesseract versus the Scan1 image set.

(Continued from previous page.)

ASCII/Unicode	Character	False Negatives	False Positives	True Positives	Actual Total
89	Y	0	1	0	0
90	Z	0	2	0	0
91	[	0	19	0	0
92	\	0	3	0	0
93	]	0	49	0	0
95	_	0	9	0	0
97	a	349	167	10,150	10,499
98	b	37	16	1,566	1,603
99	c	220	590	5,141	5,361
100	d	42	21	3,539	3,581
101	e	1,796	265	13,246	15,042
102	f	174	12	947	1,121
103	g	227	36	1,415	1,642
104	h	10	83	734	744
105	i	713	727	12,444	13,157
106	j	7	256	131	138
107	k	0	6	0	0
108	l	1,241	199	6,676	7,917
109	m	84	161	5,979	6,063
110	n	226	264	7,482	7,708
111	o	377	1,014	5,316	5,693
112	p	41	13	2,732	2,773
113	q	23	247	1,743	1,766
114	r	306	59	7,049	7,355
115	s	950	61	10,151	11,101
116	t	1,362	201	9,470	10,832
117	u	293	426	11,687	11,980
118	v	213	73	1,818	2,031
119	w	0	17	0	0
120	x	0	46	260	260
121	y	0	14	0	0
122	z	0	28	0	0
123	{	0	1	0	0
124	|	0	2	0	0
125	}	0	10	0	0
126	~	0	1	0	0
187	»	0	4	0	0
233	é	0	1	0	0
8212	—	0	1	0	0
8216	‘	0	82	0	0
8217	’	0	8	0	0
8220	“	0	8	0	0
8221	”	0	5	0	0
64257	ﬁ	0	45	0	0
64258	ﬂ	0	8	0	0
				Total Characters in Image Set	136,620

Table D.12: Character results from Tesseract versus the Scan2 image set.

(Continued on next page.)

ASCII/Unicode	Character	False Negatives	False Positives	True Positives	Actual Total
33	!	0	1	0	0
34	"	0	3	0	0
39	’	0	28	0	0
40	(	0	7	0	0
41	)	0	7	0	0
44	,	62	102	2,009	2,071
45	-	0	6	0	0
46	.	343	59	2,724	3,067
47	/	0	12	0	0
48	0	0	41	0	0
49	1	0	194	0	0
50	2	0	2	0	0
51	3	0	20	0	0
52	4	0	1	0	0
53	5	0	118	0	0
54	6	0	2	0	0
55	7	0	1	0	0
56	8	0	5	0	0
57	9	0	16	0	0
58	:	0	51	0	0
59	;	0	12	16	16
60	<	0	3	0	0
62	>	0	1	0	0
63	?	0	3	0	0
65	A	5	20	215	220
66	B	0	23	0	0
67	C	3	36	251	254
68	D	5	15	280	285
69	E	10	8	102	112
70	F	2	14	91	93
71	G	0	1	0	0
72	H	0	21	0	0
73	I	39	22	181	220
74	J	0	108	0	0
75	K	0	2	0	0
76	L	0	703	19	19
77	M	2	4	312	314
78	N	1	2	390	391
79	O	0	33	0	0
80	P	5	3	437	442
81	Q	1	2	126	127
82	R	0	3	0	0
83	S	13	125	302	315
84	T	0	11	0	0
85	U	2	28	104	106
86	V	6	155	195	201
87	W	0	16	0	0
88	X	0	1	0	0

Table D.12: Character results from Tesseract versus the Scan2 image set.

(Continued from previous page.)

ASCII/Unicode	Character	False Negatives	False Positives	True Positives	Actual Total
89	Y	0	1	0	0
90	Z	0	1	0	0
91	[	0	6	0	0
92	\	0	5	0	0
93	]	0	64	0	0
95	_	0	4	0	0
97	a	162	183	10,337	10,499
98	b	18	10	1,585	1,603
99	c	162	404	5,199	5,361
100	d	15	15	3,566	3,581
101	e	1,176	275	13,866	15,042
102	f	87	15	1,034	1,121
103	g	138	30	1,504	1,642
104	h	5	60	739	744
105	i	586	406	12,571	13,157
106	j	2	276	136	138
107	k	0	5	0	0
108	l	752	143	7,165	7,917
109	m	36	139	6,027	6,063
110	n	173	160	7,535	7,708
111	o	329	612	5,364	5,693
112	p	22	17	2,751	2,773
113	q	12	149	1,754	1,766
114	r	172	50	7,183	7,355
115	s	633	65	10,468	11,101
116	t	825	149	10,007	10,832
117	u	166	196	11,814	11,980
118	v	142	54	1,889	2,031
119	w	0	8	0	0
120	x	1	36	259	260
121	y	0	11	0	0
122	z	0	15	0	0
123	{	0	1	0	0
124	|	0	2	0	0
125	}	0	6	0	0
126	~	0	5	0	0
163	£	0	1	0	0
187	»	0	4	0	0
233	é	0	2	0	0
8212	—	0	1	0	0
8216	‘	0	116	0	0
8217	’	0	9	0	0
8220	“	0	3	0	0
8221	”	0	1	0	0
8364	€	0	1	0	0
64257	ﬁ	0	36	0	0
64258	ﬂ	0	12	0	0
				Total Characters in Image Set	136,620

Table D.13: Character results from ABBYY FineReader versus the Normal image set.

ASCII/Unicode	Character	False Negatives	False Positives	True Positives	Actual Total
44	,	51	27	21,060	21,111
46	.	64	27	30,579	30,643
49	1	0	618	0	0
59	;	0	0	135	135
65	A	3	3	2,214	2,217
67	C	1	1	2,518	2,519
68	D	4	3	3,041	3,045
69	E	1	1	1,039	1,040
70	F	1	1	1,006	1,007
73	I	2	183	2,252	2,254
76	L	0	0	149	149
77	M	6	6	3,055	3,061
78	N	6	6	4,125	4,131
80	P	6	6	4,142	4,148
81	Q	1	1	1,041	1,042
83	S	4	4	3,135	3,139
85	U	2	2	1,028	1,030
86	V	3	3	2,128	2,131
97	a	115	101	105,489	105,604
98	b	13	13	15,871	15,884
99	c	3,746	63	49,861	53,607
100	d	44	60	36,041	36,085
101	e	162	3,766	149,560	149,722
102	f	20	22	11,945	11,965
103	g	3,904	3,945	12,558	16,462
104	h	8	8	7,418	7,426
105	i	155	1,958	131,620	131,775
106	j	2	2	1,461	1,463
108	l	2,724	89	75,790	78,514
109	m	384	58	60,193	60,577
110	n	95	428	77,100	77,195
111	o	60	57	56,609	56,669
112	p	36	33	28,400	28,436
113	q	3,949	3,903	12,667	16,616
114	r	92	403	73,911	74,003
115	s	126	105	109,585	109,711
116	t	113	98	108,801	108,914
117	u	123	124	119,197	119,320
118	v	35	34	20,573	20,608
120	x	2	2	2,530	2,532
				Total Characters in Image Set	1,365,890

Table D.14: Character results from ABBYY FineReader versus the Noisy image set.

(Continued on next page.)

ASCII/Unicode	Character	False Negatives	False Positives	True Positives	Actual Total
33	!	0	149	0	0
35	#	0	15	0	0
36	$	0	1	0	0
38	&	0	4	0	0
40	(	0	1	0	0
42	*	0	309	0	0
44	,	255	2,490	20,899	21,154
45	-	0	396	0	0
46	.	3,130	151	27,247	30,377
47	/	0	35	0	0
49	1	0	12	0	0
51	3	0	3	0	0
59	;	1	0	161	162
62	>	0	1	0	0
65	A	39	0	2,065	2,104
66	B	0	55	0	0
67	C	198	1	2,273	2,471
68	D	11	22	3,026	3,037
69	E	64	9	919	983
70	F	9	8	976	985
71	G	0	135	0	0
72	H	0	228	0	0
73	I	2	403	2,373	2,375
74	J	0	1	0	0
75	K	0	51	0	0
76	L	23	1	128	151
77	M	98	67	2,951	3,049
78	N	297	0	3,896	4,193
79	O	0	22	0	0
80	P	18	7	4,088	4,106
81	Q	7	0	1,003	1,010
83	S	0	22	3,094	3,094
85	U	19	7	944	963
86	V	0	0	2,180	2,180
87	W	0	9	0	0
88	X	0	59	0	0
90	Z	0	2	0	0
97	a	10	2,041	107,201	107,211
98	b	7	11	15,196	15,203
99	c	3,307	74	51,003	54,310
100	d	2	54	37,747	37,749
101	e	129	4,041	148,661	148,790

Table D.14: Character results from ABBYY FineReader versus the Noisy image set.

(Continued from previous page.)

ASCII/Unicode	Character	False Negatives	False Positives	True Positives	Actual Total
102	f	0	163	9,002	9,002
103	g	0	262	17,834	17,834
104	h	30	10	7,446	7,476
105	i	1,285	1,774	130,275	131,560
106	j	1	0	1,517	1,518
108	l	1,737	734	77,868	79,605
109	m	1,808	27	57,688	59,496
110	n	48	575	78,970	79,018
111	o	1,375	40	55,803	57,178
112	p	6	0	30,269	30,275
113	q	258	0	16,444	16,702
114	r	22	1,486	74,082	74,104
115	s	65	54	109,771	109,836
116	t	66	343	108,975	109,041
117	u	168	15	117,810	117,978
118	v	0	0	20,669	20,669
119	w	0	4	0	0
120	x	0	31	0	0
169	©	0	74	0	0
171	«	0	1	0	0
174	®	0	4	0	0
8222	„	0	1	0	0
9830	◆	0	1	0	0
				Total Characters in Image Set	1,366,949

Table D.15: Character results from ABBYY FineReader versus the Scan1 image set.

(Continued on next page.)

ASCII/Unicode	Character	False Negatives	False Positives	True Positives	Actual Total
33	!	0	22	0	0
34	"	0	2	0	0
39	’	0	24	0	0
41	)	0	3	0	0
44	,	8	45	2,063	2,071
45	-	0	9	0	0
46	.	21	663	3,046	3,067
47	/	0	4	0	0
49	1	0	79	0	0
51	3	0	2	0	0
53	5	0	5	0	0
58	:	0	76	0	0
59	;	0	30	16	16
60	<	0	1	0	0
62	>	0	3	0	0
65	A	0	0	220	220
67	C	15	2	239	254
68	D	3	0	282	285
69	E	6	1	106	112
70	F	1	3	92	93
71	G	0	14	0	0
72	H	0	4	0	0
73	I	4	31	216	220
74	J	0	4	0	0
75	K	0	4	0	0
76	L	0	67	19	19
77	M	1	3	313	314
78	N	7	2	384	391
79	O	0	2	0	0
80	P	5	2	437	442
81	Q	0	0	127	127
82	R	0	1	0	0
83	S	1	2	314	315
84	T	0	4	0	0
85	U	1	7	105	106
86	V	0	0	201	201
87	W	0	1	0	0
93	]	0	11	0	0
94	ˆ	0	2	0	0
95	_	0	1	0	0
97	a	75	109	10,424	10,499
98	b	13	16	1,590	1,603
99	c	360	157	5,001	5,361
100	d	11	12	3,570	3,581

Table D.15: Character results from ABBYY FineReader versus the Scan1 image set.

(Continued from previous page.)

ASCII/Unicode	Character	False Negatives	False Positives	True Positives	Actual Total
101	e	270	368	14,772	15,042
102	f	7	7	1,114	1,121
103	g	27	25	1,615	1,642
104	h	15	12	729	744
105	i	126	552	13,031	13,157
106	j	0	14	138	138
107	k	0	2	0	0
108	l	485	110	7,432	7,917
109	m	408	15	5,655	6,063
110	n	38	352	7,670	7,708
111	o	50	147	5,643	5,693
112	p	3	3	2,770	2,773
113	q	27	25	1,739	1,766
114	r	30	307	7,325	7,355
115	s	71	48	11,030	11,101
116	t	133	67	10,699	10,832
117	u	49	47	11,931	11,980
118	v	0	2	2,031	2,031
120	x	4	8	256	260
121	y	0	2	0	0
169	©	0	1	0	0
8216	‘	0	1	0	0
8217	’	0	2	0	0
				Total Characters in Image Set	136,620

Table D.16: Character results from ABBYY FineReader versus the Scan2 image set.

(Continued on next page.)

ASCII/Unicode	Character	False Negatives	False Positives	True Positives	Actual Total
33	!	0	17	0	0
39	’	0	11	0	0
40	(	0	1	0	0
42	*	0	2	0	0
44	,	11	65	2,060	2,071
45	-	0	22	0	0
46	.	59	374	3,008	3,067
47	/	0	8	0	0
49	1	0	28	0	0
51	3	0	3	0	0
53	5	0	1	0	0
58	:	0	47	0	0
59	;	0	19	16	16
62	>	0	1	0	0
65	A	0	0	220	220
66	B	0	1	0	0
67	C	9	0	245	254
68	D	0	0	285	285
69	E	4	1	108	112
70	F	0	0	93	93
71	G	0	7	0	0
72	H	0	8	0	0
73	I	6	23	214	220
74	J	0	7	0	0
75	K	0	1	0	0
76	L	0	12	19	19
77	M	1	3	313	314
78	N	10	0	381	391
80	P	2	1	440	442
81	Q	0	0	127	127
83	S	0	2	315	315
85	U	0	7	106	106
86	V	0	0	201	201
87	W	0	1	0	0
93	]	0	4	0	0
95	_	0	1	0	0
97	a	40	122	10,459	10,499
98	b	4	27	1,599	1,603
99	c	339	74	5,022	5,361
100	d	6	9	3,575	3,581
101	e	180	341	14,862	15,042
102	f	1	7	1,120	1,121
103	g	15	24	1,627	1,642

Table D.16: Character results from ABBYY FineReader versus the Scan2 image set.

(Continued from previous page.)

ASCII/Unicode	Character	False Negatives	False Positives	True Positives	Actual Total
104	h	25	4	719	744
105	i	81	417	13,076	13,157
106	j	1	9	137	138
107	k	0	3	0	0
108	l	331	66	7,586	7,917
109	m	337	5	5,726	6,063
110	n	15	267	7,693	7,708
111	o	32	115	5,661	5,693
112	p	0	0	2,773	2,773
113	q	23	13	1,743	1,766
114	r	18	224	7,337	7,355
115	s	54	31	11,047	11,101
116	t	48	49	10,784	10,832
117	u	40	32	11,940	11,980
118	v	0	1	2,031	2,031
119	w	0	2	0	0
120	x	7	7	253	260
121	y	0	2	0	0
174	®	0	2	0	0
8482	™	0	2	0	0
9632	■	0	1	0	0
				Total Characters in Image Set	136,620

Table D.17: Character results from OmniPage Ultimate versus the Normal image set.

ASCII/Unicode	Character	False Negatives	False Positives	True Positives	Actual Total
33	!	0	1	0	0
38	&	0	43	0	0
44	,	36	21	21,075	21,111
46	.	32	20	30,611	30,643
49	1	0	1	0	0
59	;	0	0	135	135
61	=	0	2	0	0
65	A	2	2	2,215	2,217
67	C	3	3	2,516	2,519
68	D	0	0	3,045	3,045
69	E	46	0	994	1,040
70	F	0	0	1,007	1,007
71	G	0	1	0	0
73	I	3	3	2,251	2,254
76	L	0	0	149	149
77	M	5	4	3,056	3,061
78	N	2	2	4,129	4,131
80	P	5	5	4,143	4,148
81	Q	0	0	1,042	1,042
83	S	2	5	3,137	3,139
85	U	1	11	1,029	1,030
86	V	0	0	2,131	2,131
97	a	159	182	105,445	105,604
98	b	13	14	15,871	15,884
99	c	38	92	53,569	53,607
100	d	36	36	36,049	36,085
101	e	180	116	149,542	149,722
102	f	4	18	11,961	11,965
103	g	11	11	16,451	16,462
104	h	11	11	7,415	7,426
105	i	141	560	131,634	131,775
106	j	2	2	1,461	1,463
108	l	540	74	77,974	78,514
109	m	114	44	60,463	60,577
110	n	59	66	77,136	77,195
111	o	132	62	56,537	56,669
112	p	25	25	28,411	28,436
113	q	10	10	16,606	16,616
114	r	63	98	73,940	74,003
115	s	90	135	109,621	109,711
116	t	107	89	108,807	108,914
117	u	91	88	119,229	119,320
118	v	22	22	20,586	20,608
119	w	0	1	0	0
120	x	2	3	2,530	2,532
122	z	0	3	0	0
65533	�	0	2	0	0
				Total Characters in Image Set	1,365,890

Table D.18: Character results from OmniPage Ultimate versus the Noisy image set.

(Continued on next page.)

ASCII/Unicode	Character	False Negatives	False Positives	True Positives	Actual Total
33	!	0	13	0	0
37	%	0	2	0	0
38	&	0	4	0	0
39	’	0	15	0	0
40	(	0	6	0	0
41	)	0	46	0	0
44	,	38	52	21,116	21,154
45	-	0	16	0	0
46	.	111	33	30,266	30,377
47	/	0	3	0	0
49	1	0	24	0	0
52	4	0	2	0	0
53	5	0	4	0	0
58	:	0	5	0	0
59	;	4	2	158	162
61	=	0	6	0	0
63	?	0	3	0	0
65	A	1	4	2,103	2,104
66	B	0	22	0	0
67	C	231	11	2,240	2,471
68	D	22	15	3,015	3,037
69	E	9	6	974	983
70	F	6	13	979	985
71	G	0	288	0	0
72	H	0	9	0	0
73	I	10	10	2,365	2,375
74	J	0	5	0	0
76	L	3	5	148	151
77	M	1	4	3,048	3,049
78	N	16	5	4,177	4,193
79	O	0	15	0	0
80	P	15	24	4,091	4,106
81	Q	5	2	1,005	1,010
82	R	0	1	0	0
83	S	22	6	3,072	3,094
84	T	0	5	0	0
85	U	45	1	918	963
86	V	11	2	2,169	2,180
87	W	0	1	0	0
93	]	0	4	0	0
94	ˆ	0	3	0	0
95	_	0	15	0	0

Table D.18: Character results from OmniPage Ultimate versus the Noisy image set.

(Continued from previous page.)

ASCII/Unicode	**Character**	**False Negatives**	**False Positives**	**True Positives**	**Actual Total**
97	a	356	1,251	106,855	107,211
98	b	25	15	15,178	15,203
99	c	574	456	53,736	54,310
100	d	87	62	37,662	37,749
101	e	500	1,278	148,290	148,790
102	f	12	85	8,990	9,002
103	g	22	52	17,812	17,834
104	h	5	67	7,471	7,476
105	i	1,209	1,185	130,351	131,560
106	j	1	31	1,517	1,518
107	k	0	3	0	0
108	l	1,690	866	77,915	79,605
109	m	448	59	59,048	59,496
110	n	138	666	78,880	79,018
111	o	1,993	152	55,185	57,178
112	p	323	44	29,952	30,275
113	q	50	22	16,652	16,702
114	r	474	350	73,630	74,104
115	s	249	191	109,587	109,836
116	t	175	614	108,866	109,041
117	u	453	121	117,525	117,978
118	v	28	284	20,641	20,669
119	w	0	24	0	0
120	x	0	1	0	0
121	y	0	8	0	0
122	z	0	46	0	0
65533	�	0	20	0	0
				Total Characters in Image Set	1,366,949

Table D.19: Character results from OmniPage Ultimate versus the Scan1 image set.

(Continued on next page.)

ASCII/Unicode	Character	False Negatives	False Positives	True Positives	Actual Total
33	!	0	2	0	0
38	&	0	2	0	0
39	’	0	20	0	0
40	(	0	5	0	0
41	)	0	8	0	0
42	*	0	3	0	0
43	+	0	1	0	0
44	,	8	13	2,063	2,071
46	.	9	170	3,058	3,067
47	/	0	3	0	0
49	1	0	6	0	0
50	2	0	1	0	0
51	3	0	8	0	0
52	4	0	2	0	0
58	:	0	28	0	0
59	;	2	8	14	16
61	=	0	4	0	0
65	A	0	6	220	220
66	B	0	6	0	0
67	C	5	14	249	254
68	D	5	2	280	285
69	E	17	0	95	112
70	F	5	4	88	93
71	G	0	5	0	0
72	H	0	7	0	0
73	I	12	16	208	220
74	J	0	1	0	0
75	K	0	5	0	0
76	L	2	113	17	19
77	M	5	7	309	314
78	N	4	5	387	391
79	O	0	4	0	0
80	P	5	5	437	442
81	Q	0	0	127	127
82	R	0	5	0	0
83	S	2	10	313	315
84	T	0	5	0	0
85	U	7	10	99	106
86	V	0	0	201	201
87	W	0	3	0	0
93	]	0	27	0	0
95	_	0	1	0	0

Table D.19: Character results from OmniPage Ultimate versus the Scan1 image set.

(Continued from previous page.)

ASCII/Unicode	Character	False Negatives	False Positives	True Positives	Actual Total
97	a	484	174	10,015	10,499
98	b	14	5	1,589	1,603
99	c	156	84	5,205	5,361
100	d	21	18	3,560	3,581
101	e	1,404	204	13,638	15,042
102	f	62	31	1,059	1,121
103	g	50	19	1,592	1,642
104	h	1	19	743	744
105	i	126	236	13,031	13,157
106	j	3	1	135	138
107	k	0	1	0	0
108	l	310	127	7,607	7,917
109	m	59	28	6,004	6,063
110	n	34	233	7,674	7,708
111	o	86	1,223	5,607	5,693
112	p	16	11	2,757	2,773
113	q	16	35	1,750	1,766
114	r	75	52	7,280	7,355
115	s	208	219	10,893	11,101
116	t	211	162	10,621	10,832
117	u	71	120	11,909	11,980
118	v	7	8	2,024	2,031
119	w	0	6	0	0
120	x	0	16	260	260
121	y	0	8	0	0
122	z	0	39	0	0
65533	�	0	18	0	0
				Total Characters in Image Set	136,620

Table D.20: Character results from OmniPage Ultimate versus the Scan2 image set.

(Continued on next page.)

ASCII/Unicode	Character	False Negatives	False Positives	True Positives	Actual Total
33	!	0	4	0	0
38	&	0	3	0	0
39	’	0	5	0	0
40	(	0	3	0	0
41	)	0	8	0	0
44	,	8	5	2,063	2,071
45	-	0	3	0	0
46	.	8	96	3,059	3,067
48	0	0	1	0	0
49	1	0	3	0	0
51	3	0	9	0	0
58	:	0	21	0	0
59	;	1	1	15	16
61	=	0	9	0	0
65	A	2	2	218	220
66	B	0	10	0	0
67	C	2	4	252	254
68	D	4	1	281	285
69	E	19	0	93	112
70	F	4	1	89	93
71	G	0	6	0	0
72	H	0	8	0	0
73	I	12	9	208	220
74	J	0	5	0	0
75	K	0	2	0	0
76	L	0	20	19	19
77	M	6	2	308	314
78	N	3	3	388	391
79	O	0	5	0	0
80	P	0	4	442	442
81	Q	0	0	127	127
83	S	0	10	315	315
84	T	0	1	0	0
85	U	1	3	105	106
86	V	0	0	201	201
87	W	0	1	0	0
88	X	0	2	0	0
93	]	0	21	0	0

Table D.20: Character results from OmniPage Ultimate versus the Scan2 image set.

(Continued from previous page.)

ASCII/Unicode	Character	False Negatives	False Positives	True Positives	Actual Total
97	a	436	179	10,063	10,499
98	b	7	2	1,596	1,603
99	c	175	41	5,186	5,361
100	d	11	7	3,570	3,581
101	e	881	283	14,161	15,042
102	f	22	20	1,099	1,121
103	g	16	5	1,626	1,642
104	h	2	13	742	744
105	i	76	175	13,081	13,157
106	j	0	0	138	138
108	l	244	87	7,673	7,917
109	m	44	18	6,019	6,063
110	n	19	143	7,689	7,708
111	o	74	752	5,619	5,693
112	p	4	2	2,769	2,773
113	q	5	10	1,761	1,766
114	r	51	25	7,304	7,355
115	s	181	214	10,920	11,101
116	t	76	132	10,756	10,832
117	u	48	64	11,932	11,980
118	v	3	5	2,028	2,031
119	w	0	3	0	0
120	x	0	11	260	260
121	y	0	9	0	0
122	z	0	26	0	0
65533	�	0	12	0	0
				Total Characters in Image Set	136,620

Bibliography

[1] Dibco 2014. `http://users.iit.demokritos.gr/~kntir/HDIBCO2014/index.html`. Accessed: 2015-08-03.

[2] ABBYY. About ABBYY. *https://www.abbyy.com/en-us/company/key-facts/*, October 2016.

[3] A. S. Abutableb. Automatic thresholding of gray-level pictures using two-dimensional entropy. *Computer Vision, Graphics, and Image Processing*, 47:22–32, 1989.

[4] Adnan Amin and Sue Wu. A robust system for thresholding and skew detection in mixed text/graphics documents. *International Journal of Image and Graphics*, 5(2):247–265, Apr 2005.

[5] Itay Bar-Yosef, Alik Mokeichev, Klara Kedem, Itshak Dinstein, and Uri Ehrlich. Adaptive shape prior for recognition and variational segmentation of degraded historical characters. *Pattern Recognition*, 42(12):3348–3354, Dec 2009.

[6] Junior Barrera, Marcel Brun, Routo Terada, and Edward R. Dougherty. Boosting OCR classifier by optimal edge noise filtering. *Computational Imaging and Vision*, 18(9):371–380, 2002.

[7] Subhadip Basu, Nibaran Das, Ram Sarkar, Mahantapas Kundu, Mita Nasipuri, and Dipak Kumar Basu. A hierarchical approach to recognition of handwritten bangla characters. *Pattern Recognition*, 42(7):1467–1484, July 2009.

[8] C. I. Chang, Y. Du, J. Wang, S. M. Guo, and P. D. Thouin. Survey and comparative analysis of entropy and relative entropy thresholding techniques. *IEEE Proceedings Vision, Image and Signal Processing*, 153(6), Dec 2006.

[9] Xin Chen, Yuefang Gao, and Zhonghong Huang. Cuda-accelerated fast sauvola's method on kepler architecture. *Multimedia Tools and Applications*, pages 1–12, 2014.

[10] John Cheng, Max Grossman, and Ty McKercher. *Professional CUDA C Programming*. John Wiley and Sons, Inc., 2014.

[11] E.E. Fournier D'Albe. On a type-reading optophone. *Proceedings of the Royal Society of London A: Mathematical, Physical and Engineering Sciences*, 90(619):373–375, May 1914.

[12] A. K. Das and B. Chanda. A fast algorithm for skew detection of document images using morphology. *International Journal on Document Analysis and Recognition*, 4(2):109–114, 2001.

[13] Raphael Finkel. Multilingual ocr program. personal communication.

[14] Herbert Freeman. On the encoding of arbitrary geometric configurations. *IRE Transactions on Electronic Computers*, EC-10(2):260–268, June 1961.

[15] B. Gatos, K. Ntirogiannis, and I. Pratikakis. Icdar 2009 document image binarization contest (dibco 2009). pages 1375–1382, July 2009.

[16] Emanuel Goldberg. Statistical machine, Dec 1931. US Patent 1,838,389.

[17] Amara Graps. An introduction to wavelets. *IEEE Computation Science and Engineering*, 2(2), 1995.

[18] Josh Hershberger and Jack Snoeyink. Speeding up the douglas-peucker line-simplification algorithm. 1992.

[19] L. Hertz and R. W. Schafer. Multilevel thresholding using edge matching. *Computer Vision, Graphics, and Image Processing*, 44:279–295, 1988.

[20] Robert Hummel. Image enhancement by histogram transformation. *Computer Graphics and Image Processing*, 6(2):184–195, April 1977.

[21] J. N. Kapur, P. K. Sahoo, and A. K. C. Wong. A new method for gray-level picture thresholding using the entropy of the histogram. *Computer Vision, Graphics, and Image Processing*, 29(3):273–285, Mar 1985.

[22] D.J. Ketcham, R.W. Lowe, and J.W. Weber. Real-time image enhancement techniques. *Image Processing*, 74, July 1976.

[23] Koichi Kise, Akinori Sato, and Motoi Iwata. Segmentation of page images using the area voronoi diagram. *Computer Vision and Image Understanding*, 70(3):370–382, June 1998.

[24] Donald E. Knuth. The concept of a meta-font. *Visible Language*, 16:3–27, 1982.

[25] Karen Kukich. Techniques for automatically correcting words in text. *ACM Comput. Surv.*, 24(4):377–439, Dec 1992.

[26] C. Vasantha Lakshmi, Sarika Singh, Ritu Jain, and C. Patvardhan. A novel approach to skeletonization for multi-font ocr applications. *Lecture Notes in Computer Science*, 5909:393–399, 2009.

[27] S. Lawson and J. Zhu. Image compression using wavelets and jpeg2000: a tutorial. *Electronics and Communication Engineering Journal*, pages 112–121, June 2002.

[28] Sabri A. Mahmoud and Ashraf S. Mahmoud. Arabic character recognition using modified Fourier spectrum (MFS) vs. Fourier descriptors. *Cybernetics and Systems*, 40(3):189–210, Mar 2009.

[29] Manjunath Aradhya V. N., Hemantha Kumar G., and Shivakumara P. Skew detection technique for binary document images based on Hough transform. *International Journal of Information and Communication Engineering*, March:498–504, Mar 2007.

[30] M. J. Nassiri, A. Vafaei, and A. Monadjemi. Texture feature extraction using Slant-Hadamard transform. *World Academy of Science, Engineering and Technology*, 17, 2006.

[31] W. Niblack. *An Introduction to Digital Image Processing*. Prentice-Hall, Englewood Cliffs, NJ.

[32] K. Ntirogiannis, B. Gatos, and I. Pratikakis. Icfhr2014 competition on handwritten document image binarization (h-dibco 2014). pages 809–813, Sept 2014.

[33] Nuance. Nuance fast facts. *http://www.nuance.com/company/company-overview/fast-facts/index.htm*, October 2016.

[34] NVIDIA. Nvidia CUDA C Programming Guide v7.0. *http://docs.nvidia.com/cuda/pdf/CUDA_C_Programming_Guide.pdf*, March 2015.

[35] NVIDIA. Nvidia Parallel Thread Execution ISA v4.3. *http://docs.nvidia.com/cuda/parallel-thread-execution/*, September 2015.

[36] NVIDIA. Nvidia Profiler User's Guide. *http://docs.nvidia.com/cuda/profiler-users-guide/*, September 2015.

[37] N. Otsu. A thresholding selection method from gray-scale histogram. *IEEE Transactions on System, Man, and Cybernetics*, 9:62–66, 1979.

[38] S.M. Pizer. Intensity mappings for the display of medical images. *Functional Mapping of Organ Systems and Other Computer Topics*, 1981.

[39] Stephen M. Pizer, E. Philip Amburn, John D. Austin, Robert Cromartie, Ari Geselowitz, Trey Greer, Bart ter Haar Romeny, John B. Zimmerman, and Karel Zuiderveld. Adaptive histogram equalization and its variations. *Computer Vision, Graphics, and Image Processing*, 39:355–368, 1987.

[40] I. Pratikakis, B. Gatos, and K. Ntirogiannis. H-dibco 2010 - handwritten document image binarization competition. pages 727–732, Nov 2010.

[41] I. Pratikakis, B. Gatos, and K. Ntirogiannis. Icdar 2011 document image binarization contest (dibco 2011). pages 1506–1510, Sept 2011.

[42] I. Pratikakis, B. Gatos, and K. Ntirogiannis. Icfhr 2012 competition on handwritten document image binarization (h-dibco 2012). pages 817–822, Sept 2012.

[43] I. Pratikakis, B. Gatos, and K. Ntirogiannis. Icdar 2013 document image binarization contest (dibco 2013). pages 1471–1476, Aug 2013.

[44] Stephen V. Rice, Frank R. Jenkins, and Thomas A. Nartker. The fourth annual test of ocr accuracy, technical report 95-03. July 1995.

[45] J. Sauvola and M. Pietikäinen. Adaptive document image binarization. *Pattern Recognition*, 33(2):225–236, Feb 2000.

[46] M. I. Sezan. A peak detection algorithm and its application to histogram-based image data reduction. *Computer Vision, Graphics, and Image Processing*, 49(1):36–51, 1990.

[47] Faisal Shafait, Daniel Keysers, and Thomas M. Breuel. Performance evaluation and benchmarking of six page segmentation algorithms. *IEEE Transactions on Pattern Analysis and Machine Intelligence*, 30(6):941–954, June 2008.

[48] N. Shanthi and K. Duraiswamy. A novel SVM-based handwritten Tamil character recognition system. *Pattern Analysis and Applications*, 13(2):173–180, May 2010.

[49] Brij Mohan Singh, Rashi Nitin Gupta, Ankush Mittal, and Debashish Ghosh. Parallel implementation of devanagari text line and word segmentation approach on gpu. *International Journal of Computer Applications*, 24(9):7–14, June 2011.

[50] Brij Mohan Singh, Rahul Sharmal, Ankush Mittal, and Debashish Ghosh. Parallel implementation of niblack's binarization approach on cuda. *International Journal of Computer Applications*, 32(2):22–27, October 2011.

[51] Brij Mohan Singh, Rahul Sharmal, Ankush Mittal, and Debashish Ghosh. Parallel implementation of Otsu's binarization approach on cuda. *International Journal of Computer Applications*, 32(2):16–21, October 2011.

[52] Brij Mohan Singh, Rahul Sharmal, Ankush Mittal, and Debashish Ghosh. Parallel implementation of Souvola's binarization approach on cuda. *International Journal of Computer Applications*, 32(2):28–33, October 2011.

[53] Ray Smith. An overview of the Tesseract OCR engine. *Proc. of ICDAR 2007*, pages 629–633, 2007.

[54] Eric J. Sollnitz, Tony D. DeRose, and David H. Salesin. Wavelets for computer graphics: A primer, part 1. *IEEE Computer Graphics and Applications*, 15(3):76–84, May 1995.

[55] J. M. White and G. D. Rohrer. Image thresholding for optical character recognition and other applications requiring character image extraction. *Develop*, 27(4):400–411, July 1983.

[56] Abdelwahab Zramdini and Rolf Ingold. Optical font recognition from projection profiles. *Electronic Publishing*, 6(3):249–260, Sep 1993.

Vita

Jeremy P. Reed

Education

- B.S., Computer Science,
  Centre College, Danville, KY. May, 2001.

Employment

09/14 – Current, Software Architect, Reed Consulting, Lexington, KY

01/10 – 09/16, Research Assistant, Department of Computer Science, University of Kentucky, Lexington, KY

08/11 – 08/14, Principal Architect, Aspect Software, Inc., Louisville, KY

09/09 –07/11, Software Architect, Reed Consulting, Lexington, KY

06/05 – 08/09, Senior Systems Specialist, ACS, Inc., Lexington, KY

01/03 – 06/05, Senior Developer, REGISTRAT, Inc., Lexington, KY

09/01 – 11/04, Technical Architect, Broadband For Everyone, Inc., Georgetown, KY

Honors and Awards

- John C. Young Scholar, 2000-2001

Publications

1. J. Griffioen, Z. Fei, H. Nasir, C. Carpenter, J. Reed, X.i Wu and S.P. Rivera, “The GENI Desktop,” The GENI Book, Edited by R. McGeer, M. Berman, C. Elliot, and R. Ricci, Springer International Publishing, ISBN 978-3-319-33767-8, Sept. 2016.

2. J. Griffioen, Z. Fei, H. Nasir, X. Wu, J. Reed and C. Carpenter, “Measuring experiments in GENI’, Computer Networks”, vol 63, pp. 17–32, 2014.

3. J. Griffioen, Z. Fei, H. Nasir, X. Wu, J. Reed and C. Carpenter, “GENI-Enabled Programming Experiments for Networking Classes”, 2013, pp. 111–118.

4. J. Duerig, R. Ricci, L. Stoller, M. Strum, G. Wong, C. Carpenter, Z. Fei, J. Griffioen, H. Nasir, J. Reed and others,“’Getting started with geni: a user tutorial”, ACM SIGCOMM Computer Communication Review, vol 42, iss 1, pp. 72–77, 2012.

5. J. Griffioen, Z. Fei, H. Nasir, X. Wu, J. Reed and C. Carpenter, “The design of an instrumentation system for federated and virtualized network testbeds”, 2012, pp. 1260–1267.

6. J. Griffioen, Z. Fei, H. Nasir, X. Wu, J. Reed and C. Carpenter, “Teaching with the Emerging GENI Network”, Proc. of the 2012 International Conference on Frontiers in Education: Computer Science and Computer Engineering, 2012.

Invited Talks

1. Jeremy Reed, “Optical Character Recognition with GPUs: Document Processing Throughput Increased by a Magnitude’.’ GPU Technology Conference. San Jose, CA, March 2014.